CHARACTERIZATION AND DIAGNOSTIC OF HIGH EFFICIENCY PHOTOVOLTAIC MODULES IN COMPOSITE CLIMATE OF INDIA

A thesis submitted to the
University of Petroleum and Energy Studies

For the Award of
Doctor of Philosophy
in
Electrical and Electronics Engineering

By
Rashmi Singh

January 2020

SUPERVISOR (s)

Dr. Madhu Sharma
Dr. Chandan Banerjee

Department of Electrical and Electronics Engineering
School of Engineering
University of Petroleum and Energy Studies
Dehradun-248007; Uttarakhand

CHARACTERIZATION AND DIAGNOSTIC OF HIGH EFFICIENCY PHOTOVOLTAIC MODULES IN COMPOSITE CLIMATE OF INDIA

A thesis submitted to the
University of Petroleum and Energy Studies

For the Award of
Doctor in Philosophy
in
Electrical and Electronics Engineering

BY
Rashmi Singh
(SAP ID: 500048575)

January 2020

Internal Supervisor
Dr. Madhu Sharma
Associate Professor
Department of Electrical and Electronics Engineering
University of Petroleum and Energy Studies

External Supervisor
Dr. Chandan Banerjee
Deputy Director General
National Institute of Solar Energy, Gurugram (Haryana).

Department of Electrical and Electronics Engineering
School of Engineering
University of Petroleum and Energy Studies
Dehradun-248007; Uttarakhand

DECLARATION

I declare that the thesis entitled "Characterization and Diagnostic of High-Efficiency Photovoltaic Modules in Composite Climate of India" has been prepared by me under the guidance of Dr. Madhu Sharma, Associate Professor, Department of Electrical and Electronics Engineering, University of Petroleum and Energy Studies, Dehradun and Dr. Chandan Banerjee, Deputy Director General, National Institute of Solar Energy, Gurugram. No part of this thesis has formed the basis for the award of any degree or fellowship previously.

Rashmi Singh
Ph.D. student,
Department of Electrical and Electronics Engineering,
University of Petroleum and Energy Studies, Dehradun
National Institute of Solar Energy, Gurugram

Date: 30th June 2020.

UPES

UNIVERSITY WITH A PURPOSE

Great Place To Work. Certified APR 2019-MAR 2020 INDIA

CERTIFICATE

I certify that Rashmi Singh has prepared his thesis entitled "Characterization and Diagnostic of High Efficiency Photovoltaic Modules in Composite Climate of India", for the award of PhD degree of the University of Petroleum & Energy Studies, under my guidance. She has carried out the work at the Department of Electrical and Electronics Engineering, University of Petroleum & Energy Studies.

Dr. Madhu Sharma

Associate Professor

School of Engineering

University of Petroleum & Energy Studies, Dehradun.

Date: 30th June 2020.

राष्ट्रीय सौर ऊर्जा संस्थान
National Institute of Solar Energy

(नवीन एवं नवीकरणीय ऊर्जा मंत्रालय, भारत सरकार के अधीन एक स्वायत संस्थान)
(An Autonomous Institution of Ministry of New and Renewable Energy, Government of India)
गुरूग्राम - फरीदाबाद मार्ग, ग्वालपहाड़ी, गुरूग्राम - 122 003, हरियाणा, भारत
Gurugram - Faridabad Road, Gwal Pahari, Gurugram -122 003, Haryana, India
दूरभाष / Tel. No. : 0124-285 3060 Fax : 0124-285 3079
ईमेल / Email : dgnise.mnre@nise.res.in • admin@nise.res.in
वेबसाइट / Website : www.nise.res.in

CERTIFICATE

I certify that Rashmi Singh has prepared her thesis entitled "Characterization and Diagnostic of High Efficiency Photovoltaic Modules in Composite Climate of India", for the award of PhD degree from the University of Petroleum & Energy Studies, under my guidance. She has carried out the work at the Department of Electrical and Electronics Engineering, University of Petroleum & Energy Studies.

Dr. Chandan Banerjee
Deputy Director General
National Institute of Solar Energy, Gurugram (Haryana).

Date: 30th June 2020.

ABSTRACT

Solar energy has become one of the most important renewable energy sources. The growth of the solar photovoltaics in India reaching a cumulative installed capacity of about 53 GW at the end of November 2019 according to the report of the Ministry of New and Renewable Energy. This exponential growth was possible due to favourable policies, as well as decreasing the cost of SPV modules and balance-of-system components. As these main market drivers reach their limit, the system operating costs and long-term reliability of the SPV modules becomes more relevant in reducing the total lifetime cost of the SPV system.

In this context, characterization and diagnostic methods are increasingly important in identifying and understanding the failures and degradation modes affecting SPV modules and arrays, as well as developing relevant tools and tests for assessing the reliability and lifetime of SPV modules. The characterization and evaluation of the performance of silicon-based SPV module technology, under realistic operating condition, observed in the composite climate of National Institute of Solar Energy, India. Analysis based on the effect of radiance, ambient temperature, module temperature (back of the module), the spectrum factor and thermal factor over the performance of the SPV module has been calculated and analysed. It has been observed that the impact of the observed variation in operating condition affects SPV modules very differently according to the module type (module material property).

The estimation of monthly average effective peak power (P_{eff}), performance ratio (PR) and temperature corrected performance ratio (PR_{CORR}) has been done. The average percentage reduction in the effective peak power for the mc-si, a-si and HIT modules were 15.80%, 17.23%, and 7.15% respectively. The monthly average PR for mc-si, a-si and HIT modules were 0.70, 0.82 and 0.83 respectively. The monthly average PR_{CORR} for mc-si is 0.77, for a-si is 0.89, and for a HIT is 0.90 modules respectively. The monthly average efficiency for the for mc-si SPV module is 9.82, for a-si is 5.22, and for a HIT is 15.68 modules respectively.

The HIT modules are less affected by the variation of the operating conditions like irradiance, temperature and spectrum factor. This module exhibited the least variation in all investigated parameters. The mc-si module has a negative impact of high temperature and irradiance, performance goes decreased by high operating temperature, performance is decreased during the summer.

The annual DC degradation rate of the three-different silicon-based technology was calculated using the statistical methods of linear regression, LOESS (locally weighted scatterplot smoothing), and the CSD (classical seasonal decomposition) over a period of three years. The degradation rate using the linear regression over the effective peak power are 4.89% for mc-si, 5.08% for a-si and 1.7% for HIT modules has been calculated. The highest degradation has been observed for the a-si followed by mc-si modules whereas the HIT module shows the least degradation rate. The average degradation rates are found to be 1.07%/year, 0.27%/year and 1.26%/year for a-si, HIT and mc-si modules respectively. Further, the operational conditions and analysis of the seasonal variation over a period of three years have also been characterized.

The performance of the SPV at real outdoor condition has been studied based on the filtering techniques, performance monitoring metrics and numerical methodologies. The I-V based module diagnostic method was developed by combining the strengths of light I-V and dark I-V characterization, for the purpose of identifying series resistance. The series resistance has been calculated using the IEC 60891 edi 2.0 and mapping of the series resistance has been done with the matrix of in-plane irradiance and module temperature. The mean series resistances for mc-si, a-si and HIT modules are found to be 0.72 Ω, 18.20 Ω, and 0.61 Ω respectively using analytical techniques while 0.31 Ω, 20.62 Ω and 1.54 Ω respectively using IEC 60891 Edi. 2.0. From the results, it can be concluded that the variation in the results may be observed due to the input parameters, modelling equations and assumptions made during the calculations. The result shows that the modelling equations have been mainly derived for the mc-si technology and it is proposed that new modelling is required for the new emerging technologies like HIT and thin films modules.

It has also been found that there is a need for a stable and standardized analytical method for calculating the series resistance. The uncertainty to estimate the series resistance has been calculated for three range of irradiance i.e. 1000 W/m^2, 900 W/m^2 and 800 W/m^2 which is around 4% for all the three technologies at outdoor field condition.

The second part investigates the thermal and electrical handling capacity of the high-efficiency solar modules. The capacity to withstand the environmental and practical situation in the real field. PV arrays that are suitable for implementation in the solar inverter or incorporated in a condition monitoring system. Different condition based on the short-circuited condition was evaluated for four different technologies solar modules. It is well documented that the operating temperature of the module plays a critical role. Module designs heavily influenced by the working of cells in different conditions. The advanced structures of the new modules coming into the market are having the advantage to reduce the impact of partial shading or mismatch conditions. The power dissipation is not the, most pertinent issue instead of the maximum heat density that can occur since high heat will damage the solar cell, module encapsulates and the back tail. The non-uniformity of the power also occurs in the modules, especially over the weakest solar cells. The heat through these peaks can reach the temperature high enough to damage the modules, involving the utilization of the bypass diodes as a means of security.

. The highest degradation has been observed for the a-si followed by m-si modules whereas the HIT module shows the least degradation rate. The a-si module technologies are well suited for the hot and warm climatic zones whereas from the different performance indices the HIT module shows the best performance for the composite climate of India. The result indicates that the significance of the outdoor performance of SPV technologies with reference to location specific climatic conditions. The location specific standards are needed to be used for the accurate and precise assessment and calculation of power output, energy yields and PR of the SPV technologies.

ACKNOWLEDGEMENT

I would like to express my gratitude to many people who kindly supported me while I was doing my studies and the research presented in the thesis.

I, first and foremost, would like to express my deepest gratitude to Dr. Madhu Sharma and Dr. Chandan Banerjee, my supervisor, for encouraging me to take this research problem. It is an honour to work under their supervision. My supervisors have always been a constant source of inspiration throughout this research work. A special thanks to Director, School of Engineering Dr. Kamal Bansal for supporting me throughout my journey. I am thankful to Chancellor Dr. S. J. Chopra, Vice Chancellor Dr. Deependra Kumar Jha, CEO Prof. Utpal Gosh, Associate Dean Research Dr. Jitendra Kumar Pandey and Associate Dean Dr. Suresh Kumar for motivating me with space and environment in the serene campus of University of Petroleum & Energy Studies, Dehradun, India to carry out this work.

I am extremely grateful to my doctoral committee members Dr. Piyush Kuchhal, Dr. Sushabhan Choudhury, Dr. R Gowri, Dr. Adesh Kumar, and Dr. Rupendra Pachauri for their encouragement and insightful comments during various discussions. I am thankful to each and every faculty colleague of Electrical Engineering department for their support and cooperation. I would like to thanks Ms. Rakhi Ruhal, Mr. Sony Sandeep farmer and other CCE staff members for their help on countless occasions.

I would like extend my special thanks to my colleagues who have provided unconditional support to me all these years and especially in the last days of my submission.

Lastly, I must express my deepest appreciation to my dearest family member, Especially, I would like to thank my beloved father **Mr. Abhimanyu Singh** who appreciated my efforts and always provided cheerful encouragement during the period of study and whose love and affection provided me joy and relaxation. This achievement is for you, as what I am today is your vision and you have always made me believe in me even during my darkest days. I am grateful to my mother **Mrs. Kiran Singh** who supported me throughout my life

and always boosts up my morale. I must express my very profound gratitude to My elder brother **Mr. Raghuvendra Singh**, my younger brother **Ashish Singh** who have been there for me ever. I would also like to acknowledge moral support if my husband **Vinay Singh** for being constant source of motivation during thesis writing.

And finally, to all of those people who encouraged me throughout this process, your inspiration is what guided me, and I am truly grateful to all of you. Although this study is completed, it has opened the door for others to continue to strive to gain a better understanding of solar energy.

Thank you.

Rashmi Singh
University of Petroleum & Energy Studies
National Institute of Solar Energy.

Date: 1st January 2020.

TABLE OF CONTENTS

List of Figure

List of Table

CHAPTER 1
INTRODUCTION

This chapter presents an overview of the energy sector and summaries various renewable energy resources available in India. It deliberates renewable energy potential and achievement so far, growth trend during the plan periods and future capacity additional plans. The chapter provides motivation for the research objectives.

1.1 Indian energy scenario

Energy shows a major role in the fiscal development of a country. Earth is privileged with tremendous sources of energy, in which non-renewable energy resources are limited in nature. Non-renewable resources can be consumed entirely or used up to such an extent that they become economically inaccessible. The commercial and industrial expansion of any country is dependent on the organized development of its power and energy sectors. Electrical energy is the most needed energy transporter because of its particular quality, the wide extent of the capacity and its unmatched utilization [1]. Electricity generation in a proper framework for far away and widespread places at reasonable prices shows a significant role in the development of the country.

As on 31st May 2019, the utility electricity sector in India has an installed capacity of about 356.817 GW. During the 2017-18 Financial Year (FY) about 1,303.49 TWh gross electricity has been generated by utilities and the total 1, 486.5 TWh electricity generated by combining utilities and non-utilities in India [http.//www.cea.nic.in]. The gross electricity consumption was 1,149 kWh per capita during the 2017-18 financial year. India is the third-largest producer as well as consumer of the electricity.

Electricity production in FY 2017-18 by a source in India is shown in Fig 1.1.

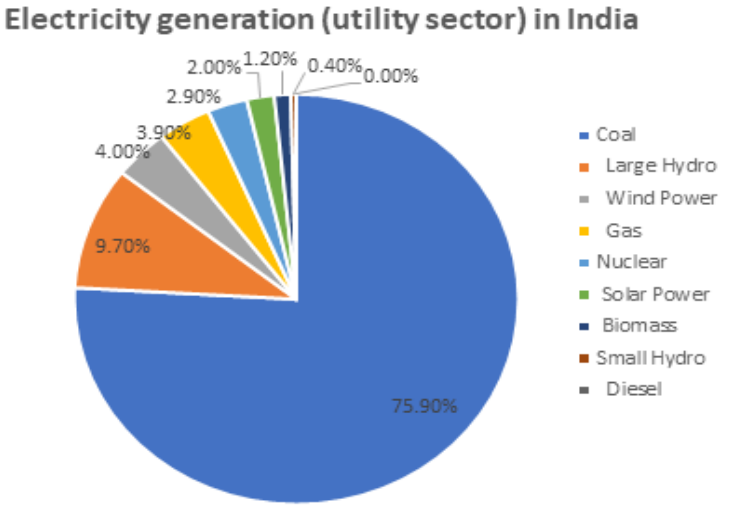

Fig 1.1. Electricity generation (utility sector) in the Financial year 2017-18 in India

The total installed capacity of the renewable energy resources, including the largest hydroelectric plants, constitute 34.86% of India's total installed capacity. India is the world's fourth-largest producer of wind power and the sixth-largest producer of solar energy. The installed power generation capacity in India as on 31st May 2019 is shown in Fig 1.2.

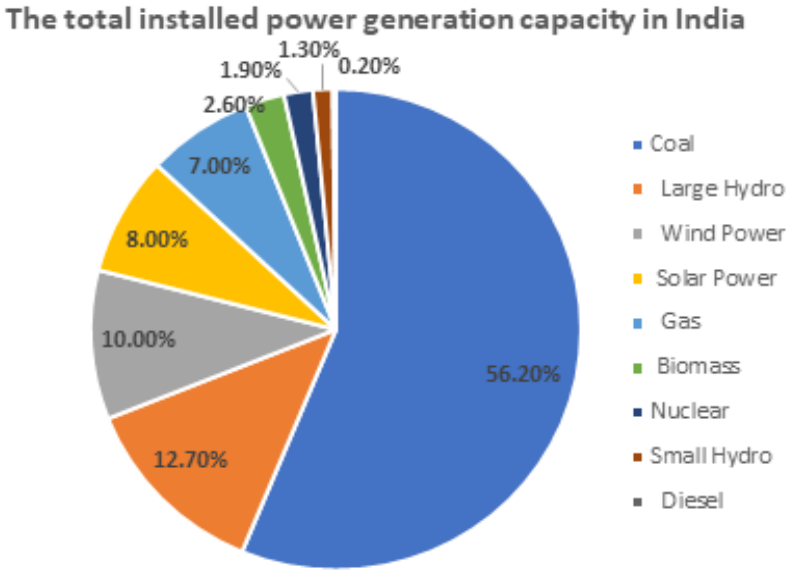

Fig 1.2. The total installed power generation capacity in India as on 31st May 2019

The coal-based installed power plant has the largest generation followed by the large hydropower plant. Similarly, in India generation from the solar systems are followed by the wind power plant. Solar energy is the preferred options in the far-flung regions, because of the convenient power sources, easy maintenance and abundant supply [2]. Solar energy is the radiant light and heat from the Sun that is utilized by a variety of technologies such as solar thermal energy, solar photovoltaics, solar pond, solar distillation, solar air conditioning, and solar concentrator etc.

There are many places in the world that are encountering fast depletion of non-renewable sources in terms of fossil fuels [https.//www.iisd.org/]. Countries are continuously working on alternative ways to generate electricity through the cleaner and promising resources. Moreover, to achieve sustainable growth, Renewable Energy Source (RES) can be one of the sustainable ways to meet the increasing global electricity demand. Considering the fact that the availability of conventional sources of energy is limited, the promotion of renewable energy generation sources is a key focus area. Renewable Energy Sources primarily constitute wind, solar, small hydro (up to 25 MW), biomass, biofuel and cogeneration. Given the increasing importance of renewable energy, especially in the context of energy security and climate change needs, tracing various policy instruments deployed for promotion of renewable energy sources is highly topical. It is all the more contextual to probe into the latest policy and regulatory initiative of REC, to understand how it gels with and to what extent it needs to be refined to align with the larger objective of green energy development.

The Jawaharlal Nehru National Solar Mission (JNNSM) later known as National Solar Mission (NSM) is a program of the state governments and the Government of India (GoI) to encourage the expansion of the solar power in India. The purpose of this initiative is to establish India as a pioneer in the field of solar energy, by developing favourable policies across the country. The former target was deploying 22 GW solar energy by 2022 under the NSM, which were revised to 100 GW. Due to this mission, there is rapid development in solar installations all over the country in the coming years. The mission

comprises of three phases which are Migration Scheme, NSM Phase-I, Batch-I and lastly NSM Phase-I, Batch-II.

As per a study conducted by the National Institute of Solar Energy (NISE), the total solar potential in the country has been estimated as 750 GW, considering the use of 3% of wasteland area [https.//mnre.gov.in/file-manager/annual-report/2016-2017/EN/pdf/1.pdf]. Acquiring land for the forthcoming solar plants would pose a significant challenge to both the policymakers as well as the project investors. When it comes to solar projects, the main goal is producing as much energy in as little space as possible. Hence, high-efficiency solar modules succeed in the residential market, where ideal roof space is every so often limited. High-efficiency solar modules will require less area for the same MW capacity than conventional Solar Photovoltaic (PV) modules.

Sun as a power harvesting sources is the best option to resolve the problems based on energy scarcity and power quality. Sun is the ultimate source of light, directly converted into direct current energy is termed as Solar Photovoltaic (PV) which is an important renewable energy source. PV technology has emerged as a useful power source, which meets the electricity needs of rural communities, solar lighting, solar drying, dispensaries, and hospitals [3]. During the 300 sunny and clear days, India gets solar energy incidence about 5000 trillion kilowatt-hours (kWh) per year. To ensure the economic growth of the country, and exterminate the energy shortage, India must utilize its massive solar potential. The progress of the solar PV sector in India has been evident through diverse initiatives. For the expansion of the solar industry, there is a need to achieve the highest reachable efficiency while reducing the manufacturing cost of the solar cell.

The efficiency of the SPV module provides an indication of the reliable and durable long-term performance guarantee. In terms of commercially available products, a high-efficiency solar module is one that is having 20-25% efficiency using solar tracking, research or theoretical cells can be even higher, though not necessarily as financially viable. It has been observed that using high-grade silicon in many high-efficiency PV modules enhance their outdoor working life-time and also having improved temperature coefficient. The area

of the solar module's installation highly depends upon the efficiency of the solar module. The solar modules with higher efficiency require less area which is highly required where an area is limited. Using the high-efficiency modules may also permit higher capacity systems to be fitted to any desired space.

At the end of 2018, the worldwide cumulative installed capacity of the PV is about 512 gigawatts (GW). The installed solar capacity in India reached 29.54 GW as of 31st July 2019 [https.//mnre.gov.in/physical-progress-achievements]. The India graph for solar radiation is shown in Fig 1.3.

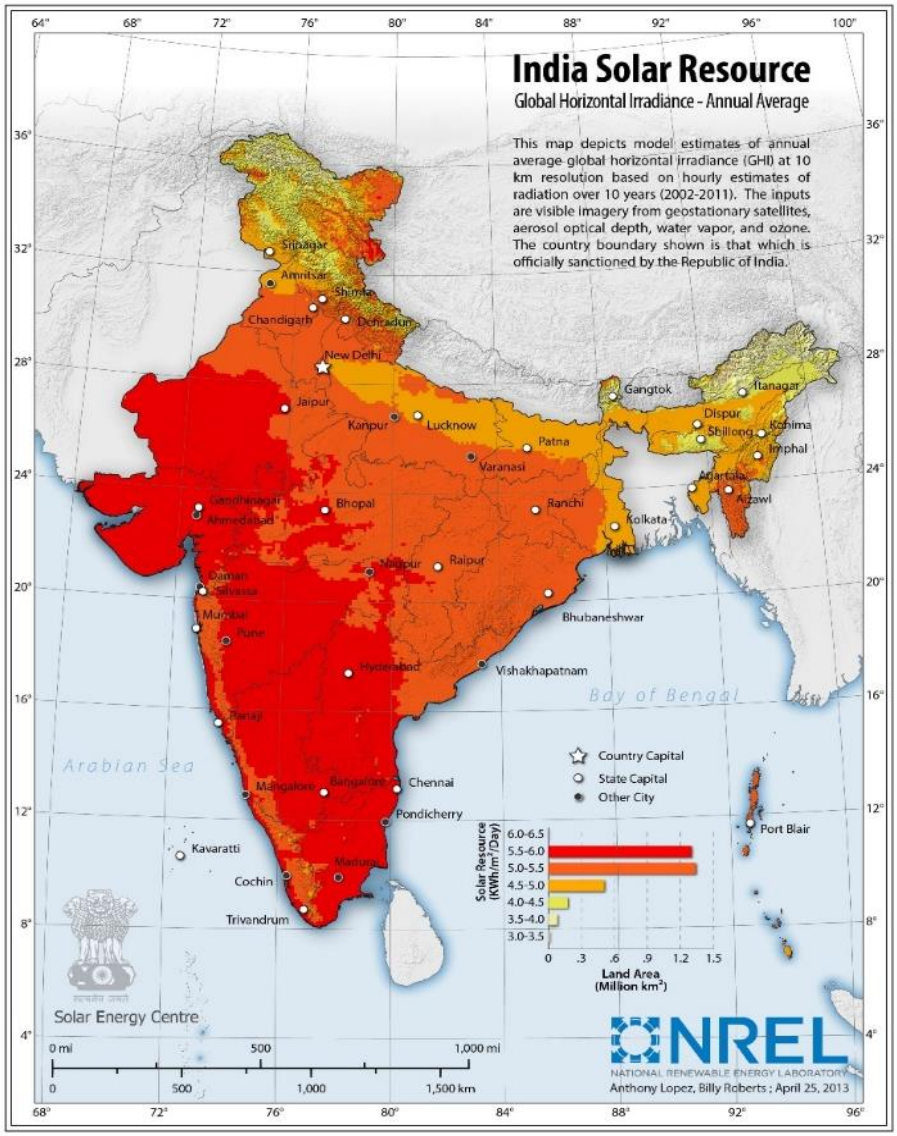

Fig 1.3. Annual average global solar radiation in India.

To enhance the production and generation of the PV industries as a suitable and commercially achievable source of energy, long-term reliability

and degradation studies over different PV technologies are utmost required. The surface receives about 47% of the total solar energy that reaches the earth presented in Fig 1.4.

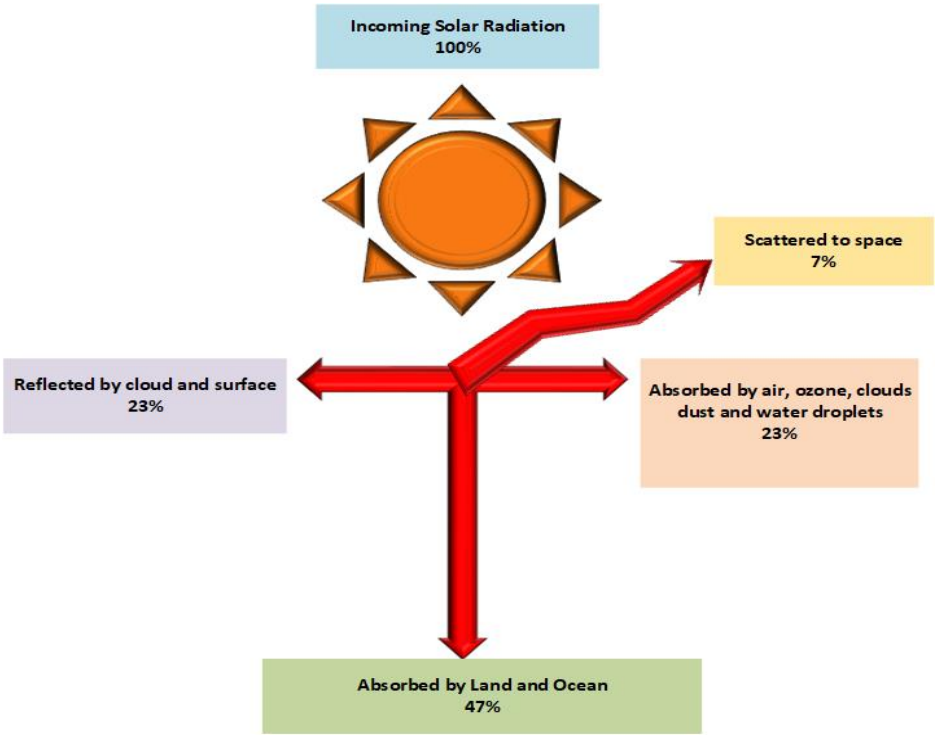

Fig 1.4: Distribution of solar radiation through absorption, transmission and scattering

The solar radiation emitted from the Sun is termed as Electromagnetic radiation. The range of electromagnetic energy covers mainly three regions. Ultraviolet (UV), Visible, and Infra-Red (IR). The solar spectrum extends from about 0.29 µm (or 290 nm) in the longer wavelengths of the ultraviolet region, to over 3.2 µm (3,200 nm) in the far Infra-Red. Solar irradiance is the power per unit area from the sun over a given wavelength range represented in the units of kW/m^2 or W/m^2. Sun's radiations travel through the atmosphere before reaching the earth. Due to the changing angle of the sun during the whole day, the distance that sunlight has to travel keeps changing. The radiations travel the shortest distance through the atmosphere when the sun is directly overhead. The spectrum of this radiation is termed as "Air Mass 1 Direct" (AM1D). Since sea level is used as a standard reference site, the global radiation with the sun overhead is referred to as "Air Mass 1 Global" (AM1G). The Solar constant is the average value of the solar irradiance outside the earth's atmosphere which

is about 1366 W/m^2. The solar irradiation is equal to the average solar irradiance multiplied by the time represented by kWh/m^2.

1.2 Solar Photovoltaic technology

In 1839, French physicist Edmond Becquerel demonstrated the photovoltaic effect, he built the world's first photovoltaic cell in his father's laboratory. In 20th February 1873, "Effect of Light on Selenium during the passage of an Electric Current" was described by Willoughby Smith in an issue of “Nature”. In 1883, the first solid-state photovoltaic cell by coating the semiconductor selenium with a thin layer of gold to form the junctions; the device was only around 1% efficient is built by Charles Fritts. During 1887, German physicist Heinrich Hertz observed the photovoltaics effects which are the creation of the current and voltage in a material upon the exposure of the light. Bells Labs created the first solar cell in the 1950s since then SPV technologies have been increasingly developing globally.

Silicon PV modules containing wafers are dominating the market, resulting in about 90% of the total production of wafer-based silicon modules. This may be due to the easy supply of raw material, i.e. silicon material which is non-toxic and plentifully accessible in the earth’s crust, recognized manufacturing processes and the high conversion efficiencies that can be achieved. Even though the PV technologies become progressive in terms of manufacturing techniques and efficiency, further research and efforts have been required to enhance the efficiency of the solar cell [4].

Sunlight is composed of minuscule particles called photons, which radiate from the Sun. A photon is a particle of light defined as a discrete bundle (or quantum) of electromagnetic (or light) energy. The generation of the electron-hole pair is happening due to the incidence of the photon which is subsequently absorbed by a photovoltaic device. The electron-hole pairs get separated by an electric field at the junction and collected through metal contacts. The entire procedure can be concluded as the three steps – (1) light absorption, (2) carrier generation, and (3) carrier collection.

The boron-doped silicon as the base together with an ultra-thin layer of n-type silicon is used in the p-type solar cells, whereas the phosphorus-doped

silicon as a base with a thin layer of p-type is structured in the n-type solar cell. The arrangement of the p and n-type silicon is used in both the solar cell structure, which constitute the p-n junction. The structures of the p-types and N-types are described below in Fig 1.5.

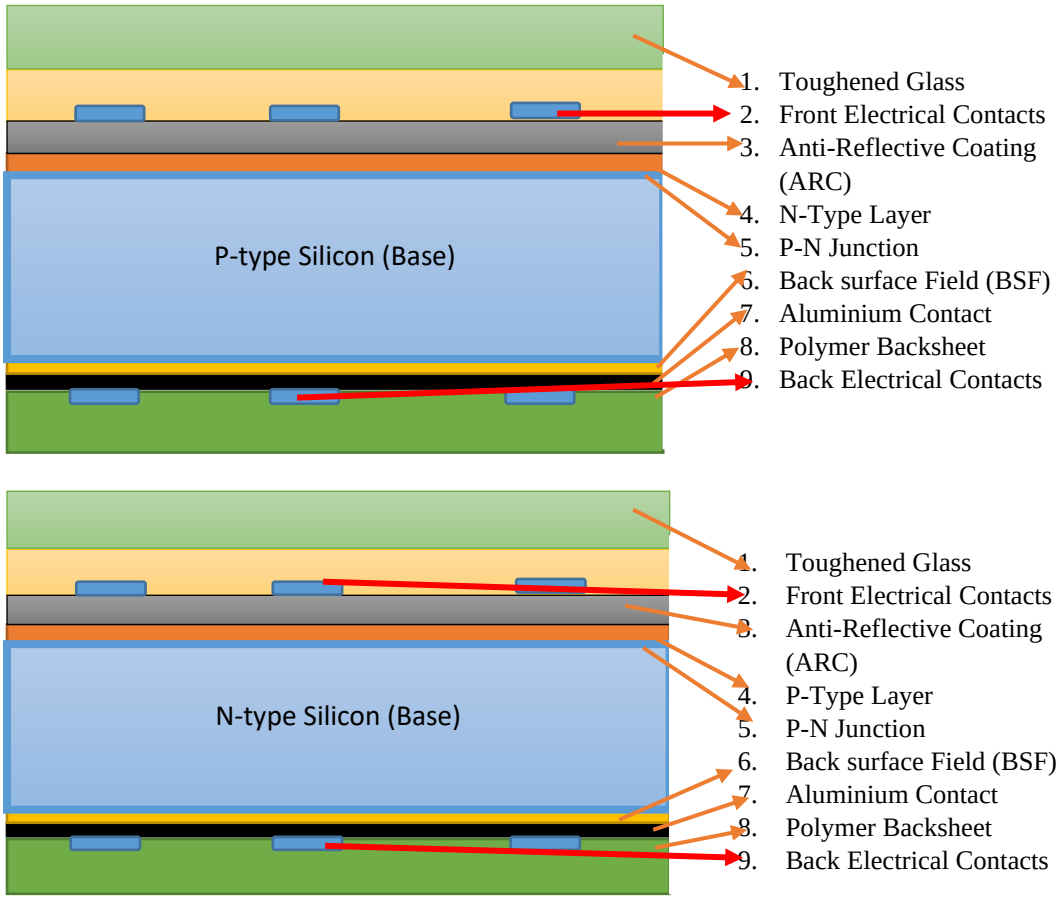

Fig 1.5. Basic construction diagram of (a) P-type silicon and (b) N-type silicon Monocrystalline solar cell.

The n-type solar cell provides increased efficiency due to the higher tolerance in the impurities and lower cell defects. The n-type solar cells free from the concerns of Light-Induced Degradation (LID), due to the boron-oxygen defects which are a familiar concern with p-type cells. It is also having a lower temperature coefficient in contrast to both mono and multi p-type solar cells. Due to the lower temperature coefficient, the solar module behaviour is stale in high-temperature zones. The construction of these types of solar cells is more expensive due to using boron diffusion process to add the thin p-type emitter layer. It is more complicated and needs higher temperatures in contrast

to the construction of the p-type cell using phosphorus diffusion process. The base of the n-type silicon solar cell is extremely pure; hence it enables higher conversion efficiency, reduced degradation over the time period. The output of these n-type solar cells results in higher generation and performance which shorten the payback period.

The solar cell classified as the homo-junction and the hetero-junction solar cells. The homo-junction can be defined as the interface that happens between similar semiconductor materials; these materials have equal band gaps but typically have different doping. A p-n junction is a homojunction occurs at the interface between an n-type (donor doped) and p-type (acceptor doped) semiconductor such as silicon. In mostly homo-junction c-si solar cells, the base is typically manufactured with about 150 μm thick boron-doped p-type wafer and the phosphorous diffused n-type emitter is about 0.2 μm to form a PN diode. The front surface passivation of the emitter and Anti-Reflection Coating (ARC) is provided from silicon nitride (SiNx). In a Silicon Heterojunction (SHJ) structure, the junction is formed through the deposition of thin doped amorphous silicon film of opposite polarity to that of the absorber.

1.3 Climatic Zones in India

The performance of a PV module and its degradation also depends on the local climatic conditions (Climatic Zones). Having both the climatic classification and the PV performance, bring us the possibility to standardize the evaluation per climatic zones [5]. Due to different geographical expansion, there is diversity in the Indian climatic zones, in which different zones experience different climatic profiles.

Based on the average annual temperature and humidity, the National Building Code (NBC) divides India into five climatic zones which are; Warm & Humid, Composite, Hot & Dry, Temperate and Cold [6]. However, Bansal and Minke provide a six climatic zone classification system which is described in the below Table 1.1. The regions having similar characteristic features of climatic zones are grouped under one.

Table 1.1. Climatic Zone Classification criteria as per Bansal and Minke [37].

Climate Mean Monthly	Mean Relative Humidity (%)	Temperature (°C)	Examples
Hot & Dry	<55	>30	Jaipur, Sholapur and Jaisalmer
Temperate	<75	25 – 30	Bangalore, Pune
Warm & Humid	>55	>30	Mumbai, Chennai and Kolkata
Cold & Cloudy	>55	<25	Jammu, Kashmir Valley, and Himachal Pradesh
Cold & Sunny	<55	<25	Ladakh
Composite	This applies when six months or more do not fall within any of the above		(including the capital city of New Delhi)

According to a recent code of Bureau of Indian Standards (BIS), the country may be divided into five major climatic zones. In the Hot & Dry mean monthly temperature >30 and relative humidity <55%; Warm & Humid have mean monthly temperature >25-30 and relative humidity >55-75%; Temperate zone having the mean monthly temperature 25-30 and relative humidity <75%; Cold zone having mean monthly temperature <25 and relative humidity all values and the Composite climatic zone having when six months or more do not fall within any of the other categories. The latest climatic zone classification criteria are defined in Table 1.2.

Table 1.2. Latest Climatic Zone Classification criteria

Climate Mean Monthly	Mean Relative Humidity (%)	Temperature (°C)
Hot & Dry	<55	>30
Temperate	<75	25 – 30
Warm & Humid	>55	>30
	>75	>25
Cold	All values	<25
Composite	This applies when six months or more do not fall within any of the above	

From the above Table 1.2, the Hot & Dry climatic zones having a mean monthly maximum temperature higher than 30 ^{o}C and mean relative humidity less than 55%. Locations having a mean monthly maximum temperature higher than 30 ^{o}C and mean relative humidity higher than 55% are considered under the warm and humid climatic zones.

The places which are having a temperature of less than 25 ^{o}C and humidity less than 55% is considered under cold and sunny. In contract similar temperature, but the humidity higher than 55% is termed as cold and cloudy. Places which experience both hot, cold & humid conditions for some part of the year and no single climatic pattern extends for six months, are clubbed in the "Composite" climatic category, and experience very dry summers, wet rainy season, and also cold winters.

1.4 Performance of the solar photovoltaic systems

The datasheet of the PV modules generally documented as per IEC 61215-2:2016 standard published by the International Electro-Technical Commission's (IEC). To evaluate the electrical performance of PV modules they are tested in Standard Test Condition (STC) which is 1000 W/m^2 and the temperature is 25 °C along with the IEC 60904-3 reference solar spectral irradiance distribution. The general testing condition for the Nominal Module Operating Temperature (NMOT) is having an irradiance of 800 W/m^2 and an ambient temperature of 20 °C into similar spectrum conditions. Later, these measurements used to verify the data sheet information of the solar module.

To ensure the capability of the PV module to withstand the outdoor exposure conditions and to evaluate the degradation impacts these tests have been conducted. These series of test in the international standard provide the data on the impact of environmental parameters over the module working in outdoor condition, however, these tests are not enough to provide much information about the solar module operating under real outdoor conditions with variation in the environmental factors. The IEC 61724-1:2017 is the worldwide followed International Electro-Technical Commission's standard for the SPV system performance monitoring, capacity evaluation methods, and energy evaluation methods of the SPV system (IEC 61724-1:2017, IEC TS 61724-

2:2016, IEC TS 61724-3:2016). The standard comprises the installation, accuracy of monitoring equipment also to the measured parameter data acquisition, quality check and performance matrices. The standard specifies procedures for the performance assessment of PV systems based on a parameter such as energy efficiency, performance ratio, and final energy yield.

1.4.1 Degradation study of solar photovoltaic module

The performance of PV depends upon various environmental parameters like solar radiation, ambient temperature, humidity, wind speed and direction which vary from location to location. The steady degradation of the PV performance while installing at the real field conditions is defined as the incapability of the module to supply its rated power due to exposure to various climatic factors. Hence, it is critically significant to examine the performance of solar modules of different technologies in outdoor conditions. However, it can vary substantially with the induction period and climatic condition. Dissimilarities in the degradation rates of the similar solar modules by installation periods are generally linked by the specific solar module material properties and location. Due to higher temperatures and moisture, the mc-si solar modules functioned in cold and composite climatic conditions shows lower degradation rates in comparison to the PV modules operated in the desert or tropical climates. The elevated degradation rates are happened due to the chain of degradation failures modes impact the performance of the system over the functioning period. These malfunctions cause a decrease in the working operations as well as a hazard towards safety [7].

It is necessary to evaluate the functioning of PV modules under various climatic zones in India. This study not only identifies the best performing SPV technologies suitable for a particular site but also give the inherent mechanism of degradation, leading to the premature failure's modules. Concerns about SPV modules underperforming (durability) or becoming failing prematurely (reliability) are major barriers to SPV diffusion and project financing. There is an many reason of failures and degradation mechanisms influencing the performance of the PV modules and systems, hence the extent of our

examination is focused on three significant kinds of degradation mechanism impact on the PV modules.

(i) Degradation due to the losses in the optical properties,

(ii) Performance characterization of the high-efficiency PV modules

(iii) Degradation due to the electrical properties of the PV module,

The optical losses may be defined as the obstacle or hurdle in the amount of light reaching the solar cell surface [8]. Optical losses basically impact the power by bringing down the short-circuit current (Isc) in the solar cell. It hinders the light which could have created an electron-hole pair in the solar cell, but does not, because the light is reflected from the front surface, or because it is not absorbed in the solar cell. The optical losses may be due to the maximized the front contact coverage of the solar cell surface, decay in the anti-reflection coatings over the surface of the solar cell, absence of surface Texturing. Under high temperature and high humidity, the moisture that penetrates into the PV module causes corrosion of the metal materials. The corrosion sometimes induces delamination between the solar cells and the encapsulating polymer. The irradiation causes the deterioration of the EVA. The adhesion loss between the solar cell and the front glass or the encapsulating polymer materials changes the optical transmission of the PV module which termed as the front glass corrosion and the optical loss reduced the performance of the PV modules. The other variables also present, which is front-glass corrosion or breakage, soiling of the solar modules, shading, and deposition of particles [9]. Absorption in the encapsulant material (EVA) is also an important optical loss mechanism, especially during degradation.

Soiling over the solar modules are highly reliant on the locations (industrial, rural or urban) and site (ground, hill or valley), weather profile and type of mounting. The shading is happening due to the improperly designed SPV systems and due to this, the activation of the bypass diode causes a substantial loss in the output power. Soiling may cause heating is localized, resulting in the development of hot-spots, and lead to PV module failure in the long term [10]. Components responsible for optical losses may lead to a visual

impression on the PV module surface which can be distinguished with a visual inspection.

The degradation of a solar cell by the illumination is not a new finding and has been the topic of research [11]. Light-induced degradation is generally defined by the increase in excess carrier concentration which causes solar cell degradation because of the different chemical processes within the solar cell as a shift in the Fermi level induced. The increase in excess carrier concentration is due to the incident irradiation over the solar cell surface. LID is a significant degradation phenomenon impacting the solar cell and module efficiency.

Degradation of the junction box connections, bus bars, string interconnect, wiring, cable connectors, and other electrical components are considered under the electrical degradation of solar modules. This may cause the declination in the power, current and safety hazards for the power plants. Corrosion and degradation in the electrical components result in an increase in the module's series resistance which later on increased the module's heating results in localized hot spots. The corrosion of the interconnect ribbons, module connectors, cell bus bars along with the corrosion of the components in the junction box can be caused by moisture ingress. To detect these types of degradation visual inspection and IR thermography of the PV modules, cables, connectors, and junction box are required [12], [7].

In order to make the PV technology cost-effective and commercially viable, it is important to study the technology, behaviour and characteristics of PV systems at the outdoor condition. Therefore, the objectives of this study are; to present the PV models for performance assessment at outdoor environment; to evaluate the behaviour of PV systems under field exposed conditions using different performance parameters; to analyse various failure and degradation modes that are adversely affecting the PV performance and reliability.

1.5 Motivation for Research

The current research in Si-based photovoltaic technologies is primarily based on two aspects; (1) Improvement in the efficiency of silicon solar cells while keeping a close watch on the cost parameters and (2) continuous improvement in the quality of critical matials such as silicon wafers and silver

paste. Together with these efforts, there is also a very pertinent need for enhancing the reliability of these modules and ensuring that these modules performance as per design for a number of years. The existing PV installation is commonly based on Aluminium Back Surface Field (AL-BSF) technology solar cells. The studies regarding the reliability and degradation of AL-BSF PV modules have been done in laboratory conditions as well as in the real field. However, such studies study on high-efficiency panels-based installations is few and far between. Especially in our country which has various climatic zones, such insulations, as well as reliability and degradation studies on them, are an oddity.

The motivation for this study essentially comes from the fact that reliability studies on the high-efficiency modules do not practically exist at least in India. And without this kind of studies, it would impossible to predict the performance of such modules in field Installations. It assumes added importance as there would outdoor performance as well as simulated indoor conditions on these modules would go a long way in determining their preparedness for field applications. The present work, therefore, focuses on such studies based on insolation at NISE, Gurugram. The aim is to compare these and predict the usefulness of the emerging high-efficiency technologies. It essentially targets several technologies, including some current and some emerging (as well as one discarded) technologies, have been studied including the three high-efficiency technologies, namely Hetero-junction intrinsic thin layer silicon (HIT), Interdigited back contact cell technology (IBC) and Passivated emitter and rear cell technology (PERC).

1.6 Thesis Structure

The study consists of seven chapters, including the present Introduction chapter. The structure is also presented in Table 3.

Chapter 1: Introduction and motivation. The first chapter presents the background and context of study; furthermore, it conveys the significance of the study followed by the motivation behind current research. Finally, it states the research gap and objective of the study.

Chapter 2: Fundamentals and literature review. This chapter discusses in detail the literature survey done on two aspects (1) Characterization of the solar modules and (2) Degradation analysis of the solar modules. The chapter defines the statement of the research problem/gap, research questions, objectives of the study and focuses on current issues related to the performance and reliability for the PV.

Chapter 3: Research Methodology and Experimental set-ups. The context of research having been established in the previous chapter, this chapter goes to explain the approach and methodology of undertaking the research. It explains the experimental design, the research methodology, sampling process, data collection, variables derived through a literature survey.

Chapter 4: To study the performance, reliability, and degradation in the composite climate of India. The interpretation of measured and calculated results, correlation of bus-bar corrosion, and module degradation have been delineated for the composite climate.

Chapter 5: A methodology for evaluating the distribution of degradation on outdoor exposure. High-efficiency module series resistance estimation techniques based on the analytical, theoretical and light I-V characteristics have been documented..

Chapter 6: Thermal stress over high-efficiency solar photovoltaic modules. Effect and analysis of the shading losses and develop the modelling of the losses as heating effects have been done.

Chapter 7: Feasibility Study of the High-Efficiency PV Modules. This paper addresses the economic assessment of high-efficiency modules in a composite climate of India (Gurugram).

Chapter 8: Conclusion. Finally, the chapter conclusions, summarize the efforts which have been done all through this study and compile the conclusions founded on the accomplished outcomes. The chapter finishes with an outlook to additional research headings empowered by the study.

Chapter 9: Reference. The later chapter deals with references used.

Table 1.3. Structure of the Thesis

Chapter 1 **Introduction**	This chapter explains the context of research and introduces the topics relevant to research; Overview of Renewable Energy Sources in India.
Chapter 2 **Literature Review**	An extensive review on journals, Reports, other relevant literature has been carried out in this phase; research problem/gap and research objective has been identified in this phase.
Chapter 3 **Research Methodology & Experimental-Setups**	The researcher has at this chapter drew insights from the data and defined the objective of the research and the methodology to achieve the objective.
Chapter 4, 5,6 and 7 **Results and Discussion (Research Objective)**	Analysis and Results
Chapter 8 **Conclusion**	Findings are discussed and contributions to research and theory are highlighted. Directions for future work are also mentioned.
Chapter 9	Reference

CHAPTER-2
LITERATURE REVIEW

A detailed literature survey has been carried out in order to compile information regarding the earlier research conducted in the field of performance monitoring, reliability and degradation studies of solar photovoltaics. This chapter starts by mentioning the performance monitoring and degradation followed by the extraction of research gaps and objective of the research work.

2.1 Solar Photovoltaic classification

Generally, PV technologies are classified as the silicon 1st generation solar cell, semiconductor compounds, and novel and emerging solar cell technologies shown in Fig 2.1. The silicon 1st generation further classified as crystalline and amorphous silicon solar cells, secondly, semiconductor compounds classified as chalcogenides and compound of group III-V and third the emerging or novel materials for the solar cells.

There are numerous commercially installed PV technologies such as Amorphous Silicon (a-si), Copper Indium Gallium Selenide (CIGS), Cadmium Telluride (CdTe), Hetero-junction intrinsic thin layer silicon (HIT), Mono-Crystalline Silicon (m-si), Multi-Crystalline Silicon (mc-si) etc., additionally few are in an examination stage such as Dye-Sensitized solar cell (DSSC), Organic cells with several dye compositions, Perovskite Solar Cell (PSC) [13], [14] etc. All silicon-based solar cells (mono, multi, and poly) is formed by employing a crystalline silicon-based wafer having two main types viz. p-type and n-type [3]. The silicon is ‘doped’ with trivalent and pentavalent elements to create a positive (p-type) or negative (n-type) charge. Phosphorous is used for the positive charges, while Boron is used for the negative charge. The many mainstream of mono and multi-crystalline cells uses p-type having a boron-

doped silicon base [4–7]. Currently, Panasonic, LG, and SunPower solar module and cell manufacturer use the n-type silicon wafers which are having various advantage over a p-type silicon wafer [8].

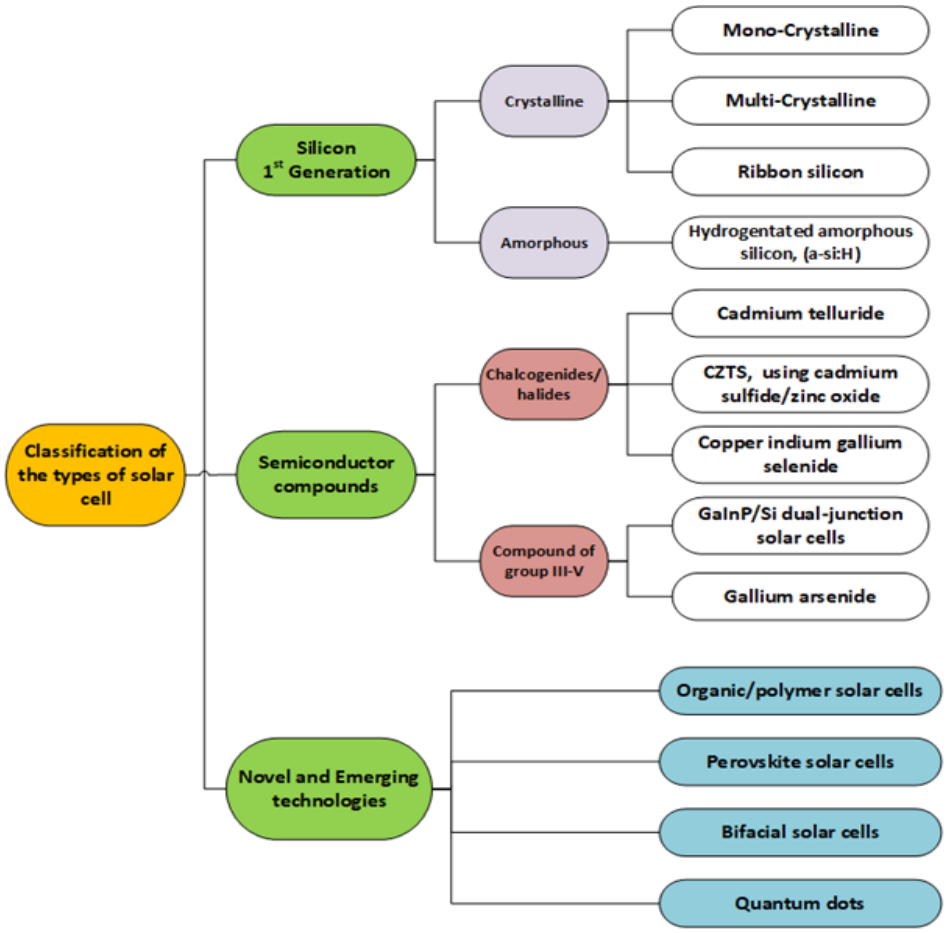

Fig 2.1. Classification of the type of solar cell.

Energy Gap or “bandgap” (Eg), is defined as the minimum threshold energy with energies below the bandgap pass through the absorber, while photons with energies above the bandgap are absorbed as shown in Fig 2.2. Accordingly, to the photovoltaics mechanism, the solar photon absorbs only above the threshold energy (minimum energy). In semiconductor materials, electrons (e^-) have energies that fall within certain energy ranges, termed as the bands. The valence band is defined as the band containing electrons with the highest energies. Similarly, the next band of possible electron energies is defined as the conduction band. The lowest electron energy in the conduction band is separated from the highest energy in the valence band by the Energy Gap (bandgap). In dark condition, all the electrons are in their lowest energy

state. When the solar photons are absorbed by the semiconductor material, photons transfer their energy to electrons in the valence band and energized these electrons to higher energy states i.e. conduction band to occupy the vacancy.

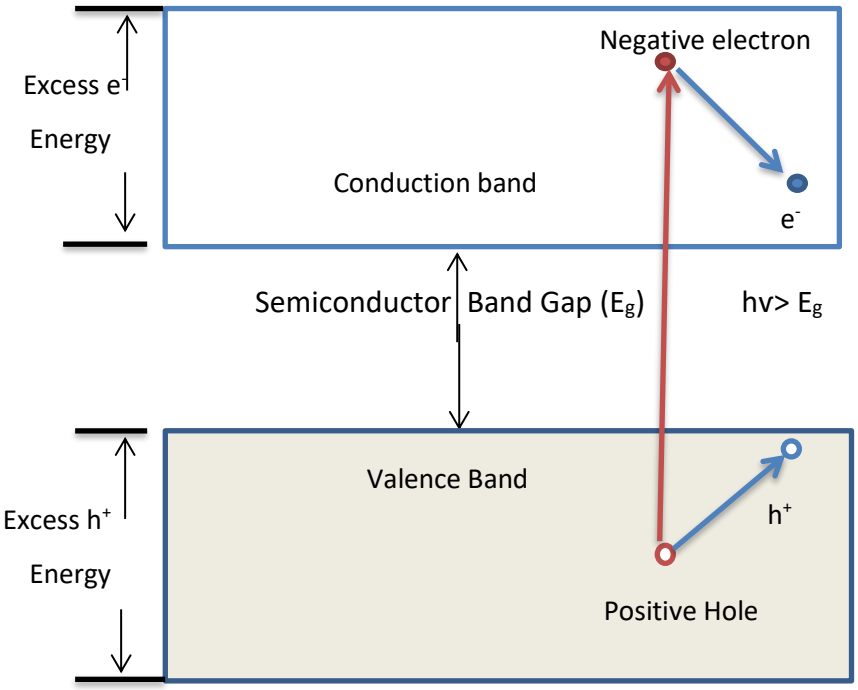

Fig 2.2. Working of the electron and proton in the energy gap

During the electron transfer mechanism, when the electron crosses the bandgap by the energy transfer from the photon, they generate negative charges in the conduction band and leave behind positive charges called holes (h+) in the valence band. Accordingly, absorbed photons in semiconductors create pairs of negative electrons and positive holes.

Due to the absorption of the light in the semiconductor, the negative (electrons) and positive (holes) charges are formed and move to opposite edges of the solar cell, where they are collected and pass through the wires connected to the cell to produce a current and a voltage thus generating electrical power.

2.2. High-Efficiency Solar Photovoltaics technology

To get better efficiency of the crystalline silicon solar cell (c-si), high-carrier-lifetime substrates are mostly needed in the blend with additional processing and advanced cell architecture, such as All Back Contact (ABC),

Emitter Wrap Through (EWT) and Laser Grooved Buried Contacts (LGBC) [15].

Notably, in crystalline silicon, there are three important concepts. Passivated Emitter Rear Cell (PERC), Inter-digitated Back Surface Cell (IBC), and Heterojunction with Intrinsic Thin layer (HIT) solar cells. The details about the three high-efficiency solar cell used for the study are as follows.

2.2.1 PERC: Passivated Emitter Rear Cell (PERC)

PERC is an abbreviation for Passivated Emitter and Rear Cell or Passivated Emitter and Rear Contact. It is a high-efficiency technology designed to attain better energy conversion efficiency by adding a dielectric passivation layer on the rear of the solar cell [16]. First developed in Australia in the 1980s by scientist Martin Green and his team at University of New South Wales. PERC cells attain better efficiency than conventional solar cells because of the following reasons.

a. The extra rear dielectric passivation layer reduces electron recombination: The back-surface (rear) passivation layer is introduced which reduces the electron recombination near the back surface, where the electrons would encounter a strong attraction force to the aluminium metallization layer. Accordingly, a greater number of electrons reach the front-surface emitter and the current density is increased inside the solar cell.

The electron recombination is the propensity of electrons to recombine, results into the hindrance in the free movement of electrons through the solar cell. This obstruction of free electron movement causes the lower efficiencies.

b. The extra dielectric passivation layer reflects wavelengths above 1180 nm out of the solar cell: The light through the solar cell without being absorbed into the back of the silicon gets reflected back from the back-surface passivation layer which enhances the ability of the solar cell to capture light in the second pass and generate more electrons, particularly for the longer

wavelength. Thus, the absorbing length of the solar cell is effectually doubled and the current density is additionally improved.

c. Maintaining the temperature of the solar cell: The reduced heating of the back-side metallization layer by reflecting out of the solar cell Infra-Red light is done by the passivation layer used in the PERC solar cell.

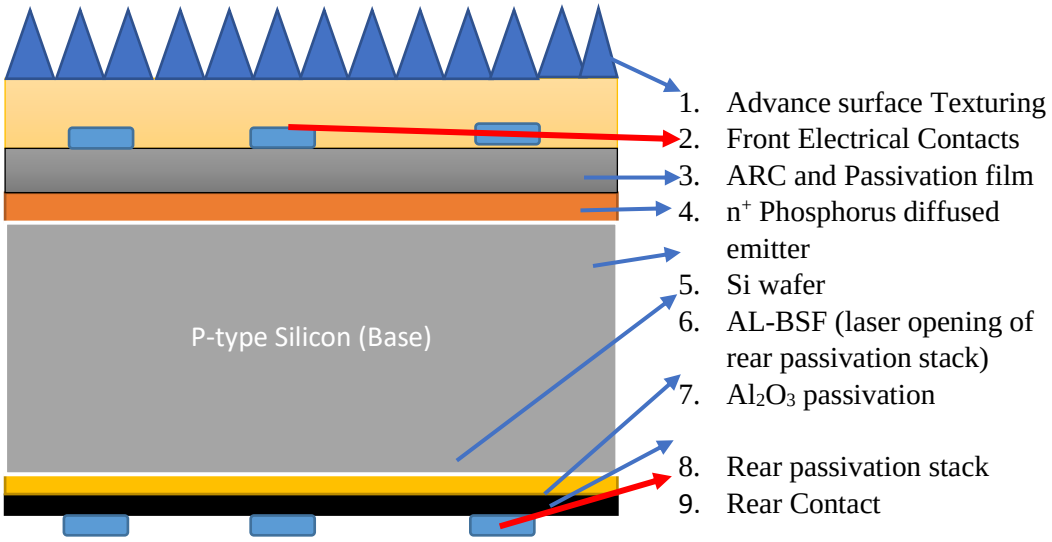

Fig 2.3. Solar cell construction diagram of PERC technology

PERC solar cell construction is shown in Fig 2.3. There is a slight advancement among the existing solar cell manufacturing and the PERC solar cell technology production lines, which motivates this solar technology more straightforward and cost-effective.

PERC solar modules having advantages of higher energy density, provide improved functioning under low irradiance and more tolerance against the high ambient temperatures. Therefore, manufacturer, installer and project coordinator can use less solar panels to accomplish the entire output or they can maximize energy output in less space.

2.2.2 IBC: Interdigitated Back Contact Solar cell

IBC stands for an Interdigitated Back Contact solar cell. It achieves higher efficiency by rearranging the front contact grids to the rear of the solar cell. The higher efficiency results from the reduced shading on the front of the

cell and is especially useful in high current cells such as concentrators or large areas. As of 2019, SunPower and LG are the only two manufacturers who produce solar panels with IBC N-type cells. IBC solar cell modules with an initial achievement of 22.1% of efficiency are introduced by SunPower and LG having an efficiency of 21.4%. The SunPower solar cell diagram is shown in Fig 2.4. The reasons of IBC cells performance better than the conventional solar cell are listed as below.

a. This solar cell has various localized junctions on the solar cell in place of a single large p-n junction. It helps to present the contact recombination loss. The incident solar light creates electron-hole pairs over the surface of the solar cell which is absorbed in the front surface, can still be accumulated at the back of the cell.

b. To avoid and reduce the recombination in the defect-rich interface, the semiconductor-metal interfaces are kept significantly small. This small cross-section of metal fingers also diminishes the resistive losses of the contacts. Two metal grids are present on the back of the IBC solar cell. In which one uses to collects the current from the p-type contact and the other use to collects the current from the n-type contact.

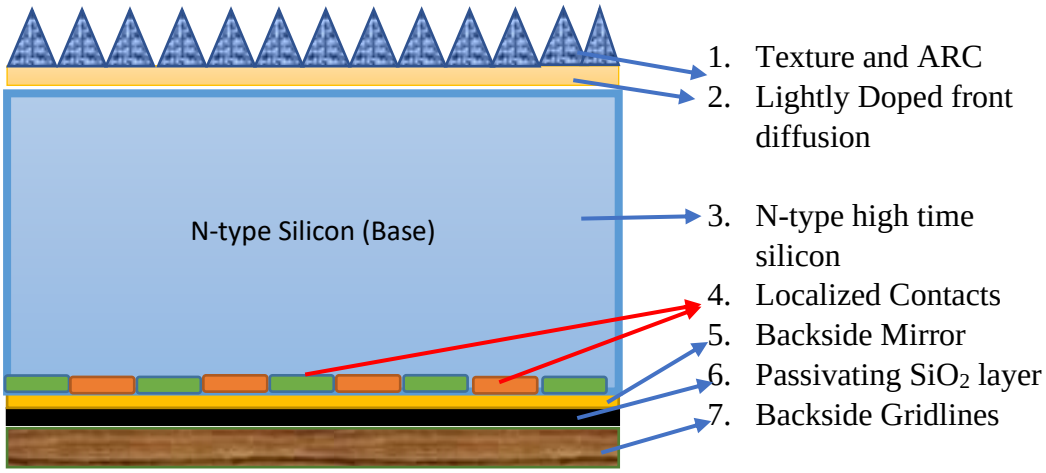

Fig 2.4. The solar cell construction of SunPower solar cell

c. The front surface acts as a passivation (silicon dioxide (SiO_2)) and formed by heavily n-doped in order to reduce the surface recombination. The

back-surface doping intensity reduces firmly to act as a p-doped region. Finally, it behaves like a p-n junction.

IBC silicon cells explained in detail above are not only more efficient but also much stronger than conventional cells as the rear layers reinforce the whole cell and help prevent micro-cracking which can eventually lead to failure.

2.2.3 Hetero-junction. HIT-Hetero junction intrinsic layer

The IBC and PERC technologies are containing the homo-junction solar cells, or a p-n junction containing depletion zone. In Hetero-junction solar cells, the junction is made from two dissimilar semiconductor materials. Hetero-structure with an intrinsic thin film (HIT) solar cell is an example of the heterojunction solar cell as this cell contain a mono thin crystalline silicon wafer surrounded by ultra-thin amorphous silicon layers and has achieved an efficiency of 24.7%. The solar cell construction of the HIT solar cell is shown in Fig 2.5. The advantage of the high-efficiency HIT structured solar cell is listed below;

a. There are two dissimilar junctions front and back in the solar cell. The front junction is constructed by a thin layer of intrinsic amorphous silicon with an accumulation of a thin layer of p-doped amorphous silicon lying on it. Correspondingly, the rear junction (i/n a-si) is composed of a thin layer of intrinsic amorphous with deposition of n-doped amorphous silicon on top.

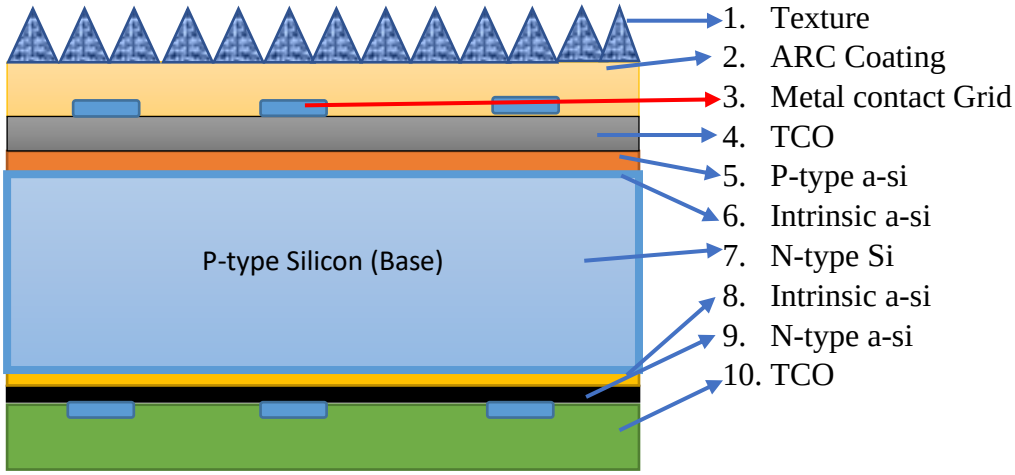

Fig 2.5. The solar cell construction of HIT solar cell

An intrinsic a-si layer can accomplish a surface passivation layer for the crystalline wafer. The p+/n+ doped a-si functions as an effective emitter/BSF for the cell. Compared to the traditional diffused c-si technology processing temperatures the a-si layers are created at a very lower temperature.

b. Compared to the c-si solar cell the HIT cell has a lower temperature coefficient which makes it suitable to use it in the high-temperature zone.

The Japanese company "Sanyo", which is currently a part of Panasonic introduced the concept of the crystalline silicon wafer-based hetero-junction solar cell. HIT permits to use in a bi-facial configuration (i.e. it can accumulate light from the front as well as scattered and diffuse light falling on the rear of the solar cell) due to the n-type backside contact scheme as seen in IBC. These technologies are having the advantage of high-efficiency in the same module area for the installation in the outdoor field.

2.3 Performance characterization of photovoltaic modules

This International Standard series sets down IEC requirements for the design qualification and type approval of terrestrial flat plate module materials such as crystalline silicon module types as well as thin-film PV module.

2.3.1 IEC Standard 61215-2: 2016

The datasheet of the SPV modules provides the parameters tested as per IEC standard as per IEC 61215-2: 2016 [17]. The block diagram of the IEC 61215-2: 2016 is presented in Fig 2.6. The purpose is to determine the thermal and electrical characteristics as well as the capability of withstanding prolonged exposure in outdoor conditions. The genuine lifetime expectation of PV modules will depend on their electrical design, climatic factor and the undefined circumstances under which they are functioning.

The SPV module is tested at Standard Test Condition (STC), i.e. 1000 W/m^2 irradiance, 25 °C cell temperature and Air Mass 1.5, and at Nominal Module Operating Temperature (NMOT), i.e. 800 W/m^2 irradiance, 20°C ambient temperature and Wind Speed 1.0 m/s, along with the IEC 60904-3 reference solar spectral irradiance distribution for both conditions.

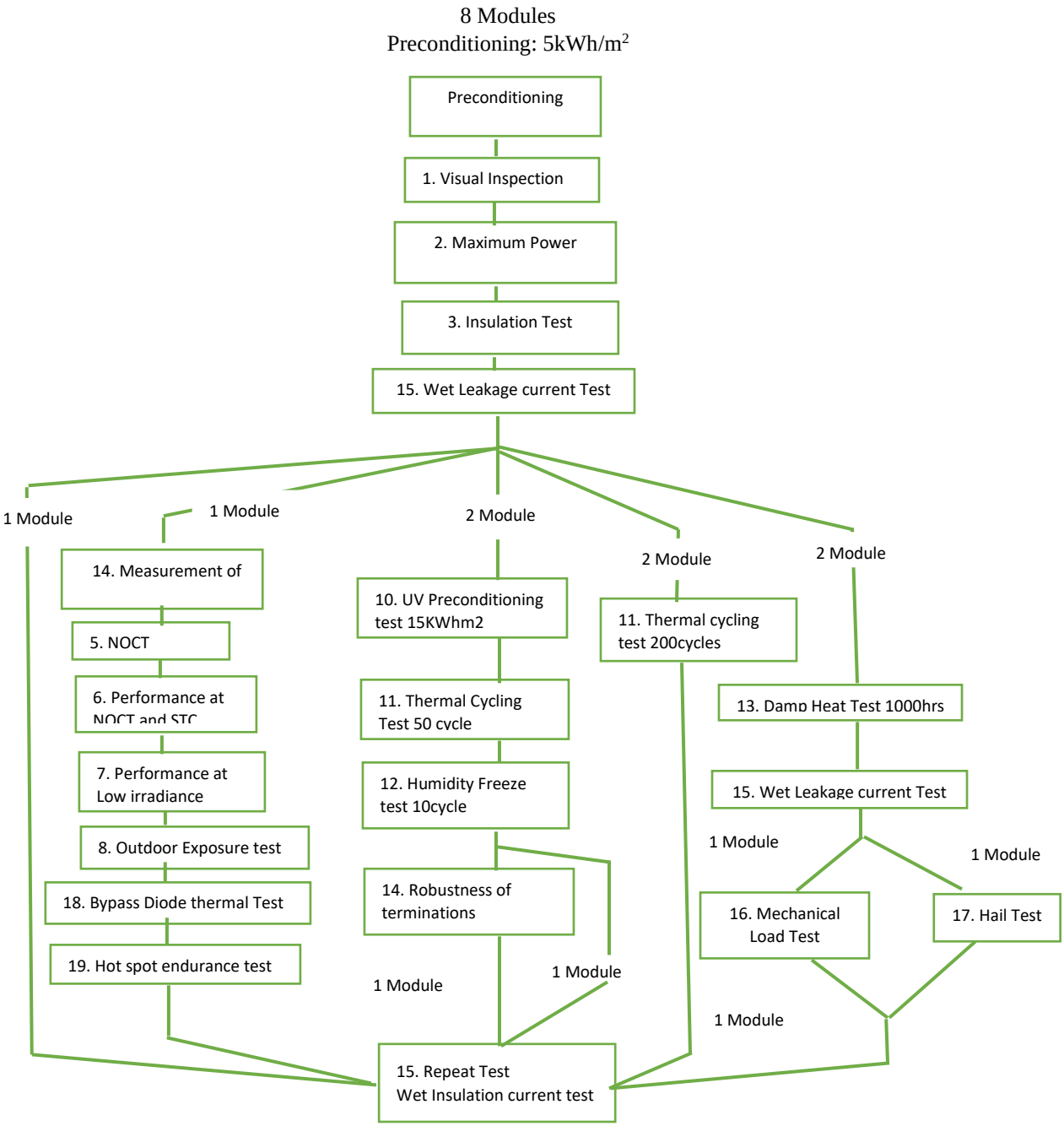

Fig 2.6. Block diagram of the standard IEC 61215-2.2016 [17].

Analysing the performance and characterization of SPV modules is extreme significance, as it enables in evolving acceptable qualification standards. Table 2.1 shows the name of the tests along with the objective and the name of the equipment used for the testing done in the IEC 61215-2.2016.

Table 2.1. The name of the test along with the objectives and equipment in IEC 61215-2: 2016.

S.no	Name of Test	Objective	Equipment
1	Visual Inspection	To detect any visual defects in the PV module.	A microscope, an illumination of 1000 lux.
2	STC Measurement	Performance of the module with load at Standard Test Conditions.	A solar simulator (The Quick Sun 700A Sun Simulator).
3	Insulation Test	To determine whether the module is sufficiently well insulated between current-carrying parts and the frame or the outside world.	High Voltage Insulation Tester.
4	Wet Leakage Current Test	To evaluate the insulation of the module under wet operating conditions and verify that corrosion due to moisture ingress.	water container for wetting the module, High Voltage Insulation Tester.
5	Measurement of Temperature Coefficients	To determine the temperature coefficients of current (α), voltage(β), and peak power (δ)	Using the environmental chamber and sun simulator.
6	NOCT Measurement	The equilibrium mean solar cell junction temperature within an open-rack mounted module in the following standard reference environment (SRE).	Tilt angle. 45 degree, 800 Wm-2, Tamb 20 °C, Wind speed. 1 ms-1, Electrical load. Nil (open circuit).
7	Performance at STC and NOCT	How the performance of the module varies with load at NOCT (800 Wm^{-2}, with the IEC 60904-3 reference solar spectral irradiance distribution).	Using the environmental chamber and sun simulators.
8	Performance at Low Irradiance	To determine how the electrical performance of the module varies with load at 25^0C and an irradiance of 200 Wm^{-2} in accordance with IEC 60904-1.	using the available sun simulator by setting the intensity at 200Wm^{-2}.
9	Out Door Exposure Test	To reveal any synergistic degradation effects which may not be detected by laboratory tests.	Exposure. 60 kWh/m^2, Outdoor test bed & Structure
10	Bypass Diode Thermal Test	To assess the adequacy of the thermal design and relative long –term reliability of the by-pass diodes.	An environmental chamber to a temp of 75 0C ± 50 0C, Temp probe for measuring and recording accuracy of ±10 °C, Power supply for applying a current equal to 1.25 times the STC short-circuit current of the module under test throughout testing.
11	Hot-Spot Endurance Test	To determine the ability of the module to withstand hot-spot heating effects,	Opaque screens for shadowing and sun simulator.IR Camera. The sharp thermal resolution, Temperature range up to 1200 °C.
12	UV Preconditioning Test	To precondition the module with ultra-violet (UV) radiation before the thermal cycle/humidity freeze tests to identify those materials and adhesive bonds that are susceptible to UV degradation.	UV exposure system to control the temperature of the module while it is irradiated by UV light (280-385 nm, at 60 °C ± 5 °C).

13	Thermal Cycling Test	To determine the ability of the module to withstand thermal stress caused by cyclic changes of temperature.	Environmental chambers with automatic temperature control, Power supply for applying a current equal to the STC peak power current.
14	Humidity Freeze Test	To evaluate the ability of the module to withstand the impact of high temperature and humidity.	Environmental chambers with automatic temperature control and humidity.
15	Damp Heat Test	To determine the ability of the module to withstand the effects of long-term penetration of humidity.	Environmental chamber with humidity and temperature control.
16	Robustness of Terminations Test	To evaluate that the module will withstand such stresses like the terminations and attachment of the terminations to the body.	A set of weights along with the hanging arrangement.
17	Mechanical Load Test	The purpose of this test is to determine the ability of the module to withstand wind, snow, static or ice loads.	Mechanical load tester, Instrumentation to monitor the electrical continuity, applied 2400 Pa uniform load for 1 h to front and back.
18	Hail Impact test	The objective of this test is to ascertain the mechanical integrity of the PV module during hail impact.	Test conditions. — Circular Ice balls of 25mm diameter are bombarded with a velocity of 23 m/sec.

These tests have been carried out at laboratories using environmental chamber and specified devices. For each test, the temperature, humidity and irradiance profile are introduced via software during the tests.

2.3.2 Solar PV module characterization and diagnostic methodology

To increase the global production of the PV generation, creating a commercially feasible and long-term reliable product are utmost important [18], [19]. The performance parameter has been summarized in Table 2.2 for different locations and climatic zones.

Table 2.2. Performance metrics over SPV devices for performance monitoring.

S.no	Plant size and location	Parameters	Results	Reference
1	Mono, multi and a-si solar module technologies at Sudano-Sahelian climate, hot	PR	The a-si SPV modules performance is better with an average performance ratio of 92%. Due to the	[20]

	climate regions like West Africa		relatively low-temperature coefficients.	
2	10 SPV monocrystalline and p-si generators in Spain	Numerical integration of the Oster Wald's model.	The validation exhibits good correlations at higher irradiation greater than 800 W/m^2.	[21]
3	CIS, HIT, a-si, mono-si, and mc-si installed in the city of Saida in Algeria has a Mediterranean climate.	PR	The HIT and a-si perform better than other technology.	[22]
4	Four identical mono-c-Si PV systems with different back sheet materials at Warm climatic conditions of Cyprus.	Electrical and thermal performance over a period of five years	Energy performance improvements can be achieved by improving the heat dissipation of the modules using innovative packaging materials.	[23]
5	c-si, CdTe & mc-si technologies in a humid continental climate of Prague.	Effective peak power (PM*) technique. DC output power, and PR.	The highest degradation rate has been observed for CdTe SPV which is −5.55%/year.	[24]
6	Four crystalline silicon SPV modules at Ispra, in the North of Italy having a moderate subtropical climate zone for a period of 20 years of outdoor exposure.	Infra-Red (IR), under forwarding bias and under the illuminated condition, and electroluminescence (EL).	The annual degradation rate was −0.24% for the module on the bonnet and between −0.84 to −2.75% for the other SPV modules.	[25]
7	Poly-Si, a-si and CdTe SPV modules studied at Madrid, Spain.	Air mass, Seasonal variation of yields and losses, the Seasonal spectral effect on different technologies and thermal effects.	The PR are 81.89% (poly-Si), 81.01% (a-si) and 81.01% (CdTe), whereas the inverter conversion efficiencies were 89.92% (poly-Si), 89.63% (a-si) and 89.73% (CdTe).	[26]
8	One-year results of mc-si, p-si and a-si SPV modules at Düzce Province, in Turkey having a hot-summer Mediterranean climate.	Efficiency, PR, and CUF	PR were found out as 73%, 81% and 91% for a-si, polycrystalline and monocrystalline PV panels, respectively. Panel efficiency was calculated at	[27]

			4.79%, 11.36% and 13.26% in the same order.	
9	A 20 kW SPV system at Bangalore.	CUF, PR and Seasonal analysis.	The CUF of 16.5% for the SPV system. Average PR is around 85%.	[28]
10	Mono-crystalline silicon at the composite climate of India.	The Voc, Isc, Pmax, Imp, Vmp and the fill factor, as a function of time of field exposure, Visible defects.	The qualification standard (s) needs to be reviewed and revised under actual field conditions in India.	[29]

Evaluating emerging SPV module technology, according to the other climatic conditions and selecting the most efficient module has been the major objective in the current scenario for efficient utilization of the technology [30], [31]. [32] presented that solar spectrum is an important parameter which impacts the for a-si cells, both single-junction and double-junction devices. The solar spectrum is a very crucial parameter for accurate system performance modelling. Alonsa and Abella studied the impact of the solar spectrum distribution over energy yield for eight different SPV solar cell on a monthly and yearly period [33]. [34] presented field exposed performance monitoring of m-si photovoltaic array at Athens. Under similar outdoor operating conditions, the efficiency has been found to be about 18% lower than that under laboratory STC. [25] has been performed a comparison of electroluminescence (EL) and Infrared (IR) images over a 20 years field aged module of c-si SPV technologies. The comparison provides the state of PV modules, the moisture ingress, broken fingers in the most damaged solar cell. [35] has been used the temperature corrected performance ratio and the effective peak power of the PV modules to calculate the degradation of m-si, c-Si and HiT technologies over a period of three years in the Saharan environment. It has been found that the highest degradation rate, ranging from 1.53%/year to 1.92%/year for the HiT technologies. Kichou et al have been studied the behaviour of CdTe, c-Si and m-si technologies installed in a humid continental climate for two years. It has been found out that c-Si and m-si SPV modules exhibited seasonal changes having a slight performance degradation. The CdTe SPV modules show the

poorest degradation rate of −5.55%/year [24]. [36] presented a single-diode model-based improved procedure for more accurate modelling and energy yield prediction of photovoltaic modules. The SPV model has been validated using real data collected by the SCADA system of a 12-MW SPV farm. [23] has been done the performance analysis of alike m-si modules with dissimilar backsheet materials. The modules were installed in the warm climatic conditions of Cyprus to form grid-connected systems. It has been found out that in spite of the use of black buckets, temperature enhancements were achieved verifying that the backsheet effect the cell temperature and improve performance by functioning at a lower temperature. Fairbrother et al presented the (polyethylene naphthalate (PEN)-based) back sheet degradation of SPV modules in Maryland (USA). It has been concluded that the modules with higher elevations and the modules near the edge have faced greater amounts of backsheet degradation [37]. In India, the solar radiation databases used for the annual energy yield predictions of 39 solar PV power plants located across the country national under the solar mission. The main aim of the study is to identify the losses during solar energy conversions [38].

The steady degradation of the SPV performance while installing at the real outdoor field conditions is defined as the incapability of the module to supply its rated power due to exposure to various climatic factors [18], [39]. The geographical locations having high solar insolation may accelerate the mechanism of the degradation in the solar devices, due to the higher ambient temperatures [40], [41], [42]. Hence it is necessary to estimate the effects of the different temperature and irradiation profile on the performance degradation of the solar panels [43], [44], [45], [46].

Hence, it is critically significant to examine the performance degradation of solar modules of different technologies in outdoor conditions at different climatic conditions [47]. To monitor the performance of the solar module and solar system, different performance matrices are taken into account. The aim is to examine and observe the solar system, diagnostics of the degradation and failure modes occurring into the system and finally mitigation of the faults. Due to these performance monitoring, there is an enhancement in

the lifetime of the system as well as lower the maintenance cost of the plant [48].

a. Performance Ratio: The SPV reference irradiance at Standard test condition is equal to the 1000 W/m^2. The performance ratio (PR) is determined as the ratio of the final yield of the system (Y_f) to the reference yield (Y_r). The PR is expressed as equation (1),

$$Performance\ Ratio\ (PR) = \frac{Final\ Yield\ (Y_f)}{Reference\ Yield\ (Y_r)} = \frac{1000}{Total\ in-plane\ Irradiance} \cdot \frac{Final\ Energy\ Output}{Maximum\ Power,_{STC}} \quad (1)$$

The PR delivers the yield of the system in real operating conditions regarding the yield at STC normalized input irradiance. To compare the performance of two distinct SPV systems, the PR can be normalized using the thermal factor (T_F) and spectrum using spectrum factor (S_F) to standard test condition, termed as a Normalized Performance ratio (PR_{NOR}). The expression of the thermal factor is presented below in equation (2);

$$T_F = \frac{1}{1+\gamma_p(T_M - T_{STC})} \quad (2)$$

Where T_F is a thermal factor, T_M is module temperature, T_{STC} is standard test condition temperature and γ_p is the temperature coefficient of power at the maximum power point of SPV the module.

The influence of spectral parameter over the SPV technologies is due to the bandgap of the solar cell material which regulates a threshold photon energy that can generate free carriers. The absorption of carrier generation by photon varies as a function of their wavelength of the material. The constraints used for the spectrum factor has been counted on using SMART software (The Simple Model of the Atmospheric Radiative Transfer of Sunshine) [49]. The mathematical expression for the spectrum factor is as follows equation (3);

$$S_F = \frac{\int \zeta STC(\lambda)_{.} SR(\lambda) / \int \zeta(\lambda)_{.} SR(\lambda) d\lambda}{\int \zeta STC(\lambda)_{.} d\lambda / \zeta(\lambda) d\lambda} \quad (3)$$

where S_F is spectrum factor, ζSTC is standard spectrum at STC, ζ is the solar spectrum of the location, SR is the relative spectral response of the SPV technology, and λ is the wavelength (nm). The effect of the spectral variation on devices performance with a narrow spectral response such as a-si technology is much evidence in the literature. The normalized PR of SPV technology can be determined by equation (4);

$$PR_{NOR} = PR \times T_F \times S_F \quad (4)$$

The normalized performance ratio of each module for the different year is presented in the contour Fig in which the normalized performance ratio is plotted against the module temperature ($^{\circ}$C) and in-plane irradiance (W/m^2).

b. Normalized Efficiency

The normalized efficiency of the DC side of the SPV system is described as the ratio of the normalized power to the input irradiance for a particular time instant. The normalized power is obtained by the product of output power to the thermal factor. The normalized efficiency is given by equation (5) & (6);

$$\eta_{DC} = \frac{P_{DC}}{A \, X \, G_T} \quad (5)$$

$$P_{NOR} = \frac{G_{STC} \times P_{DC}}{G_T} \times T_F \quad (6)$$

where η_{DC} is the efficiency of the DC side of the system, A is the area of the SPV modules, P_{DC} is the overall power of the SPV modules, G_{STC} is irradiance at STC, T_F is the thermal factor, P_{NOR} is the normalized power and the G_T is the solar irradiance.

2.4 Degradation analysis of the SPV devices

Degradation of any component of the solar power plant is one of the reasons for performance loss over a period of time [105–107]. Analysing the degradation of SPV modules is also of extreme significance, as it enables in evolving acceptable qualification standards [53], [54]. It is essential to characterize and analyse the type of degradation for the field aged PV modules

along with deformation in emerging solar modules. The impact of electrical and environmental parameters over the PV modules are documented in Table 2.3.

Table 2.3. Impact of electrical and environmental parameters over the PV modules.

Parameters	Degradation on PV Modules and consequences
Sun (UV+IR+VS) + Irradiation	• Discolouration (yellowing), reduced power output • moisture ingress, • Degradation of cell material which reduced the power output.
Temperature	• Impact on different thermal expansion coefficients • Opening of soldering joints due to unequal thermal expansion, • Degradation of electrical parameters with temperature, hotspot and burn mark on the cell [55].
Voltage	• Potential Induced Degradation of the electrical parameters of modules • The major component of loss is the FF loss due to creation of shunts in solar cells. • Degradation is nonuniform across the module and is seen to be more severe near the frame. Degradation is accelerated by voltage, temperature, humidity and dust [56].
Current	• Corrosion/ageing of cell and interconnects inside the modules
Light-Induced Degradation	• Impact on the performance of the high-efficiency modules. • Results in lower minority carrier lifetime • Can be brought back to near original state through regeneration
Wind	• Various kinds of mechanical fatigue • The vibration that damages the underlying structure
Soiling	• Reduces the short circuit current of the modules • Shading effect which may lead to the formation of hotspots.
Humidity	• Moisture ingress.

These characterization methods support to find out defects in design and engineering, identify complications with the system installation in that location and climate conditions. This helps to considerate the failure modes and why they happen; with the goal that we can develop module reliability tests for identifying and anticipating them. The procedure of identifying these module failures and degradation, requires various characterization, performance metrics and degradation analysis. The general methods are (a) visual inspection, (b) Infra-Red (IR) imaging (c) Current-Voltage (I-V) characterization.

2.4.1 Visual inspection

The visual inspection is the most efficient and quickest technique to observe defects in the solar module [18], [57], [58]. It is most appropriate for recognize the features causing optical losses, physical breakage, defects causing a change in the solar cell colour or visible defects as well as the decolouration of the optical layer over the solar cell [59], [10].

Still, this approach is inadequate in identifying degradation or failures causes a change in electrical parameters, unless these leave a visual print over the modules, such as snail-trail, moisture ingress, burn marks or corrosion [60], [61]. The examples of the visible inspections of the solar modules in the outdoor field are presented in Fig 2.7. The Fig 2.7 shows the visual defects such as (a) Haziness in glass (b) Corrosion in cell interconnects and string interconnects (c) Hot-spot (d) Metallization discolouration (e) Encapsulant discolouration (yellowing or browning) and (f) Backsheet cracking/tearing degradation. The front glass provides protection to the solar cells from the outside environment while allowing light to pass unhindered to the solar cells underneath. However, improper handling and cleaning have been found to cause haziness in the glass, brown and white spots (paint marks), scratches, and even complete shattering (often caused by the impact of hard objects falling on the glass) as shown Fig 2.7 (a). Metallization on top of the solar cells (fingers and busbars), and the interconnect ribbons conduct the current generated in the PV module to the terminal box at the backside of the module.

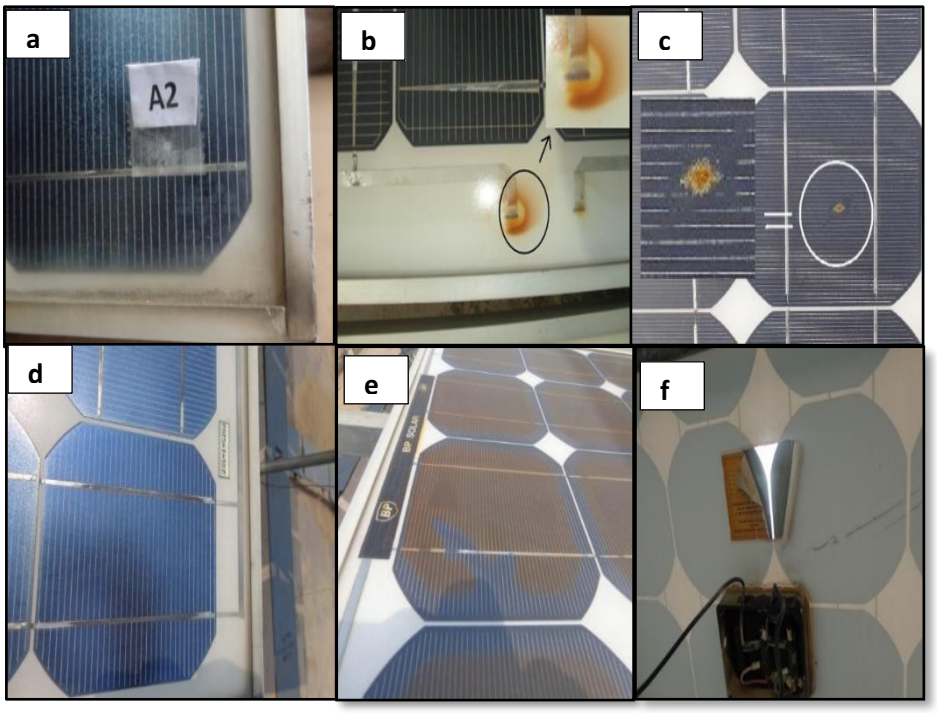

Fig 2.7. Visible inspections of the solar modules in the outdoor field

Discolouration of the metallization can occur due to corrosion and also sometimes due to improper manufacturing practices (like deposition of solder flux leading to brown discolouration on the cell interconnect ribbon). Examples are shown in Fig 2.7 (b). Hot-spot heating occurs when there is one low current solar cell in a string of at least several high short-circuit current solar cells and on a long time becomes brown pinhole structure as shown in Fig 2.7 (c). Metallization discolouration is mainly due to corrosion in the old modules, and hence it can be expected that as the discolouration increases over the years, there would be an increase in series resistance, which would degrade the fill factor as shown in Fig 2.7 (d). Discolouration of the encapsulant is one of the major reasons behind the reduction in short-circuit current (Isc) and consequently power output (Pmax) of field-aged PV modules as shown in Fig 2.7 (e). The backsheet is the outermost protective layer of the module, which serves to provide electrical insulation and prevent the ingress of moisture into the module. However, the backsheet can easily get scratched due to improper handling, can get burnt due to hot spots in the modules, can lose adhesion (causing bubbles

and delamination) due to moisture ingress, and also degrade thermally leading to chalking. Some of these effects are shown in Fig 2.7 (f).

2.4.2 Infra-Red imaging

Infra-Red (IR) imaging methodology recognizing the electrical failures and degradation caused by the increased heat (thermal stress) inside the PV modules, cables, and connectors [13], [62], [63]. It is also a non-destructive process for detection of defects in PV Modules. The example of the Hot-Spot of PV modules is shown in Fig 2.8.

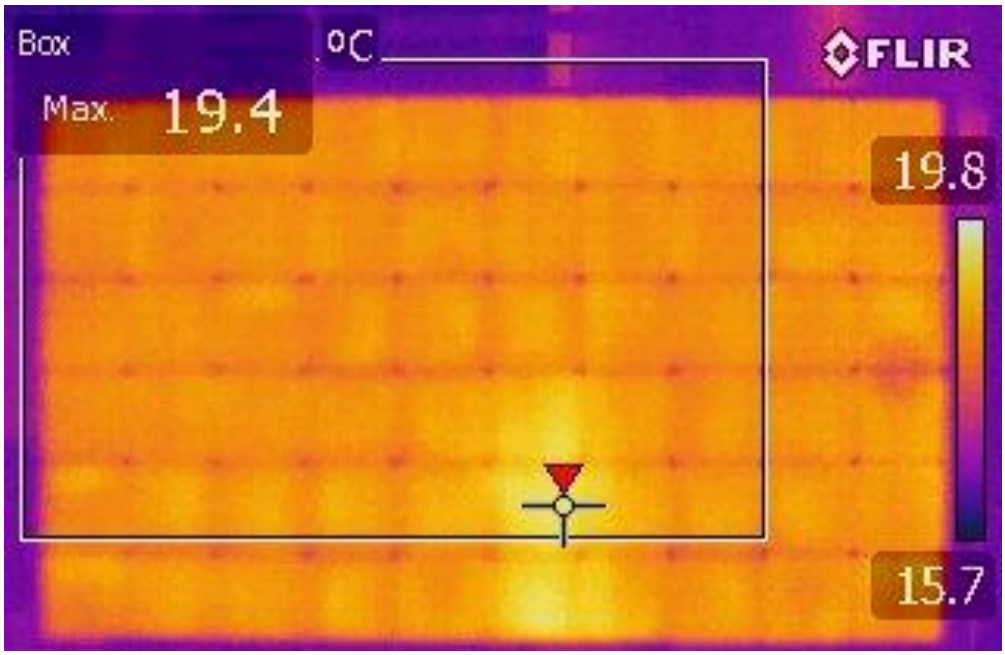

Fig 2.8. Example of the Infra-Red images of typical solar modules along with indicators.

All materials, which are above 0 degrees Kelvin (-273 degrees C), emit Infra-Red energy in the surroundings [64], [65]. If some cells of the solar modules are hotter than the other cells, the hot areas will show up clearly in the thermal image taken by the thermal sensors [66].

Depending on the size and location, these hot spots and areas can help to recognized several different faults in the solar modules or in solar cells. If an entire module is hotter than usual that might indicate a problem such as interconnection problems. If single cells or sequences of cells are showing up

as a hot spot or a warmer ‘patchwork pattern’, that can be recognized as defective bypass diodes, in internal short-circuits, or in a cell mismatch [67], [68]. Thermal images obtained under load, no-load, and short-circuit conditions. This is the important performance indicator in the study of the reliability of the high-efficiency solar module should be compared in the outdoor or in the stimulated condition for the testing [69]. For details knowledge of the failure, the electrical and visual study on the module is necessary which is conducted at NISE

2.4.3 Current-Voltage (I-V) characterization curve

to recognize the electrical and optical properties of the solar modules Current-Voltage characterization is used [70], [71], [72], [73]. PV module I-V measurement system consists of a natural or artificial simulated light source, a test bench to illuminate the solar module under test, temperature control, facility for monitoring, and a data acquisition system to measure the current-voltage curve when the voltage across the module or current through the module is varied with an external electronic load or power supply [74], [75], [76]. Other parameters are evaluated based on the obtained parameters. I-V characteristics curve of the solar cells is given in Fig 2.9.

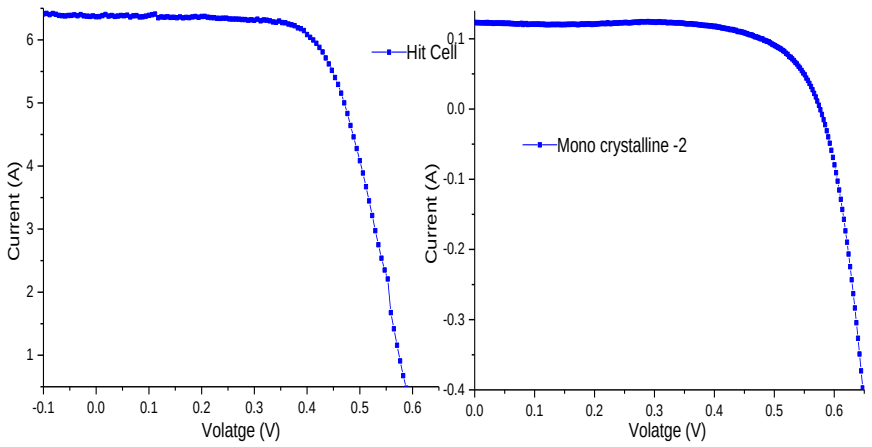

Fig 2.9. I-V characteristics curve of the HIT and Monocrystalline solar cell

The determination of the open-circuit voltage (Voc), short-circuit current (Isc), Maximum Voltage (Vm), Maximum current (Im) and Maximum power

(Pmax) has been done from the I-V characteristics curve. The series resistance (Rs) and shunt resistance (Rsh) can be estimated using the slopes near Voc and slope near Isc in the I-V characteristics curve respectively [15], [77], [78]. The open-circuit voltage (Voc) is the maximum voltage available from a PV module when the current across the solar cell is zero. The short-circuit current (Isc) is the current through the PV module when the voltage across the cell is zero. The maximum power (Pmax) is defined as a point on the I-V curve of a PV module under illumination, the product of maximum current (Im) and maximum voltage (Vm). The fill factor (FF) is essentially a measure of the quality of the solar cell or PV module.

Using the single diode and double diode model with five or seven parameters on the light or dark I-V measurements can be used to investigate the extent of degradation [79–81]. This procedure of the analysis of single and double diode model has been carried out over the three silicon-based technology modules in Publication I for examining the characteristics of different silicon-based technology modules [82].

2.4.4 Statistical tools to estimate the degradation rate

The degradation rate of the SPV technologies may be investigated using three commonly used statistically trend extraction methods. Linear Regression (LR), Classical Seasonal Decomposition (CSD) and Locally weighted scatterplot smoothing (LOESS) [83], [84]. Linear regression is the most commonly used methods for trend extraction and can be expressed as equation (7).

$$y = \beta_o + \beta_1 x \qquad (7)$$

Where x is independent variable also termed as a predictor, y is the dependent variable also termed as the response variable and β_o is the intercept of the line.

The degradation rate can be calculated using the intercept and slope of the linear curve over the long-term performance parameter time-series data [24]. Thereby the annual degradation rate (D_ψ) is calculated linearly with time T (years) expressed as [85] equation (8);

$$DR = 100 \times \frac{12\beta_1}{\beta_o} \quad (8)$$

The degradation rate can also be calculated using the classical seasonal decomposition over the time series for each SPV technology by extracting the trend and seasonality parameters. The CSD used to the decomposition procedure to extract the trend, seasonality and the residual factor of nine modules. The trend has been calculated by applying a 12-month centered moving average (CMA) to the PR time series. The k is the seasonal period, which is 12 as the number of months in a year has been considered. The expression for calculating the trend is as follows equation (9);

$$T_t = \frac{1}{2}\left(\frac{1}{k}\sum_{i=t-m}^{t+m-1} Y_i + \frac{1}{k}\sum_{i=t-m+1}^{t+m} Y_i\right) \quad (9)$$

where Tt is the trend at time t, (t>m), and m is defined as the half-width of a moving average, m=$\frac{k}{2}$. After the calculation of the trend, linear regression is applied to calculate the degradation rate. The seasonal indices, Si has been calculated by taking the average of the de-trended series for each month of the year [83] as equation (10);

$$S_i = Y_i - T_t \quad (10)$$

where seasonal indices Si, Y_i is the original data and T_t is a trend at time t. The residual component is the most significant component in the seasonal decomposition as it indicates the adequacy of the fitted model. The annual degradation rates have been obtained by applying the linear least-square fit of the calculated trend data of the time series. The gradient of the line represents the monthly degradation loss which can be multiplied by months in a year i.e. 12, to obtain the final degradation rate.

LOESS methodology has been also used to analyse the degradation rate of the SPV modules. In this method, the slope of the linear fit of each technology

is the indication of the degree of degradation. The annual degradation (Dψ) has been used as under [86] as represented in equation (11-13).

$$D_{\psi} = \frac{\delta PR}{\delta t} \times 365 \quad (11)$$

$$\delta PR = \frac{PR_{final} - PR_{initial}}{PR_{initial}} \quad (12)$$

$$PR\,(t) = PR_{initial}(1 - D_{\psi} \times t) \quad (13)$$

where t is in years and the annual degradation, δt is the number of days in the evaluation period, δPR is the relative difference, $PR_{initial}$ is the initial PR value in the calculation period and PR_{final} is the final PR value in the calculation. The typical methods used in the degradation analysis have been summarized in Table 2.4.

Table 2.4. Typical methods and metrics used in degradation rate analyses.

S. no	Statistical Methods	Advantage	Limitations	Reference
1	Linear Regression (LR)	Simplicity; less time consuming	Sensitive to outliers and seasonal variations; uncertainty increases by missing data.	[87]
2	Classical Seasonal Decomposition (CSD)	Reduce the uncertainty in the degradation rate by removing noise and seasonal effects.	The trend would not be available for the starting and the last 6 months.	[83]
3	Locally Weighted Scatterplot Smoothing (LOESS)	Used for forecasting as well as for understanding the time series.	A number of factors are more.	[83], [84]

Based on the above three methods the degradation rate has been calculated for nine SPV modules and comparison has been made.

2.5 Series resistance estimation of the photovoltaic solar modules

An accurate estimate of power output based on the electrical behaviour, including series and shunt resistance as well as the environmental conditions, are required for optimum designing [88], [89]. Accruing a precise model parameter of the PV system is very critical for the performance monitoring, control management, efficiency estimations and maximum power point tracking [90], [91]. The precise measurement of series resistance is essential for performance monitoring and the reliability assessment of the PV technology deployed in the outdoor field [92], [93].

In 1960, Swanson proposed the graphical method to estimate the series resistance of a solar cell using the current-voltage (I-V) characteristic of the solar cell at two different illuminations which were firstly utilized by Wolf and Rauschenbusch in 1963 [94]. Since then, several methods and models for the series resistance estimation have been reported in the literature such as single diode model, double diode model, single and double exponential diode model, Lambert-W function, Explicit model, etc. [95], [96], [97].

From methodology, these models can be broadly classified into three groups. The first group includes the models which are based on theoretical concepts and numerical analysis of the I–V curves including several techniques comprising regression, fitting based on genetic functions [98]. In the second group, the graphical analysis based on measured I–V characteristic curve in dark and varying irradiance are used [99]. The third group of uses a combination of the theoretical analysis of the I–V characteristic curves and one or two diode models for the estimation of the series resistance of solar cell [100], [101].

2.5.1 Estimation of the Series resistance using the theoretical concepts and numerical analysis of the I–V characteristic curves

The electrical circuit for the SPV module is presented using single or double diodes along with the parasitic resistance (series and shunt resistance), are recognized as a single diode model or double diode model. The total five and seven DC parameters of single and diode models respectively can be reduced to four and six parameters respectively by assuming the shunt resistance

to be infinite [102], [103]. The majorly used the four parameters and five parameters are explained in Table 2.5. The model expressed using four parameters i.e. Ipv, Io, η and Rs is termed as the four-parameter model. In the five parameters model, the shunt resistance has been added among the four parameters.

Table 2.5 The expression for four parameters and five parameters using the Single diode model.

S.no	Model expression	Advantage	limitations
1	Four-parameter model $I = I_{PV} - I_O \left[exp\left(\frac{q(V + R_s)}{\alpha kT}\right) - 1 \right]$	Simplicity, computational efficiency and derivation of the less parameter, less time-consuming	Less accuracy when subjected to temperature variation.
2	Five-parameter model $I = I_{PV} - I_O \left[exp\left(\frac{q(V + R_s)}{\alpha kT}\right) - 1 \right] - \frac{V + IR_s}{R_{sh}}$	precise parameter estimations, better accuracy	Accuracy deteriorates at low irradiance. Increase the complexity of the model.

The theoretical/analytical concepts of estimating the series resistance are further classified into the following three models, i.e., a single exponential model, the double exponential model and Lambert W-function.

a. Single exponential model. The single exponential model is based on the single diode model of SPV modules. The mathematical equation of the lumped electric model having a single diode and parasitic resistances is expressed by equation (14).

$$I = I_{ph} - I_o \times \left(e^{\frac{V+IR_S}{nV_t}} - 1 \right) - \frac{V+IR_s}{R_{sh}} \qquad (14)$$

The equation is comprised of a photo-generated current (Iph), a series resistance (Rs), reverse saturation current (Io), and a shunt resistance (Rsh), n

is the ideality factor of a diode, the thermal Voltage (V_t=kT/q), Boltzmann constant (k), the temperature of SPV module (T) and the electronic charges (q).

The single diode model is obtained by the Shockley diode equation in which ideality factor has been integrated for the diffusion. The equivalent (electrical) circuit-based models are used to simulate and estimate the solar cell parameters. The losses due to the contact resistance between the solar cell surface, the resistance in the current flow and the resistance of the electrode is incorporated using the Rs to the ideal single diode model. The equivalent circuit diagram of the single and double exponential models is presented in Fig 2.10.

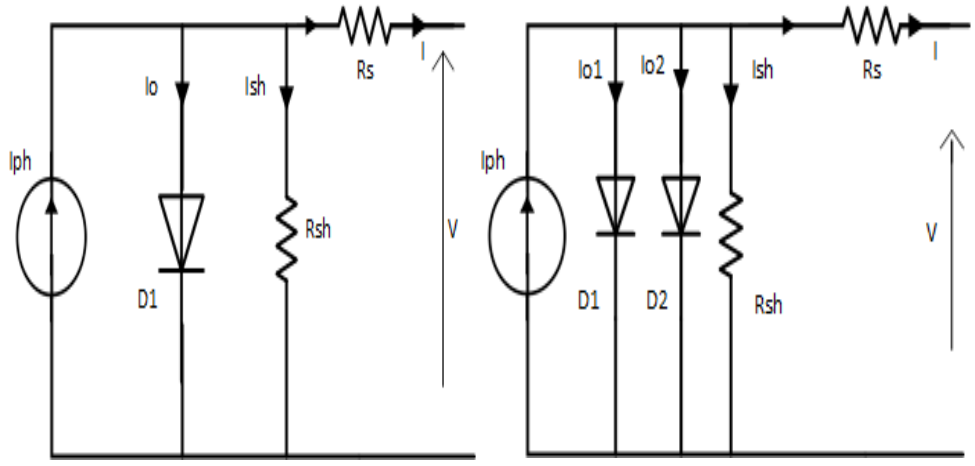

Fig 2.10. Equivalent circuit of the single and double exponential model with parasitic series and shunt resistance

The single diode model (one diode model) is majorly used method due to its simplicity and derivation of the less parameter, less time-consuming. Picciano, 1969 developed a method which estimates series resistance using the I-V characteristics curves [104]. Charles et al.,1981 assumed the classical one-diode equivalent circuit valid for given light intensity to determine Rs and Rsh from the experimental data of the fourth-quadrant characteristic using a programmable calculator [105]. Chan et al., 1986 have carried out a comparative study of three methods for determining solar cell parameters including Rs from the single diode model, i.e., iterative 5-point method, curve-fitting method, and analytical 5-point method, out of which the analytical 5-

point method gives more accurate and reliable results [106]. Jia et al., 1988 introduced a method for evaluating the series resistance of SPV devices based on the single exponential lumped constant parameter model [107]. The above methods used the intensity as a parameter in various form for the determination of the series resistance. The expressions proposed for the estimation of series resistance using the single diode model are summarized in Table 2.6.

Table 2.6. The expression for estimating the series resistance using the Single diode model.

S.no	Expression	Advantage	Limitation	Reference
1	$Rs = Rso - \frac{1}{\frac{1}{Rsh} + BI_S A_1}$ $Rsh = \frac{1}{\frac{1}{(R_{Sho} - R_s) - BI_s A_2}}$ $R_{SO} = -\left(\frac{dV}{dI}\right) v = v_{oc}$ $R_{sho} = -\left(\frac{dV}{dI}\right) I = I_{sc}$ $B = \frac{q}{AkT}$ $A_1 = exp(BV_{OC})$ $A_2 = exp(BR_s I_{sc})$	Provide information at low intensities and temperatures where the impact of the shunt resistance increases and at high illumination and temperatures where the influence of series resistance increases.	Complex, a methodology using multiple parameters.	[106]
2	$Rs = R_L \times \left(\frac{V_{oc}}{V_L} - 1\right)$	The method has an advantage that the solar cell does not require heat sinking and problems arises due to varying temperature are avoided.	Due to considering R_{sh} infinite less accurate.	[108]
3	$R_s = R_{so} - \frac{\eta V_t}{I_s} exp\left(\frac{-V_{oc}}{\eta V_t}\right)$	Simple methodology.	The methodology does not provide the behaviour of the solar cell at low illumination.	[105]

4	$Rs = \frac{Vm}{Im} \cdot \frac{\frac{1}{Vt}(Isc - Im)\left[Voc + Vt.ln.\left(1 - \frac{Im}{Isc}\right)\right] - Im}{\frac{1}{Vt}(Isc - Im)\left[Voc + Vt.ln.\left(1 - \frac{Im}{Isc}\right)\right] + Im}$	The effects of light, temperature, and diode junction ideality on the series resistance are accounted.	Used various approximation and consider Rsh infinite.	[107]
5	$\Delta V = (R_s^{'} - R_s)I + \beta A.ln\left(\frac{I_o}{I_o'}\right)$ $\beta = \frac{kT}{q}$ A=correlation coefficient; derived from the curve.	Extract parameters from experimental f (I) characteristic;	Various parameters estimation is required.	[108]
6	$V = V_{oc} - IR_s + \frac{1}{\Lambda} ln\left\{\frac{I_{sc} - 1}{I_{sc}} + exp[\Lambda(I_{sc}R_s - V_{oc})]\right\}$ $\Lambda = \frac{I_m V_m}{I.V}$	All the parameters can be calculated from experimental data of a solar cell I-V Characteristics curve.	Depends upon the measurement of I-V characteristics curve	[109]
7	$R_s = \frac{1}{\lambda} \times \frac{1}{(I_2 - I_1)} ln\left[\frac{I_{ph} + I_o - I_2}{I_{ph} + I_o - I_1}\right] - \left(\frac{V_2 - V_1}{I_2 - I_1}\right)$	The dependency between series and shunt resistance and the fluctuation of the junction voltage with series resistance is justified.	Need to calculate various parameters.	[110]
8	$R_s = -\frac{1}{2}\left\{\left[(a-b)^2 + \frac{2q}{Isc}(a-b) + \left(\frac{Voc}{Isc}\right)^2\right]^{\frac{1}{2}} + (a+b) + \frac{Voc}{Isc}\right\}$ $a = \left(\frac{dI}{dV}\right)_{V=0}^{-1}$ $b = \left(\frac{dI}{dV}\right)_{I=0}^{-1}$ $q = Voc\frac{\gamma + 2}{\gamma} - \frac{2AkT}{e}$ $\gamma = exp\frac{eVoc}{AkT} - 1$	Determination series resistance is based on the analysis of its I-V the characteristic curve at fixed illumination.	Dependency on the I-V curve, complex parameters.	[111]

9	$R_S = \frac{nkT}{qI_f} ln\left\{\frac{I_r P - \left(V_r + V_f + I_f P\right)}{I_o P}\right\} - \frac{V_f}{I_f}$ $I_f = I_{ph} - I_o \times \left(e^{q\left(\frac{V_j}{nkT}\right)} - 1\right) - \frac{V_j}{R_{sh}}$ $I_r = I_{ph} + I_o + (V_r - I_r R_s)/R_{sh}$ $V_j = V_f + I_f R_s$ Vj is the Junction Voltage (V).	Series resistance is increased by enhancing the illumination and the junction voltage, but Rsh is independent of illumination impact.	Need various mathematical model to calculate different required parameters.	[112]
10	$R_s = \frac{\Delta V}{I_m} = \frac{V_{ideal} - V_{max}}{I_m}$	Graphical programming language LabVIEW is used.	Less accuracy.	[113]
11	$\left(\frac{dI}{dV}\right)_{I=0}^{V=Voc,ref}$ $= -\frac{\left(Io, \frac{ref}{\eta Tref}\right) e^{Voc \frac{ref}{\eta Tref}} + \frac{1}{R_{sh}}}{1 + R_s\left(\left(Io, \frac{ref}{\eta Tref}\right) e^{Voc \frac{ref}{\eta Tref}} + \frac{1}{R_{sh}}\right)} = -\frac{1}{R_{so}}$ $Rsh = Rsho$	The system was solved by a double process of trial and error for the parameters R and n. based on a mathematical algorithm.	Complex methodology.	[114]
12	$m_{oc}^{-1} = \left[R_s + \frac{nkT}{q} \times \frac{1}{I_{sc} - \frac{V_{oc}}{R_{sh}}}\right]$	The series resistance decreases by an increase in intensity.	Other equation required to calculate the parameters.	[74]
13	$\boldsymbol{Rs = CoRso}$ $C1 = (1 - \frac{Im}{Isc}) exp\ (-\frac{Vm}{C2Voc})$ $C2 = \frac{\frac{Vm}{Voc} - 1}{log\left(1 - \frac{Im}{Isc}\right)}$ $I = Isc\left(1 - C1(exp\left(\frac{v}{c2voc}\right) - 1)\right)$ $I = Isc\left(1 - exp\left(-\frac{1}{C}\right)\left(exp\left(V\left[\frac{1}{CVoc} + \frac{C^b}{Vm}\right]\right) - 1\right)\right)$ $b = \left(-1.2 + \frac{Voc}{Vm} + \frac{Isc}{Im}\right)$ $C = C2$ $\frac{dI}{dV} = -Isc\left(\frac{1}{CVoc} + \frac{C^b}{Vm}\right) exp\left(\left[\frac{VocC^b}{Vm}\right]\right)$ $Rso = -\frac{CVocVmexp\left(-\left[\frac{VocC^b}{Vm}\right]\right)}{(C^{b+1}Voc + Vm)Isc}$	Required only the Manufacturer's nameplate data to determine the series resistance	Complex methodology.	[115]

$$Co = -\frac{bC^{b-1}(C^{b+1}Voc + Vm)}{(C^{b}Voc + Vm)} exp\left(\left[\frac{VocC^{b}}{Vm}\right]\right)$$

$$\boldsymbol{Rs = \frac{C^{\frac{Isc}{Im}}VmVoc}{Isc\left(C^{\frac{Isc}{Im}}Voc + Vm\right)}}$$

$$a = (Isc - Im)\left(\frac{Vm}{Im} - Rs\right)$$

$$Rs = \frac{(Vm(Isc - Im) - CImVoc)log\left(1 - \frac{Im}{Isc}\right)}{Im\left(Im + (Isc - Im)log\left(1 - \frac{Im}{Isc}\right)\right)}$$

$$a = \frac{RsIm}{log\left(1 - \frac{Im}{Isc}\right)} + CVoc$$

$$Rsh = \frac{(Vm - a)(Vm - RsIm)}{(Vm - RsIm)(Isc - Im) - aIm}$$

14	$Rs = Rs = \frac{rs.Voc}{Isc}$ $voc = \frac{Voc}{Vt}$ $FFo = \frac{voc - ln(voc + 0.72)}{voc + 1}$ $FF = \frac{Vm\,Im}{Voc\,Isc} = \frac{Pm}{Voc\,Isc}$ $rs = \frac{1 - FF}{FFo}$	Model and quantify the impact of the ambient temperature, the incident Intensity, and the wind speed over SPV technology in real-time.	Consider Rsh infinite enhance the error.	[116]
15	$Rs = \frac{R_{L2}I_{T2} - R_2I_{T1}}{I_{T1} - I_{T2}}$ The Subscripts are results from Load resistor 1 & 2	Independent of influences created by mismatches between the simulator and solar spectra.	depends on logarithmically on pulse-to-pulse light varying illumination.	[117]
16	$R_{s,STC} = \frac{V_{mp,STC}}{I_{mp,STC}} - \frac{2V_{mp,STC} - V_{oc,STC}}{\left(I_{sc,STC} - I_{mp,STC}\right)\left[\left(ln\left(1 - \frac{I_{mp,STC}}{I_{sc,STC}} + \frac{I_{mp,STC}}{I_{sc,STC} - I_{mp,S}}\right.\right.\right.}$	The combined approach of the analytical and mathematical solution has been introduced.	Complex method.	[118]
17	$Rs = \frac{V_m}{I_m} - \frac{B}{I_L - I_m}$ $B = \frac{2V_m - V_{oc}}{\frac{Im}{Im - I_L} + ln\left[\frac{I_L - I_m}{I_L}\right]}$	Data extracted from the curve characteristics	Less accurate, ideality factor constant	[104]
18	$Rs = Roc - \frac{(Vm + RocJm - Voc)}{Jm + \{(ln(Jsc - Jm) - ln(Jsc)\}Jsc}$ $Roc = \left(\frac{dJ}{dV}\right)^{-1}_{V=Voc,J=0}$	The conductivity of the front, bulk and emitters	Less accurate	[119]

		will increase with increasing power. Therefore, the value of Rs decreases with increasing power.			
19	$Rs = \frac{1}{Imp}\left[Voc - Vmp - nVt.ln\frac{Vmp + nVt.Imp\,Rs}{nVt}\right]$	Does not required Rsh value for the estimation.	The solution cannot be reached without resorting to an iterative procedure for the estimation of Rs which a logarithmic term.		[120]

The single diode model (one diode model) is majorly used method due to its simplicity and derivation of the less parameter, less time-consuming. From the literature survey, it has been concluded that using the intensity with various varieties, is a majorly used for determination of series resistance. It also has been found out that the shunt resistance has been assumed to be ideal, i.e., infinite, in the most of the single diode methods which result in an error in the estimation of series resistance. The single diode model assumes that the ideality factor is constant for all conditions. Whereas the ideality factor is a function of the voltage across the device. At high voltage, the ideality factor is near to one, when the recombination in the device is dominated by the surfaces and the bulk regions. However, at lower voltages, recombination in the junction dominates and the ideality factor approaches two. The single diode model has been considered to be less accurate than the double diode model by numerous authors [80].

The five-parameter model led to more precise parameter estimations than the simplified four-parameter model, which assumes that the shunt resistance is infinite and thus neglects it causes uncertainty in the results. However, the said methods have the disadvantage of involving a large number of parameters in the calculations rendering it very complicated. The methods based on the least-squares, numerical techniques, and exact solutions are complicated. The extraction of parameters is more comfortable using the

computational tools and software as MATLAB Mathematica, Transys, Lab view and several others. The primary efforts which are done by the various researchers are in improving the accuracy, precision and less computational time while solving the equations.

b. Double exponential model. The double diode model (or double exponential model) requires an additional diode in a detailed manner to account for the losses due to the recombination of the carrier in the junction space charge region and the losses due to the surface recombination as given by Shockley diode equation (15), Shockley, 1948 [121], [122].

$$I = I_{ph} - I_{01}\left(e^{\frac{V+IR_S}{V_t}} - 1\right) - I_{02}\left(e^{\frac{V+IR_S}{2V_t}} - 1\right) - \frac{V+IR_S}{R_{sh}} \qquad (15)$$

Khanna et al., (2016) has suggested that the value of shunt resistance would be nearly the same for both single exponential models and double exponential models. However, the values of series resistance would be lower for the double exponential model as compared with the single exponential model. Further, it has also been concluded that the series resistance decreases linearly with the junction voltage [123]. The expressions for estimation of the series resistance using the double exponential model are given in Table 2.7.

Table 2.7. The expression for estimation of the series resistance using the Double diode model.

S.no	Expression	Advantages	Limitation	Reference
1	Method A. Constant Voltage $R_s = \frac{\frac{KT}{q} ln\left[\frac{I_2}{I_1}\right] + I_2 R_{ext2} - I_1 R_{ext1}}{I_1 - I_2}$ Method B. Constant Current $R_{ext} + R_s = \frac{1}{I} \times \left[V + \frac{KT}{q} ln\left[\frac{I_{01}}{I}\right]\right]$ $R_{ext} = External\ Resistor\ (\Omega)$	For method A, required only two experimental dark measurements for constant voltage.	The method is not valid when the Rs have an impact on the photoconductivity of the upper solar cell layer.	[124]
2	$y = \frac{1}{n_d V_t}(-Rs + x)$	Special emphasis on the low Rs.	Rs determined	[122]

	$y = \frac{ln\left(\frac{I}{I1}\right)}{I - I1}$ $x = \frac{V - V1}{I - I1}$		by using the linear regression.	
3	$Rse = -\left(\left(\frac{\partial II}{\partial V}\right)_{V=Voc}\right)^{-1} - \left(\frac{kT}{e\eta} Il\right)^{-1}$	In a curve-fitting procedure simplex minimization algorithm is used for the estimation.	Less accurate.	[125]
4	$I_5 = I_{O1}\left(exp\left[\frac{V_5 - RsI_5}{Vt}\right] - 1\right) + I_{O2}\left(exp\left[\frac{V_5 - RsI_5}{\alpha Vt}\right] - 1\right) + \frac{V_5 - RsI_5}{Vt} - I_L$ $a = \frac{V_{oc}}{V_t\left[ln\left[I_L + I_{O2} - I_{O1}\left(exp\left(\frac{V_{oc}}{V_t} - 1\right)\right)\right]}$	Computation on double diode model,	The equations must be repeated until the value of the "α" satisfied the desired precision.	[73]
5	$R_S = \left(\frac{\partial V}{\partial I}\right)_{OC} - \frac{V_T}{I_{DO}exp\left(\frac{V_{oc}}{V_T}\right) + \frac{I_{RO}}{m_R}exp\left(\frac{V_{oc}}{m_R V_T}\right) + \frac{V_T}{R_{Sh}}}$	Modified double diode model for CIS, amorphous silicon triple junction, a-Si, amorphous silicon double junction, Sanyo HIT, CdTe, mc-si, and mono-crystalline has been used.	Required multiple parameters.	[126]
6	$Rs = \frac{(V_A - V_{oc})}{I_{sc}}$ V_A=Large Voltage (V)	The two-diode model along with a dark I-V characteristic has been used.	Less accuracy.	[127]

7	$F(I,V) = I - I_{ph} + \emptyset(X) = 0$ $\emptyset(X)$ $= I_{S1}\left[exp\left[\frac{X}{n_1 V_t}\right] - 1\right]$ $+ I_{s2}\left[exp\left[\frac{X}{n_2 V_t}\right] - 1\right] + \frac{X}{R_{sh}}$ $X = V + IR_s$ $1 + (R_s - R_{sho})\emptyset'(I_{sc}, R_s) = 0$ $1 + \left(R_s + \frac{Vm}{Im}\right)\emptyset'(Xm) = 0$ $Xm = Vm + ImRs$	Only single Illumination curve is required for estimation of the series resistance.	Complex, time-consuming methodology.	[128]

In various silicon technology devices, the recombination components are a complex function of the carrier concentration. The primary assumption used in the double diode model is considering both diodes ideality factors as constant or variable and considering various fitting parameters to estimate the diode parameters. As the number of carriers increases with the applied voltage, the recombination at the rear surface changes dramatically with voltage in the solar cell. In such cases, accuracy may be achieved using the single diode but allowing both the ideality factor and the saturation current to vary with voltage. In such cases, which are quite common in silicon devices, a double diode fit yields erroneous value.

c. Lambert W-function. The Lambert W-function method of calculating parasitic resistance (series and shunt resistances) in the solar PV cell was proposed by Jain & Kapoor, 2004 and is based on the exact closed-form solution [129]. It has also been utilized to study series resistance of organic solar cells in which W-function equations have been estimated using Maple software [130]. The Lambert W-function is given by equation (16 & 17);

$$W \exp(W) = x \tag{16}$$

$$i = Iph - \frac{V + iRs}{Rsh} - I_0\left(e^{\frac{(V+iRs)}{nVth}} - 1\right) \tag{17}$$

Where terminal current (A) and voltage (V) are i and V respectively, the thermal voltage (V) (kT/q) is V_{th} and Rs (Ω) and Rsh (Ω) are shunt resistance and series resistance resp. The expression for estimation of the series resistance using the Lambert W-function is presented in Table 2.7.

Table 2.7. The expression for estimation of the series resistance using the Lambert W-function.

Expression	Remark	Ref.
$I = \frac{nKbT}{qRs} lambertw\left[\frac{qRs}{nKbT}\left(I_{sc} - \frac{V_{oc}}{Rs + Rsh}\right) exp\left(\frac{-qV_{oc}}{nKbT}\right)\right.$ $\left. \times exp\frac{q}{nKbT}\left(RsI_{sc} + \frac{RshV}{Rsh + Rs}\right)\right] + \frac{V}{Rs}$ $- I_{sc} - \frac{RshV}{Rs(Rsh + Rs)}$	Analyse various solar devices, including dye-sensitized solar cells, tandem silicon solar cells, silicon solar modules, and multi-junction structures organic solar cells	[70]
$Rs, o = Rso - \frac{nV_{th}}{Io} e^{\left(\frac{-Voc}{nV_{th}}\right)}$	Required some initial value for the execution of the process. The increased calculation time required to execute the numerical algorithm	[131]
$Rs = A(W_{-1}(Bexp(C)) - (D + C))$ $A = \frac{aV_T}{I_{mp}}$ $B = -\frac{Vmp\ (2\ Imp - Isc)}{Vmp\ Isc + Voc\ (Imp - Isc)}$ $C = -\frac{2\ Vmp - Voc}{aV_T} + \frac{(Vmp\ Isc - Voc\ Imp)}{(Vmp\ Isc + Voc\ (Imp - Isc))}$ $D = \frac{Vmp - Voc}{\alpha V_T}$	The method is straightforward, explicit, and non-iterative; no iterations or initial values for the process are required. Manufacturers' data sheets are required for the estimations.	[132]

IEC 60891 Edi 2.0 is an international standard which defines the procedure for translating the measured I-V characteristics of SPV modules to the desired temperature and irradiance condition. The validation of the series resistance estimation method using IEC 60891 Edi 2.0 standard for solar modules technologies has been attempted by [133]. Trentadue et al., 2016 pursue standard IEC 60891 Edi. 2 (2009) for the internal series resistance determination and examine the uncertainty and repeatability of the procedure.

It has been found out that the series resistance of SPV would be estimated with an uncertainty of 10% [134]. There are three standard procedures placed down by the IEC 60891 Edi.2.0 given in Table 2.8.

Table 2.8. The expression for estimation of the series resistance using the IEC 60891 Edi.2.0.

Procedure	Expression	Description	Reference
Simplified Method	$I_2 = I_1 + I_{sc} \times \left(\frac{G_2}{G_1} - 1\right) + \alpha(T_2 - T_1)$ $V_2 = V_1 - R_S \times (I_2 - I_1) - kI_2 \times (T_2 - T_1) + \beta(T_2 - T_1)$	The most straightforward method for more natural understanding, determination of the Rs and curve correction factor.	
The alternative algebraic correction method	$I_2 = I_1 \times (1 + \alpha_{rel} \times (T_2 - T_1)) \times \frac{G_2}{G_1}$ $V_2 = V_1 + V_{oc1} \times \left(\beta_{rel} \times (T_2 - T_1) + \alpha \times ln\left(\frac{G_2}{G_1}\right)\right) - R'_S \times (I_2 - I_1) - k' \times I_2 \times (T_2 - T_1)$	Methods provide better yields results for large irradiance corrections (>20 %).	IEC 60891 Edi. 2.0 [135],[136].
Interpolation method	$V_3 = V_1 + a \times (V_2 - V_1)$ $I_3 = I_1 + a \times (I_2 - I_1)$	The method does not require correction parameters as input. It can be applied to a minimum of three current-voltage curves.	

The deviation in the value of the estimated Rs using various methods occurs due to multiple factors such as mathematical error, instrumental error, calculation error and humanoid error. These discrepancies are due mostly to (i)

differences amongst the different estimation methods and (ii) dissimilarity in necessary materials used for solar cells, their structures as well as the fabrication methods.

2.6 Uncertainty analysis of the estimated data

The uncertainty in the measurement devices and in the measurement is calculated according to the 'Guide to the expression of uncertainty in measurement' [GUM, (JCGM 100.2008, 2008)]. The objective of the study is to incorporate various causes of uncertainty while collecting the data, filtration and analysis over the data. The uncertainty calculation has been done on the three different technologies for three irradiance range. Table 2.9. presenting the uncertainty including Type "A" and Type "B" is used to report in the literature review.

Resistance = f (Irradiance, Temperature, Current, Voltage)

Table 2.9. The parameter for the assessment of uncertainty using GUM

Type of Uncertainty	**Parameter**	**Mathematical Representation**	**Degree of Freedom**
TYPE A. Evaluation of standard uncertainty.	Arithmetic Mean or Average	$q = \frac{1}{n}\sum_{k=1}^{n} q_k$	
	The variance of the probability distribution of q	$S^2(q_k) = \frac{1}{n-1}\sum_{j=1}^{n}(q_j - q)^2$	The degree of freedom= n-1
	The experimental standard deviation of the mean S2 (q), Variance of mean	$S^2(q) = \frac{S^2(q_k)}{n}$, $S^2(q) = \sqrt{\frac{1}{n-1}\sum_{j=1}^{n}(q_j - q)^2}$	
TYPE B. Evaluation of standard uncertainty	Combined standard uncertainty.	$U_C = \sqrt{U_A^2 + U_{B1}^2 + U_{B2}^2 + U_{B3}^2 + U_{B4}^2 + U_{B5}^2 + U_{B6}^2 + U_{B7}^2}$ -	The degree of freedom= n-1
	Expanded uncertainty. For a 95.45% level of confidence the coverage factor K=2	$U = K\,U_C(eff)0$	

The calculation and valuation of SPV degradation is an essential contribution to the assessment of the performance evaluation based on the real

outdoor condition [137]. To avoid the uncertainty of predicting the degradation rate, there is a requirement of the detailed knowledge over the degradation during the field conditions [92]. Jordan et al. investigated four methodologies as a function of years, seasonality and noise. Additionally, sensitivity to outliers and soiling actions were investigated. Year-on-year (YOY) approach is suitable best among four different methods as this is having less impact of the seasonality and outliers [138]. [118] introduced a new method to define the single-diode and double-diode model having five and seven parameters more accurately. The 'fsolve' of MATLAB embedded with 'Levenberg–Marquardt (LM)' algorithm has been applied for determining the accurate parameters. [139] discussed different degradation modes and their correlation with the linear degradation within the measurement uncertainty while other degradation modes lead to non-linear degradation.

2.7 Effect and analysis of the shading losses as heating effects

When a solar cell or a number of solar cells operates in the reverse bias condition within the cell and dissipating the power and work as a load in its place of generating, the well-known phenomenon is termed as Hot spots [140], [141], [142]. In this, the solar cell reaches an elevated temperature in comparison to other cells in the PV modules. Due to attaining the higher temperature within the solar cell, the degradation rates also accelerate for the particular solar cell within the module. The hotspot also results in faster degradation of the material used for the module's encapsulation [142]. The hotspot occurs due to shading of the nearby structure, construction, chimney or any tree, local or asymmetrical dusting, obstacles from the natural resources as leaves etc. Solar cells exposed to higher temperatures will put down at a higher rate than others and, if operation at high temperatures occurs during a protracted time, pulling it to permanently run in reverse bias and rendering useless the rest of the cellular telephones below the same bypass diode [143]. There are two localized heating phenomena affecting the PV modules in outdoor testing condition. First problems relate with the weak solder joints and second is due to the micro-cracks on the module cells. Even if the cell does not result damaged, the exposure to high temperatures will result in faster degradation of the

material used for the module's encapsulation reducing the radiation that turns over the solar cell. Both conditions would worsen over time [142].

To minimize the impact of the Hot-Spot in the solar modules, these modules are incorporated with the bypass diodes [129, 130]. The international standard IEC 61215:2016 describes the procedure for hotspot resistance testing and the functioning of the Bypass diodes [146], [147]. One of the functions of by-pass diodes is to limit hotspot effects to a minimum, however, even with their use, hotspots can still occur in SPV modules [140]. Various thermal imaging procedures are used to detect the hot-spot phenomenon in the solar PV plants [148].

The Infra-Red image of the PV modules having the Hot-spot temperature profile is shown in Fig 2.11.

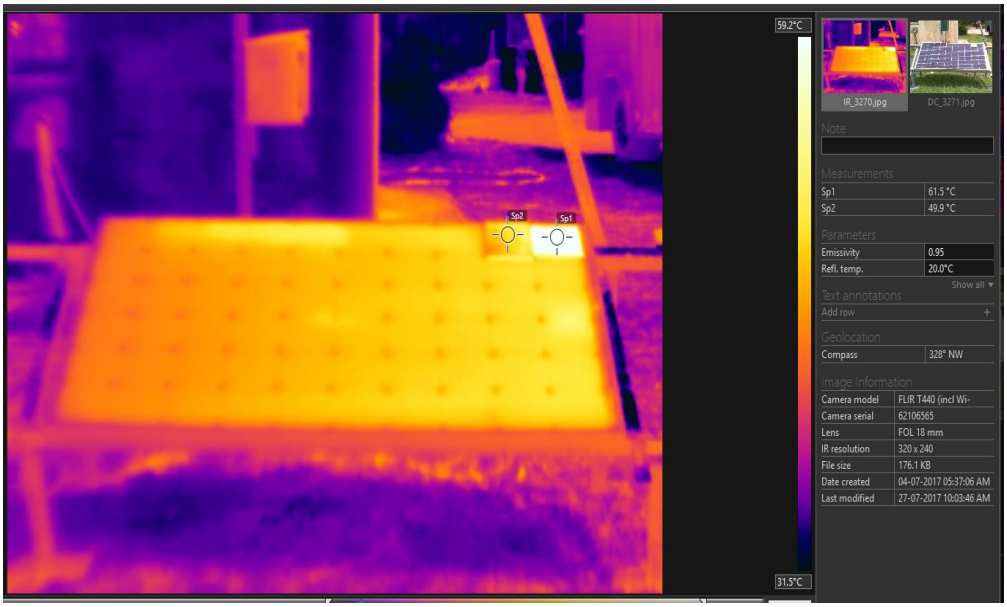

Fig 2.11. The Infra-Red image of the PV modules having the Hot-spot temperature profile.

Infra-Red (IR) imaging is a non-destructive tool to collect the information regarding the temperature distribution and profiling of the photovoltaic cell within the solar modules or in the solar power plant. Table 2.10 describes much literature in which the Infra-Red thermography used for experimental performance monitoring. Various imaging techniques such as electroluminescence (EL), photoluminescence (PL), and Infra-Red (IR) technologies are being used to detect the hotspot phenomenon in the SPV

modules [149,150]. Sinha et al., 2016 has established a model to simulate the active thermography approach for the characterization of de-lamination in the SPV module [151]. Table 2.10 shows the Infra-Red imaging used for performance monitoring.

Table 2.10. Infra-Red imaging used for performance monitoring.

Experimental in-situ approach	Camera used	Detector	Reference
Passive thermography Approach Studies the degradation effects over field aged (18–22 years) SPV modules.	TROTEC-IC080LV Thermo camera	The Detector is an uncooled micro-bolometer with spectral range 7.5 to 14 μm.	[69]
Passive thermography Approach Drone-based aerial thermography of defective modules and cells in large photovoltaic Power plants.	Optris PI450 and the RGB Camera GoPro Hero3+		[152]
Active thermography approach- An electro-thermal model was developed for the characterization of delamination in SPV module.	A high-speed (150 Hz) cooled IR camera	Cooled IR Camera	[153]
Active thermography approach - Quantitative values for local reverse current and series resistance images in hot-spots can be easily obtained in 10 ms. and 800 ms. respectively.	Different cameras can be used to detect radiation in different wavelength ranges	-	[154]
Passive thermography Approach – IR thermography to show the Infra-Red luminance of the PV panel surface.	Impac IVN 780-P.	Temperature range of -40 to +1000 ^{0}C	[149]
Passive thermography Approach Processing and Interpretation of the thermo-graphical images acquired on a grid-connected photovoltaic plant (20 kwp).	FLIR thermacam B4	Non-cooled detector. Temperature between -20 °C and +55 °C.	[155]
Passive thermography Approach Detailed characterization of PV modules.	FLIR E- 60 Infra-Red Camera		[148]
Passive thermography Approach The thermal and electrical effects caused by outdoor hot-spot testing in crystalline silicon modules.	AGEMA Thermo vision 1570 camera	Focal plane array uncooled Micro-bolometer detector)	[156]
Passive thermography Approach Analyze a sample of 200 defective PV modules from two PV plants.	Infra-Red camera (FLIR-Infracam, 7.5-13 µm)		[10]
Passive thermography Approach Quality control of different thin-film module technologies (a-Si, CdTe, and CIS) was investigated using IR thermography.	Uncooled IR-camera.	The Wavelength sensitivity of the IR-detector is 7.5μm and15μm.	[157]

Radiation emitted by an object is detected in a non-contact way by an Infra-Red detector and using the Stefan-Boltzmann's law. Using equation (18), the temperature of the body is obtained.

$$q/A=\varepsilon\sigma T^4 \quad (18)$$

Where, q=rate of energy emission (w)

A=the area of the emitting surface (m2)

T=Absolute Temperature (K)

σ = Stefan-Boltzmann's constant (5.676 x 10^{-8} Wm^{-2} K^{-4})

ϵ = Emissivity of the emitting surface for a fixed wavelength and absolute temperature

Fig 2.12 represents the passive and active thermography techniques along with their applications.

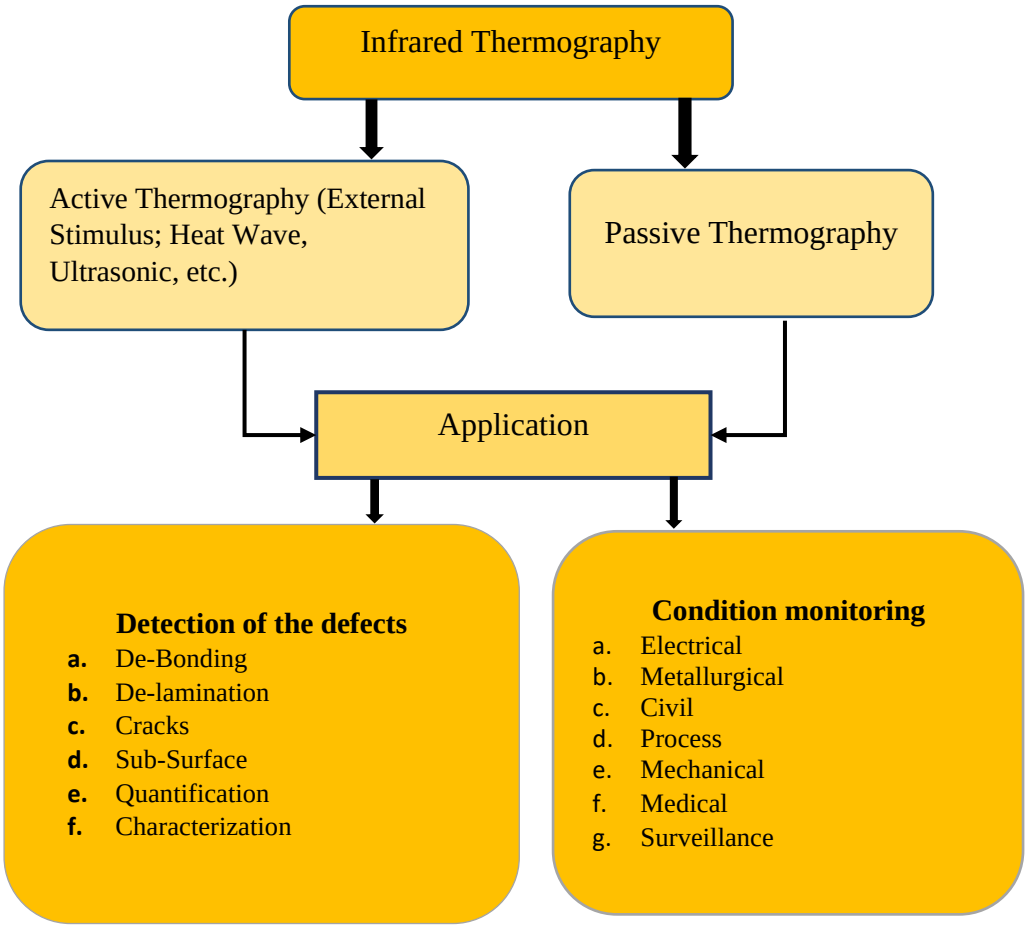

Fig 2.12 Graphic representation of the Passive and Active thermography techniques along with their applications.

Through literature review, an effort is made to find out the progress of high-efficiency solar PV modules in the World, with special emphasis on India. This comprehensive review aided the researcher in supporting the present study through the identification of the research gap in the existing literature.

2.8 India's seasonal classification based on months.

India is a big tropical country and is famous for its diverse climatic features. India's climate can be categorized into six principal categories and this has been determined by the Koppen climate classification. The seasons in India can be broadly categorized in the following Table 2.11.

Table 2.11. Classification of the seasons in India

Name of the season	Tenure
Winter	The months of January and February, Mid of November to the last of December.
Summer	The starting from March to end of June
Monsoon (rainy) Season	The months from July to Mid-September
A post Monsoon period	The months from Mid-September to Mid-November

The categorization has been done on the basis of the astronomical distribution of the twelve months in a year into six fragments.

2.9 Characteristics of composite climate

The composite zone covers the central part of India, such as New Delhi, Lucknow, Kanpur and Allahabad. The design criteria are more or less the same as for hot and dry climate except that maximizing cross ventilation is desirable in the monsoon period.

India is mainly a composite type of climatic condition. These climates usually occur in large landmasses near the tropics of cancer and Capricorn, which are sufficiently far from the equator to experience marked seasonal changes in solar radiation and wind direction. In composite climate condition, two seasons occur normally. Approximately two-thirds of the year is hot- dry

and the other third is warm- humid. Localities further north and south have a third season but described as cool-dry. The temperature in this climatic region follows the following order shown in Table 2.12.

Table 2.12. The temperature of the composite climate.

Season	Hot-dry	Warm humid	Cool-dry
Day-time mean max	32-43^{o} C	27-32 ^{o} C	Up to 27 ^{o} C
Night-time mean min	21-27 ^{o} C	24-72 ^{o} C	4-10 ^{o} C
Diurnal mean range	11-22 ^{o} C	3-6 ^{o} C	11-22 ^{o} C

Humidity is low throughout the dry periods at 20-55% with a vapour pressure of 1300 to 1600 N/m^2. During the wet period, it rises to 55-95% with a vapour pressure of 2000 to 2500 N/m^2. Monsoon rains are intense and prolonged; occasionally 25-38 mm can fall in an hour. Annual rainfall varies from 500-1300 mm with 200-250 mm in the wettest month. There is little or no rain during the dry seasons.

2.10 Research Gap

Based on the literature reviewed, the researcher has identified the following research gap, which further motivates the researcher to carry out the proposed research.

- Selection of suitable module technology for different climate is a difficult task. Knowledge about the performance of solar power plants will result in incorrect investment decisions, a better regulatory framework, and favourable government policies. It is imperative to acquire a profound comprehension of the fundamental of the degradation mechanisms so as to ensure guarantee the steady performance of the PV module and devices.

- For reliable operation of PV modules, it should be designed to withstand the climatic stress during its operational lifetime. However, for each climatic condition, the level of stress and its effect on the reliability will be different. In this area, for the Indian climatic conditions, only scanty literature is available for the high-efficiency solar modules. It is significant to fill the

knowledge gap on PV module analysis in the composite climatic zone and later predict for other zones. These statistics can deliver productive advice to manufacturers to produce improved PV modules for composite climates.

- It is also necessary for system investors to effortlessly regulate which type of PV module technology gives the superlative functioning at the specified environments in the different climatic zones. Since there is no significant study on the identification of the leading barrier and challenges to the growth of high-efficiency solar modules in India, there is a need for a comprehensive study to be conducted. To study and understand these parameters including the environmental and electrical factor, an effort will have done at NISE.

Hence, it is critically significant to examine the performance of high-efficiency solar modules in outdoor conditions.

2.11 Research objectives

Based on the research gap, the following objectives are set for this thesis;

1. To study the performance, reliability, and degradation of several technologies, including some current and some emerging (as well as one discarded) technologies in the composite climate of India.
2. To develop a methodology for high-efficiency PV modules for assessing and quantifying the distribution and extent of degradation, failures, and mismatch within a PV module on outdoor exposure.
3. Effect and analysis of the shading losses and develop the modelling of the losses as heating effects.
4. Feasibility study of the high-efficiency PV modules.

2.12 Conclusion

The literature review of all the aspects based on performance metrics of solar photovoltaic modules and the array is put together. A detailed literature

survey has been carried out in order to compile information regarding the earlier research conducted in the field of performance of solar photovoltaics and described in the subsequent section.

A comprehensive literature survey using up-to-date research articles has been presented, highlighting the advantages and limitations of different methods of estimating series resistance. The expressions used for the estimation and performance analysis have been tabulated.

CHAPTER 3
RESEARCH METHODOLOGY & EXPERIMENTAL SET-UP

The literature review has been done in the previous chapter which widened the understanding of SPV modules characterization and performance monitoring mechanism in India. This present chapter discusses the research methodology and experimental setup used for the analysis of the issues revealed by the literature survey. The SPV technologies modules, data logger system and the scientific instruments used are discussed briefly in the below sections.

3.1 Scope for the design of work

Considering the significance of high-efficiency solar modules, the work is carried out on high-efficiency solar modules consisting HIT (Hetero-junction intrinsic thin layer silicon), Sun-Power and PERC (Passivated Emitter and Rear Cell or Passivated Emitter and Rear Contact) along with the a-Si (amorphous single-junction silicon), (m-si) mono-crystalline silicon and mc-si (multi-crystalline silicon). It has been tried to fulfil the gap existing between well-defined wafer-based technologies and thin-film technologies and not yet reported performance of high-efficiency at the composite climate of India.

3.2 Methodology adopted to fulfill the Objective-I "To study the performance, reliability, and degradation of high-efficiency modules in the composite climate of India."

For objective, I, the performance of the SPV at real outdoor condition has been studied based on the filtering techniques, performance monitoring metrics and numerical methodologies. A set of nine SPV modules consisting multi-crystalline (mc-si), Heterojunction with Intrinsic Thin layer (HIT) and amorphous silicon (a-si) each were characterized for a period of three years under the composite climate of India.

This objective comprises, comparative performance analysis of the different silicon-based module technologies under the composite climate based on monthly average effective peak power, monthly average performance ratio, monthly average temperature corrected performance ratio and monthly average efficiency; secondly to estimate the degradation rate based on the linear regression over the effective peak power. The detailed methodology used for the performance analysis has been presented in the flowchart as shown in Fig 3.1 and discussed in the subsequent subsections.

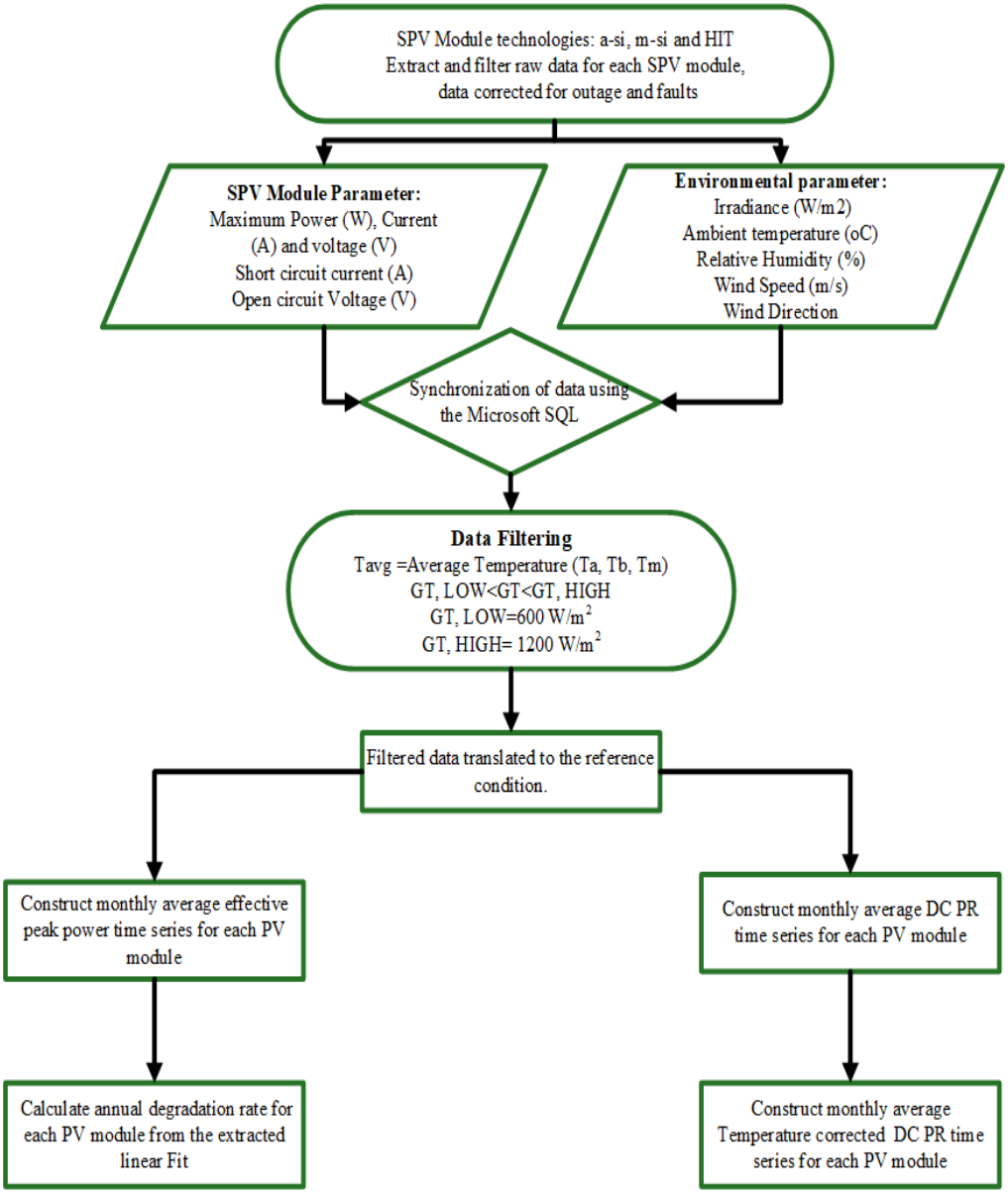

Fig 3.1. Methodology for the performance assessment of the SPV technologies

3.2.1 Effective peak power and Thermal Factor of the SPV modules

The investigation of the performance of the SPV technology based on the effective peak power (P_{eff}) has been done using the following equations (19);

$$P_{eff} = \frac{G_{STC} \times P_{DC}}{G} \times T_F \quad (19)$$

where P_{eff} is the effective peak power, G_{STC} is irradiance at STC, P_{DC} is the DC output power, G is the irradiance and T_F are the thermal factors respectively. The thermal factor is well-defined as follows eqn. (20).

$$TF = \frac{1}{[1+\delta(T_m - T_{STC})]} \quad (20)$$

where T_m is the module temperature, T_{STC} is the module temperature at STC, δ is power temperature coefficient of the SPV module.

The assessment of the P_{eff} has been carried out as the product of the normalized values of the maximum current and maximum voltage gained from the equation provided in the IEC 60891 edi 2.0, the equations are as follows eqn (21 & 22);

$$I_r = I_m + I_{sc}\left(\frac{G_r}{G_m} - 1\right) + \alpha(T_r - T_M) \quad (21)$$

$$V_r = V_m - R_s(I_r - I_m) - KI_r(T_r - T_m) + \beta(T_r - T_m) \quad (22)$$

where I_r is the rated current, I_m is the measured current, I_{sc} is the short circuit current, R_s is the series resistance, V_r is the rated voltage, V_m is the measured voltage, k is the curve correction factor and α is the temperature coefficient of the module.

The estimation of the effective peak power from the outdoor data has been performed after filtering the low irradiance data sets. Only measurements taken at irradiance greater than 800 W/m^2 were used in the analysis and calculations to avoid uncertainties when recalculating power to STC conditions and omit some false values caused by low irradiance. Above this irradiance, the threshold shape of the varying solar spectrum closely resembles that of spectral AM 1.5G reference spectrum. Hence no spectral effects corrections are taken into account in the equations used to calculate the effective peak power for all nine modules.

3.2.2 Performance Ratio, temperature corrected performance ratio and efficiency

The actual electrical properties of the SPV modules are different from the reference STC characteristics, hence the performance ratio is calculated to evaluate the performance of the SPV modules. PR is a dimensionless quantity and defined as the ratio of the real energy production to the product energy at the STC. It indicates the overall effects of the losses on the rated output on the environment as well as electrical components. The expression of the performance ratio is as the following Eqn. (23);

$$PR = \frac{Final\ yield\ (Y_f)}{Reference\ Yield\ (Y_r)} \quad (23)$$

The final yield of the SPV module (Y_f) is defined by the ratio of the final or actual energy output of the SPV module to the total power of the SPV module under STC. The expression of the final yield is written as follows eqn. (24);

$$Final\ Yield\ (Y_f) = \frac{Final\ Energy\ Output\ (kWh)}{Maximum\ Power,_{STC}\ (kW)} \quad (24)$$

The reference yield (Y_r) is defined as the ratio between total daily in-plane solar irradiance to the reference irradiance in a unit area defined under STC and is expressed with the below equation (25);

$$Reference\ Yield\ (Y_r) = \frac{Total\ in{-}plane\ Irradiance\ \left(\frac{kWh}{m^2}\right)}{1000\ \left(\frac{kW}{m^2}\right)} \quad (25)$$

The temperature correction of the Performance ratio has been by multiplying the performance ratio with the thermal factor of the technology calculated using the Eqn. 26,

Temperature corrected performance ratio (PR_{CORR}) = PR X T_F (26)

3.2.3 Normalized PV module efficiency and Spectrum Factor

The efficiency of the PV module is well-defined as the ratio of the DC power output to the product of the total in-plane solar irradiance and the module area. The instantaneous PV module efficiency (η_{PV}) is expressed as follows eqn. (27);

$$\eta_{PV} = \left(\frac{P_{DC}}{G_T \times A_M}\right) \times 100 \quad (27)$$

where P_{DC} is the DC output power, G_T is the total in-plane solar irradiance W/m^2, A_M is the PV module area m^2.

Spectrum Factor: The influence of spectral parameter over the SPV technologies is due to the bandgap of the solar cell material which regulates a threshold photon energy that can generate free carriers. The absorption of carrier generation by photon varies as a function of their wavelength of the material. The constraints used for the spectrum factor has been counted on using SMART software (The Simple Model of the Atmospheric Radiative Transfer of Sunshine) [49]. The mathematical expression for the spectrum factor is as follows Eqn. (28);

$$S_F = \frac{\int \zeta STC(\lambda)_{.} SR(\lambda) / \int \zeta(\lambda)_{.} SR(\lambda) d\lambda}{\int \zeta STC(\lambda)_{.} d\lambda / \zeta(\lambda) d\lambda} \quad (28)$$

where S_F is spectrum factor, ζSTC is standard spectrum at STC, ζ is the solar spectrum of the location, SR is the relative spectral response of the SPV technology, and λ is the wavelength (nm). The effect of the spectral variation on devices performance with a narrow spectral response such as a-si technology is much evidence in the literature. The normalized PR of SPV technology can be determined by Eqn. (29);

$$PR_{NOR} = PR \times T_F \times S_F \quad (29)$$

The normalized performance ratio of each module for the different year is presented in the contour Fig in which the normalized performance ratio is plotted against the module temperature (^{0}C) and in-plane irradiance (W/m^2).

3.2.4 Effect on the seasonal normalized performance ratio for three years

The calculation and analysis of the effects of the observed variation in real operating condition on annual and three-year performance have been done. For the analysis of the seasonal performance fluctuations, the study period is divided into three seasons, namely Summer (March, April, May, June), Winter (November, December, January, February) and Monsoon (July, August September, October).

3.2.5 Series resistance estimation methodology

Degradation within the SPV modules manifests as changes in the electrical resistive properties. This may arise due to the deterioration in the series resistance of the SPV modules. The ability to detect the increase in the series resistance (R_s) of modules would be tremendously useful in SPV module degradation studies. The assessment of the series resistance for nine SPV modules has been done using the procedure-I provided in the IEC 60891 Edi.2.0 [82]. To decrease the irradiance without any change in the module temperature and spectrum the wire mesh screen has been used over the SPV module shown in Fig 3.2.

Fig 3.2. Test set-up using mesh for calculation of series resistance of the SPV modules

The transmissivity of the complete mesh screen has been estimated using the irradiance above and below the mesh to check spatial uniformity. The error in transmissivity has been found out to be less than 2% for the complete mesh. The mathematical formula described below.

$$I_2 = I_1 + I_{SC} \times \left(\frac{G_2}{G_1} - 1\right) \quad (30)$$

$$V_2 = V_1 - R_S \times (I_2 - I_1) \quad (31)$$

$$P_2 = V_2 \times I_2 \quad (32)$$

$$\Delta = 100 * \frac{\max(P_1, P_2) - \min(P_1, P_2)}{mean(P_1, P_2)} \quad (33)$$

Where I_1 (A) and V_1 (V) are the values on the measured I-V characteristics, I_2 and V_2 are the values on the resulting corrected characteristics, G_1 is the irradiance (W/m^2), Isc is the corresponding measured short circuit current (A), G_2 is the irradiance at the standard conditions (W/m^2), Rs is the internal series resistance (Ω), P_2 is the power corresponding to the corrected I-V curve (W) and Δ is the deviation of power from P_1.

3.2.6 Statistical tools to estimate the degradation rate

The degradation rate of the SPV technologies has been investigated using three commonly used statistically trend extraction methods. Linear Regression (LR), Classical Seasonal Decomposition (CSD) and Locally weighted scatterplot smoothing (LOESS) [83], [84]. The data filtration and performance monitoring of three modules each of the mc-si (160 W), HIT (210 W) and a-si (75 W) have been carried out at the composite climate for a period of three years. A comparison of the annual degradation rate of three silicon-based SPV technology nine modules based on the real outdoor measurements. The degradation rate of the nine modules is obtained using the linear regression, classical series decomposition and LOESS applied to the monthly performance ratio time series over three years. The time series of the performance ratio has been constructed using the IEC 61724-1:2017. The analyses of the technologies, by employing the statistical techniques of the linear regression, CSD and LOESS have been done on the constructed time series.

Linear regression is the most commonly used methods for trend extraction and can be expressed as Eqn. (34).

$$y = \beta_o + \beta_1 x \tag{34}$$

Where x is independent variable also termed as a predictor, y is the dependent variable also termed as the response variable and β_o is the intercept of the line.

The degradation rate can be calculated using the intercept and slope of the linear curve over the long-term performance parameter time-series data [24]. Thereby the annual degradation rate (D_ψ) is calculated linearly with time T (years) expressed as [85] Eqn. (35);

$$DR = 100 \times \frac{12\beta_1}{\beta_o} \tag{35}$$

The degradation rate can also be calculated using the classical seasonal decomposition over the time series for each SPV technology by extracting the trend and seasonality parameters. The CSD used to the decomposition procedure to extract the trend, seasonality and the residual factor of nine modules. The trend has been calculated by applying a 12-month centred moving average (CMA) to the PR time series. The k is the seasonal period, which is 12 as the number of months in a year has been considered. The expression for calculating the trend is as follows Eqn. (36);

$$T_t = \frac{1}{2}\left(\frac{1}{k}\sum_{i=t-m}^{t+m-1} Y_i + \frac{1}{k}\sum_{i=t-m+1}^{t+m} Y_i\right) \quad (36)$$

where T_t is the trend at time t, (t>m), and m is defined as the half-width of a moving average, m=$\frac{k}{2}$. After the calculation of the trend, linear regression is applied to calculate the degradation rate. The seasonal indices, Si has been calculated by taking the average of the de-trended series for each month of the year [83] as Eqn. (37);

$$S_i = Y_i - T_t \quad (37)$$

where seasonal indices Si, Y_i is the original data and T_t is the trend at time t. The residual component is the most significant component in the seasonal decomposition as it indicates the adequacy of the fitted model. The annual degradation rates have been obtained by applying the linear least-square fit of the calculated trend data of the time series. The gradient of the line represents the monthly degradation loss which can be multiplied by months in a year i.e. 12, to obtain the final degradation rate.

LOESS methodology has been also used to analyze the degradation rate of the nine SPV modules. In this method, the slope of the linear fit of each technology is the indication of the degree of degradation. The annual degradation (D_ψ) has been used as under [86].

$$D_\psi = \frac{\delta PR}{\delta t} \times 365 \quad (38)$$

$$\delta PR = \frac{PR_{final} - PR_{initial}}{PR_{initial}} \quad (39)$$

$$PR\ (t) = PR_{initial}(1 - D_\psi \times t) \quad (40)$$

where t is in years and the annual degradation, δt is the number of days in the evaluation period, δPR is the relative difference, $PR_{initial}$ is the initial

PR value in the calculation period and PR_{final} is the final PR value in the calculation.

3.3 The methodology to fulfill the objective-II "To develop a methodology for high-efficiency PV modules for assessing and quantifying the distribution and extent of degradation, failures, and mismatch within a PV module on outdoor exposure."

For objective-II, the distribution and impact of degradation within a PV module at outdoor real condition various methodologies have been carried out. In this regards the estimation of the series resistance of the PV modules has been determined using several theoretical, analytical and graphical methodologies. The measurement of series resistance is vital for outdoor performance modelling and evaluation of solar photovoltaic and helps to identify the degradation of field aged SPV modules. The objective is to present a comparative analysis of various methodologies for estimation of the series resistance of three different technologies namely, hetero-junction intrinsic thin layer silicon, amorphous single-junction silicon and Multi-crystalline silicon.

An extensive literature survey of different series resistance estimation methods has been presented, and a case study to compare the total of ten different methods has been carried out. The methods have been broadly classified into three groups of different approaches of series resistance estimation. Further, the present study also deals with the determination of series resistance by measuring the current-voltage characteristics of three different solar photovoltaic technologies at various ranges of irradiance and temperature that serves as a combination of real-time test environments during outdoor exposure.

The series resistance of three different solar photovoltaic technologies has been estimated using nine different analytical methods as well as IEC 60891 Edi 2.0 procedure and the comparative study has been carried out. The effect of irradiance and temperature on the series resistance has also been evaluated. Flowchart of the methodology followed in the series resistance study is shown in Fig 3.3.

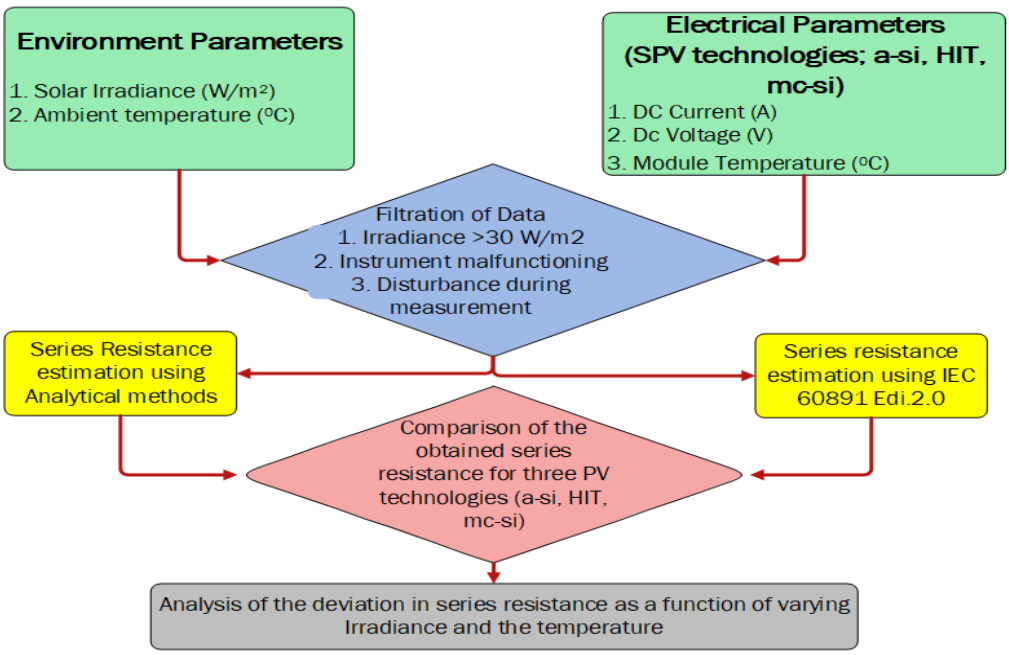

Fig 3.3. Flowchart of the methodology followed in the study

3.3.1 Estimation of series resistance using the analytical method

The actual power generation data of each SPV technology array along with the weather data are initially integrated arranged using the Microsoft access making a SQL programmer. For analysis the measured data in the irradiance range of 70-150 W/m^2, 150-250 W/m^2, 250-350 W/m^2, 350-450 W/m^2, 450-550 W/m^2, 550-650 W/m^2, 650-750 W/m^2, 750-850 W/m^2, 850-950 W/m^2, 950-1050 W/m^2, have been normalized to voltage and current at alternative reporting condition for 100 W/m^2, 200 W/m^2, 300 W/m^2, 400 W/m^2, 500 W/m^2, 600 W/m^2, 700 W/m^2, 800 W/m^2, 900 W/m^2 and 1000 W/m^2 respectively and 25°C module temperature [49]. The electrical parameters measured at the real operating conditions have been translated to alternative conditions using Eqn. (41) to Eqn. (43) to carry out the analysis under desired conditions.

$$V_{MP.ARC} = V_{MP} + \beta(T_{ARC} - T_M) \quad (41)$$

$$I_{MP.ARC} = I_{MP}\left(\frac{G_{ARC}}{G_T}\right) + \alpha(T_{ARC} - T_M) \quad (42)$$

$$P_{MP.ARC} = V_{MP.ARC} * I_{MP.ARC} \quad (43)$$

. The data obtained from the translation procedure have been utilized for nine different analytical techniques, as summarized in Table 3.1.

Table 3.1. The different analytical method for estimation of the series resistance

Method No	Formula	Remark	Reference
1	$Rs = \frac{Vm}{Im} \cdot \frac{\frac{1}{Vt}(Isc - Im)\left[Voc + Vt\left(1 - \frac{Im}{Isc}\right)\right] - Im}{\frac{1}{Vt}(Isc - Im)\left[Voc + Vt\left(1 - \frac{Im}{Isc}\right)\right] + Im}$	Simplified calculations; diode junction ideality factor at the maximum power point can be determined by the formula; one diode model	[35]
2	$Rs = \frac{Vm}{Im} - \frac{1}{B(Iph - Im)}$ $B = \frac{\left[\frac{Im}{Iph - Im}\right] + \ln\left[\frac{Iph - Im}{Iph}\right]}{2\,Vm - Voc}$	One diode model; the ideality factor of the diode has a constant value over the entire I–V characteristic.	[30]
3	$Rs = CoRso$ $Rso = -\frac{CVoc\ Vm \exp\left(-\left[\frac{Voc\ C^b}{Vm}\right]\right)}{(C^{b+1}\ Voc + Vm)\ Isc}$ $Co = -\frac{bC^{b-1}\left(C^{b+1}\ Voc + Vm\right)}{(Voc\ C^b + Vm)} \exp\left(\left[\frac{Voc\ C^b}{Vm}\right]\right)$	Reliable and accurate; expose the computational models of the series resistance Rs	[48]
4	$Rs = \frac{C^{\frac{Isc}{Im}} VmVoc}{Isc\left(C^{\frac{Isc}{Im}} Voc + Vm\right)}$	Extract the parameters by using the standard diode model;	[48]
5	$Rs = \frac{(Vm(Isc - Im) - CImVoc)\log\left(1 - \frac{Im}{Isc}\right)}{Im\left(Im + (Isc - Im)\log\left(1 - \frac{Im}{Isc}\right)\right)}$	For estimation required only nameplate values	
6	$Rs = \frac{Vm}{Im} - \frac{2Vm - Voc}{Im + (Isc - Im)\ln\left\{1 - \left(\frac{Im}{Isc}\right)\right\}}$	Maximum Point method. One diode model; For estimation required only nameplate values	[158]
7	$Rs = \frac{Voc}{Isc} - \frac{Vm}{Im}$	The Simplified maximum point method, One diode model; Rs value can be obtained by this approach from a single I-V curve,	[113]
8	$Rs = \frac{\Delta V}{Im} = \frac{Videal - Vm}{Im}$	One diode model was applied, and only one I-V characteristic needs to be raised; Due to less parameter in considerably less precision.	[159]
9	$Rs = \frac{rs.Voc}{Isc}$	Methodology to model the Rs using the three environmental factors, the ambient temperature, the incident irradiance and the wind speed.	[116]

3.3.2 Estimation of series resistance using IEC 60891

In order to measure the series resistance using the IEC 60891 Procedure I, a test setup has been developed to measure electrical parameters at different irradiance levels. The test modules have been covered with a wire mesh screen to reduce the irradiance level without any change in the spectrum and module temperature as shown in Fig.3.4.

Fig 3.4. Mesh used to take the I-V at the same temperature

The mesh used for the analysis needs to be spatially uniform, and for this, the transmissivity of the mesh has been determined for different parts using the irradiance above and below the meshes. The error in transmissivity level is found to be less than 2% for the entire mesh. The I-V characteristics of the modules have been measured using the PVPM under different ambient conditions with and without the wire mesh screen [160].

The measurements have been taken at different irradiance levels, constant ambient temperature, and continuous spectrum. For the two consecutive sets of I-V measurements, the difference in the temperature of the test module and pyranometer is held constant within ± 2 °C. The I-V curve data are used to determine the Rs of solar modules using the procedure I described in international standard IEC 60891 Edi. 2.0. The measured data in the irradiance

range of 50-150 W/m^2, 150-250 W/m^2, 250-350 W/m^2, 350-450 W/m^2, 450-550 W/m^2, 550-650 W/m^2, 650-750 W/m^2, 750-850 W/m^2, 850-950 W/m^2, 950-1050 W/m^2, have been corrected to voltage and current at alternative reporting condition for 100 W/m^2, 200 W/m^2, 300 W/m^2, 400 W/m^2, 500 W/m^2, 600 W/m^2, 700 W/m^2, 800 W/m^2, 900 W/m^2 and 1000 W/m^2 respectively at 25°C, 35°C and 50°C module temperature.

The estimation of Rs has been carried out using the procedure I of IEC 60891. The first I-V curve (with I_1, V_1 as the coordinates) measured at higher radiation is taken as the reference curve, and the corresponding power P_1 is considered as the reference power. The reference I-V curve is then translated by putting the value of series resistance as 0 Ω, to begin with, and the deviation Δ of power from P_1 determined. This process is repeated by changing the value of series resistance in steps of 0.01 Ω until the value of Δ reaches up to 0.5% or less. Total of three I-V characteristic curves will be read at varying irradiance and will be transferred to their mean irradiance. The Rs value transported after the curve correction considered to the minimum value of Δ (Rs mean).

3.3.3 Uncertainty analysis of the estimated data

The uncertainty in the measurement devices and in the measurement is calculated according to the 'Guide to the expression of uncertainty in measurement' [GUM, (JCGM 100.2008, 2008)]. The objective of the study is to incorporate various causes of uncertainty while collecting the data, filtration and analysis over the data. The uncertainty calculation has been done on the three different technologies for three irradiance range. The uncertainty including Type "A" and Type "B" is used to report in the thesis. The mathematical expressed in presented in Table 3.2.

Resistance = f (Irradiance, Temperature, Current, Voltage)

Table 3.2. The parameter for the assessment of uncertainty using GUM

Type of Uncertainty	Parameter	Mathematical Representation	Degree of Freedom
TYPE A. Evaluation of standard	Arithmetic Mean or Average	$q = \frac{1}{n}\sum_{k=1}^{n} q_k$	

uncertainty.	The variance of the probability distribution of q	$S^2(q_k) = \frac{1}{n-1}\sum_{j=1}^{n}(q_j - q)^2$	The degree of freedom = n-1
	The experimental standard deviation of the mean S2 (q), Variance of mean	$S^2(q) = \frac{S^2(q_k)}{n}$, $S^2(q) = \sqrt{\frac{1}{n-1}\sum_{j=1}^{n}(q_j - q)^2}$	
TYPE B. Evaluation of standard uncertainty	Combined standard uncertainty.	$U_C = \sqrt{U_A^2 + U_{B1}^2 + U_{B2}^2 + U_{B3}^2 + U_{B4}^2 + U_{B5}^2 + U_{B6}^2 + U_{B7}^2 + U_B^2}$	The degree of freedom = n-1
	Expanded uncertainty. For a 95.45% level of confidence the coverage factor K=2	$U = K\,U_C(eff)0$	

3.4 The methodology adopted to fulfill the objective-III "Effect and analysis of the shading losses and develop the modelling of the losses as heating effects."

The motivation for this study mostly comes from the fact that reliability studies on the high-efficiency modules are practically not existed in India, and without this kind of studies, it would be impossible to predict the operation of modules in field installations. To address the need and study the thermal stress in a different module technology under arbitrary patterns of illumination, a methodology has been developed for studying different Infra-Red images by short-circuiting the SPV modules for 10 mins. The experiment is also extended by the short-circuiting the solar module up to 2 hours and the hotspot, so obtained can be regarded as the worst-case scenario. Under normal operation of the solar module at maximum power points, the hotspots are expected to be much less severe (since the module at MPPT would not be dissipating the total input energy as heat as would happen in the case of short-circuited modules).

The work focuses on studies based on the temperature distribution of solar module technologies. It primarily targets the total four different

technologies, Mono-crystalline (m-si), Multi-crystalline (mc-si) modules including two high-efficiency technologies, namely Silicon hetero-junction technology (HIT), Interdigitated back-contact cell technology (IBC). The methodology adopted in this work essentially entails exposing some of the modules to outdoor conditions and recording their electrical output parameters through a data logger on a continuous basis. Along with these, Infra-Red imaging techniques used for a definite time interval to identify the possible forms of defects and their progression in the solar modules. The four solar module technologies are deployed in the outdoor field since 2014 working in a loaded condition. The I-V tracer and weather and weather monitoring station have been used for the measurement of current-voltage characteristics and environmental parameters respectively. The methodology used for the study is presented below in Fig 3.5.

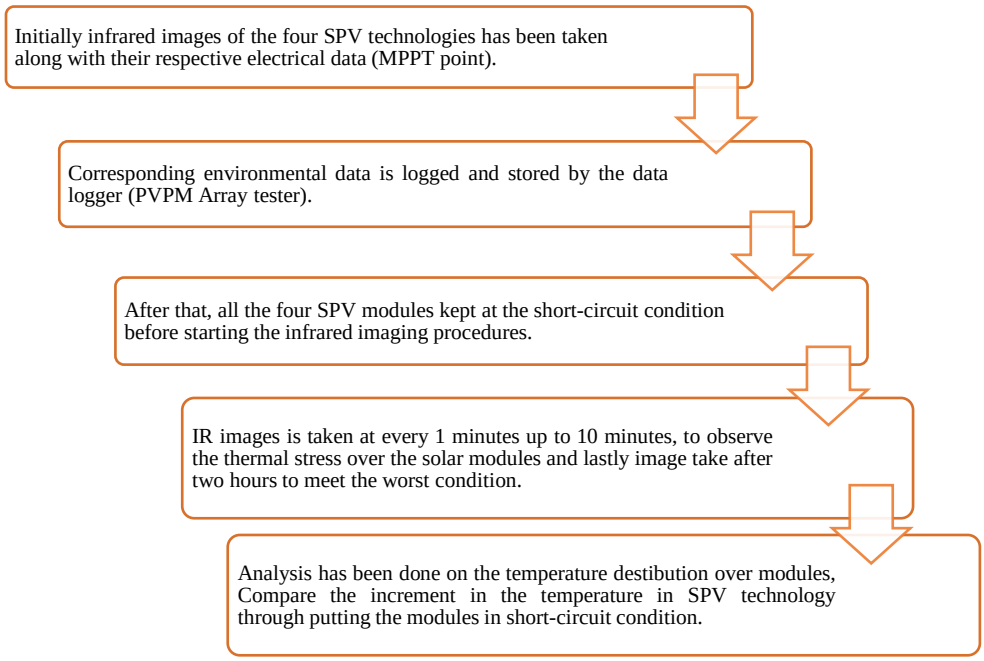

Fig 3.5. Flowchart of the methodology followed in the Infra-Red analysis.

The study covers the different temperature profiling configuration in the association of the solar cells in PV modules and monitors the thermal impact and its corresponding electrical parameters simultaneously. Schematic block circuit diagram of the experimental set-up including the data logger is shown in Fig 3.6.

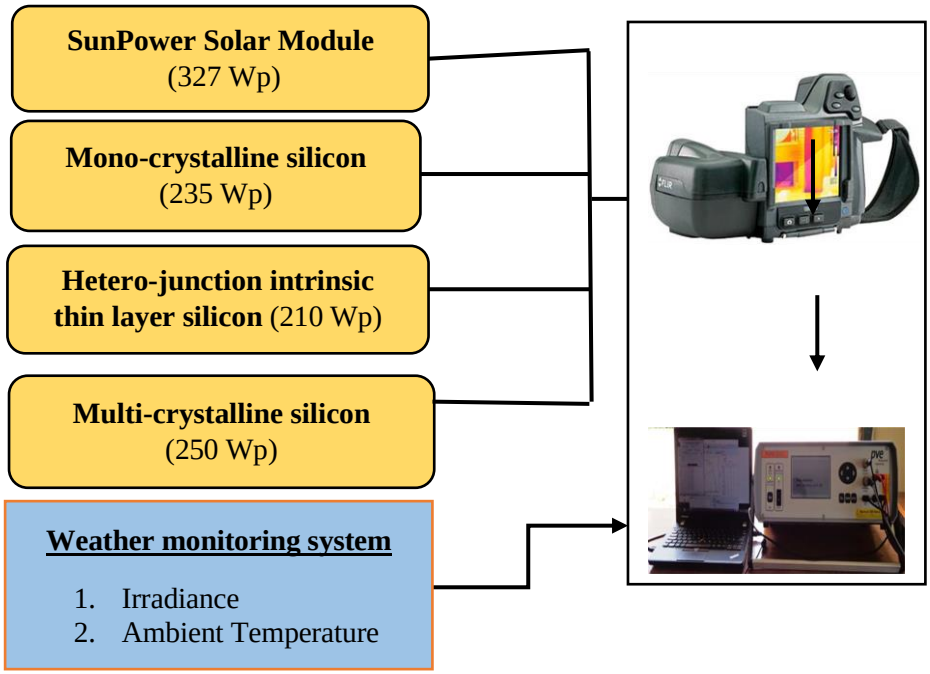

Fig 3.6. Schematic block circuit diagram of the experimental set-up including the data logger.

The experiment focused on performing various shadow configuration, the utilization of the bypass diodes in the modules, usually three diodes placed in series connection over 60 solar cells in modules. The Infra-Red images of the SPV modules have been taken at the interval of 10 minutes for 2 hours in short-circuited condition, to find the heated up solar cell. The hot spots obtained in the short-circuited state can be considered as the worst-case scenario since this causes the solar cell to sink tremendous amount of power which is the product of the reverse bias voltage and the module operating current. Whereas in the MPPT condition, the hot spots are expected to be less severe, but more representative of actual operating conditions. The shading profile has been created in the percentage as the numbers of cells are different in each solar module. The different shading configurations in loaded conditions are as follows;

- Solar modules Unshaded condition
- 10% of one string in the solar modules
- 50% of one string in the solar modules

- 100% of one string in the solar modules
- 10% of two string in the solar modules
- 50% of two string in the solar modules
- 100% of two string in the solar modules
- 10% of three string in the solar modules
- 50% of three string in the solar modules

Since the IR images have been taken at a different time of day having different ambient conditions, it is necessary to normalize the measured temperature data to the reference condition to enable the comparisons between the different images. The temperature has been normalized to the reference condition of 1000 W/m^2 and 40 °C using the relation (Dubey et al., 2017);

$$T_{normalized} = 40 + \frac{(T_{measured} - T_{ambient}) * 1000}{Irradiance} \quad (44)$$

Where $T_{normalized}$ is translated (normalized) temperature.
$T_{measured}$ is module temperature (obtained from IR images)
$T_{ambient}$ is an ambient temperature measured at the site.

The IR images and electrical measurements have been analyzed under several configurations, to assess the performance of SPV module after three years of outdoor operations, about the identification of the hotspot defect. Subsequently, the use of the thermography techniques is emphasized and elucidated for the detection and characterization of the SPV modules degradation. The results comprise of the thermal impact of the surrounding temperature over the PV modules in outdoor condition, Hotspot formation, Impact of various shading configuration in the loaded state, analysis of the electrical behaviour of the field aged solar module technologies.

This section has outlined the theoretical framework for the study, pragmatism, and discussed why it is particularly suited to this study. The data collection method for quantitative and qualitative methods was discussed. This completes the discussion on the research methodology adopted for the study as well as the fulfilment of the research objectives. The next section discusses the

various experimental set-up and instruments used in the study to identify the performance and challenges.

3.5 Climatic condition: The composite climate of Gurugram

The experiments based on the characterization, performance assessment and degradation rate calculation along with the measurement uncertainties have been carried out in the National Institute of Solar Energy, Gurugram in India. The latitude and longitude of Gurugram is 28.4595° N, 77.0266° E respectively, with an altitude of 216 m above sea level.

The hourly, daily, monthly average irradiance at the test facility for three consecutive years is presented in Fig 3.7. It shows that the highest irradiation occurring during the March followed by April and lowest in January for 2010, highest in March, April and lowest in August for 2011 same pattern is followed in 2012.

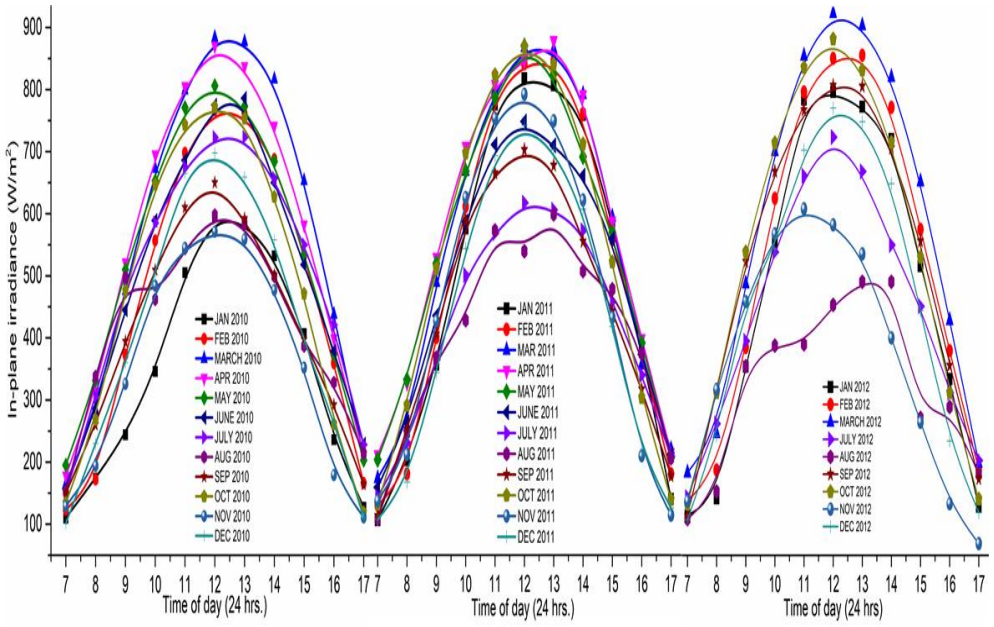

Fig 3.7. The time series of daily, hourly monthly average in-plane irradiance (W/m^2) for three years

From Fig 3.8, the highest frequency occurred in the lower range at 200 W/m^2 whereas in a higher range the highest irradiance frequency range is at 800 W/m^2. It is evident that for the site the most frequent condition (MFC) is having a radiance range between 750 Wm^2-850 W/m^2 at a temperature range between 35 °C - 45 °C.

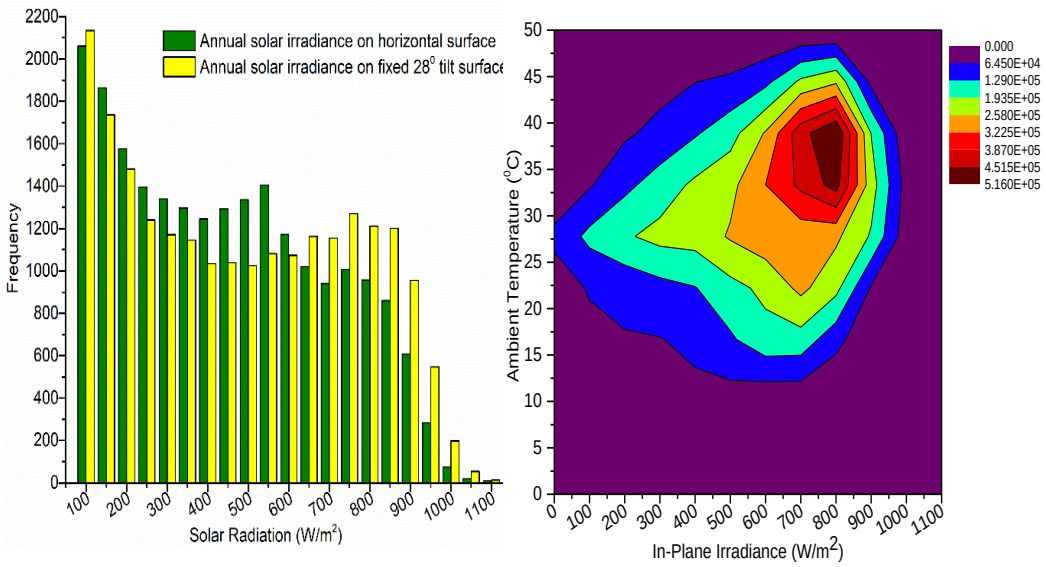

Fig 3.8. Distribution of yearly solar irradiance in the horizontal surface and on fixed 28° tilt surface and the most frequent condition at Gurugram.

The time series of the ambient temperature (°C), wind speed (m/Sec) and the relative humidity (RH) measured over three years are plotted in Fig 3.9.

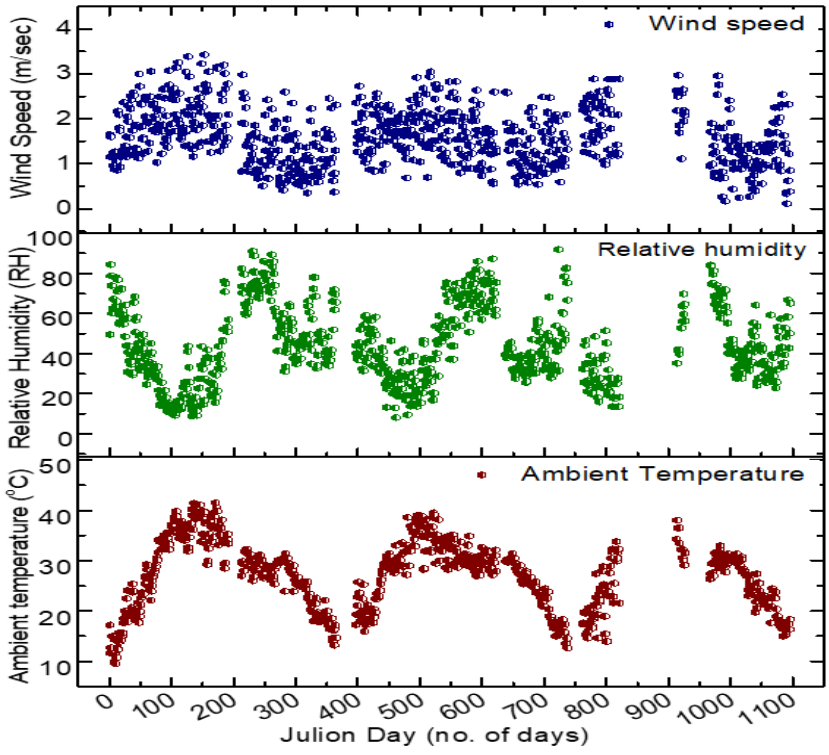

Fig 3.9. The time series of wind speed, relative humidity and the ambient temperature for three years.

It is apparent that the seasonality impact visible over the ambient temperature, relative humidity, and wind speed. The duration of the summer was the warmest whereas the lowest ambient temperature occurred in the winter season. Also, the relative humidity is complimenting to the ambient temperature, i.e. when the temperature is higher the humidity shows its lowest value. The wind speed is between the 0.3 m/sec to 3.8 m/Sec thought out the three years.

For the experimental site, the hottest month is June considered by the average temperature value of 36.23 ^{o}C whereas the minimum average is about 14.78 ^{o}C in the month of January. The monthly average wind speed is presented in Fig 3.9. The highest monthly average value of the wind speed is recorded in the month of June whereas the lowest in November month. The wind speed and wind directions are a very crucial and imperative factor for the evaluation of the PV module's productivity due to its influence on the cooling of the surface of the SPV module by heat convection. The monthly average values of the wind speed are in the range of 1.008-2.32 m/Sec. Moreover, another climatic factor which would influence the performance of is the monthly average humidity. The monthly average values of the relative humidity during the testing period is in the range of 13.45-73%. The highest relative humidity is recorded in August whereas the lowest in April month.

3.6 Outdoor experimental set-up

The description of the electrical parameter, I-V characteristics curves and thermal parameters like the temperature of PV modules along with weather data representing the ambient temperature, wind speed and in-plane solar irradiance are compiled in this section. In this study, the performance evaluation of three-year outdoor exposure solar modules was carried out using the methodology discussed in chapter 3.

3.6.1 Data Acquisition Hardware and Sensors; Data Sources.

Electrical parameters of SPV modules have been monitored and collected using a data logger and an SPV scanner (Kernel System, PVC01802). The global solar radiance was measured using a pyrometer of EKO, MS 802C. The solar radiation intensity is measured on the horizontal surface and at the tilt

of PV panels using two Pyranometers. The linearity of the pyranometers is 0.5% from 0 to 2800 W/m^2 and sensitivity of 7 mV/W/m^2.

The total irradiance in plane of array (POA), the ambient temperature (Tamb), the wind speed (Sw) and wind direction (aw), Relative Humidity (RH), atmospheric pressure (atm) along with the electrical data like maximum power (P_m), current (Im) and voltage (Vm), open-circuit voltage (Voc), short circuit current (Isc), module temperature (Tm) was measured and recorded simultaneously. The module temperature is measured at three different places of SPV modules i.e. upper, bottom and middle. The average of the module temperature been used in the study for the input of the calculations. The outdoor facility of test set-up along with the weather sensors for data monitoring is shown in Fig 3.10.

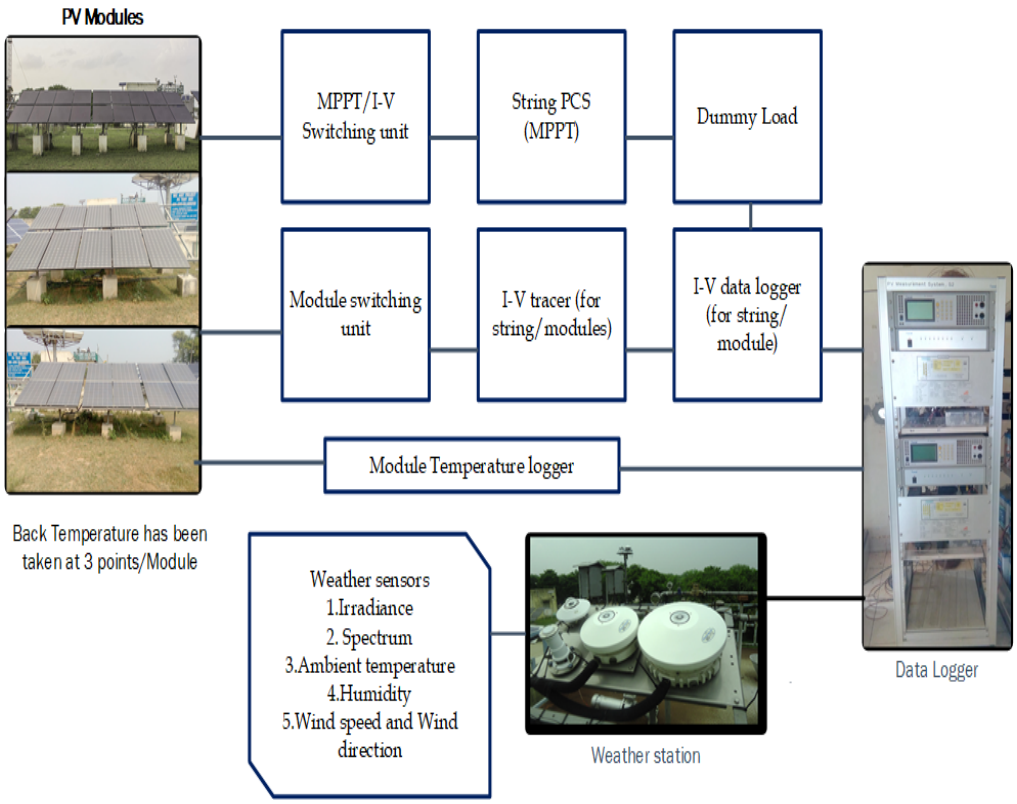

Fig 3.10. The schematic diagram of the experimental set-up for data monitoring system

All the sensors were calibrated during the testing and data analysis period. The system description is presented in Table 3.3.

Table 3.3. Specification of weather station instruments.

Instrument	Significance	Accuracy	Make
Pyranometer	To measure the solar irradiance	±10 W/m²	EKO, MS 802C
Humidity and Temperature probe	To measure the humidity and module back surface temperature	±1.7% for RH, ±0. 2 °C for temperature	Vaisala
MS-710 and MS-712 Spectro-radiometer	To measure the spectrum.	The wavelength, accuracy ±0.2 nm Accuracy of 0.5°	EKO
Wind sensor	To measure the wind speed and wind direction.	± 0.3 m/s, ± 3°	Young

Periodic calibration and inspection of the measuring sensors have been a performance to ensure the true values of the measurement. Additionally, all sensor cabling and connection terminals are periodically checked to avoid the moisture ingress, cracks and lose connection.

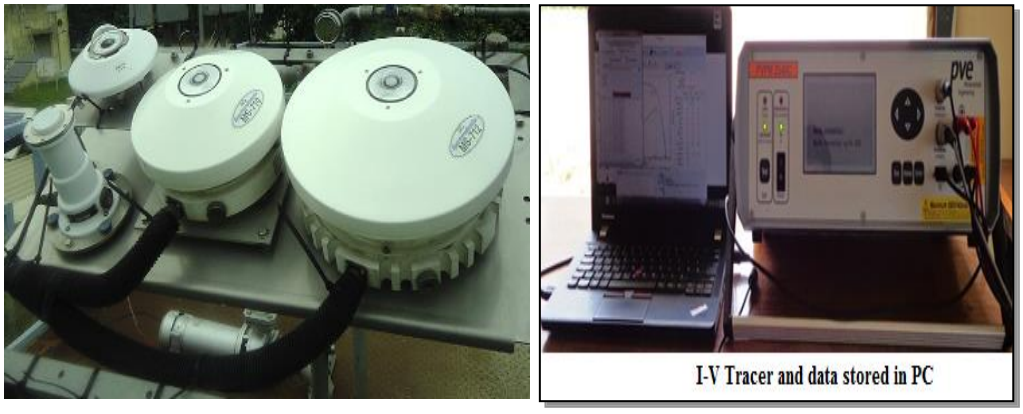

Fig 3.11. The weather monitoring and I-V tracer system at NISE

The I-V characteristics of the modules have been also measured using the PVPM under different ambient conditions as per the need of the different experiment shown in Fig 3.11. The technical specification of the PVPM is given in Table 3.4.

Table 3.4. Technical specification of the PVPM.

Model	PVPM2450C
Voltage DC (V)	Accuracy ±2 % for voltage.
Current DC (A)	Accuracy ±2 % for current
Temperature	-40°C- +120 °C with pt1000
Irradiance	Model. SOZ-03, 0-1300 W/m^2

The temperature sensor is thermally attached by a thermal conducting adhesive and insulated from the ambient temperature effect. The monitoring set-up achieves and stores the real-time measurement of the solar device continuously. The I-V tracer equipment is connected to a Data Acquisition System (DAS) which is further connected to the PC.

The SPV modules technologies were mounted on the same stand-alone frames in the same inclination angle of SPV modules at outdoor testbed. The SPV modules were placed on the south-facing structure at a fixed tilt angle of 28^o with the horizontal plane. The SPV technologies as the mc-si containing 42 cells, HIT containing 104 cells and a-Si comprising 110 cells, PERC having 60 cells and SunPower modules containing 60 cells have been used for the performance monitoring and analysis. All the modules were ground-mounted on metal frames over a height of 1 meter and installed at south facing with a tilt angle of 27.5 for optimal energy yield at Gurugram. The technical specifications provided by the manufacturer for each SPV module technology documented in Table 3.5.

Table 3.5. The technical specification of the SPV modules used in the study

Parameter	**PV modules specification**					
Type	PERC	Hetero-junction silicon	SunPower	Multi-crystalline silicon	Mono-crystalline	Single junction a-Si
Maximum power (W)	295	210	327	160	235	75
Maximum voltage (V)	32.5	59.7	54.7	21.28	30	67
Maximum current (A)	9.08	3.52	5.98	7.52	8	1.12

Open circuit voltage (V)	39.7	73.6	64.9	25.60	37	91.8
Short circuit current (A)	9.55	3.79	6.46	8.42	8.60	1.4
The temperature coefficient of voltage(%/K)	-0.29	-0.30	–176.6 mV/K	-0.34	-0.31	-0.39
The temperature coefficient of the current(%/K)	+0.05	+0.05	3.5 mA /K	+0.06	0.052	+0.05
The temperature coefficient of the power (%/K)	-0.39	-0.30	– 0.38 %/K	-0.43	-0.41	-0.35
Spectral response range (nm)	300 – 1200	350-1200	300-1200	350-1200	350-1200	330-800

Periodic cleaning of the environmental sensors and system was further performed when the SPV system and array were cleaned too. The SunPower array is shown in Fig 3.12.

Fig.3.12. A testbed of the SunPower based MAXEON^{TM} technology

3.7 PV modules performance analysis and degradation

This measurement is done to study which module of the array is degrading faster, or the position dependence of degradation in PV modules. The software consists of programs for sensing weather sensors, estimating, averaging, integrating and tabulating weather parameters.

3.7.1 Electrical Characterization measurement arrangement

The important measurement to estimate PV array parameters is V_{OC}, I_{SC}, P_{MAX}, FF, R_{Sh} and R_S; along with these parameters, it scans complete I-V at every preselected interval. This would enable to estimate the energy yields for a day. After completing the scanning, the remaining period between scans the array will be operating at the maximum power point should be within the measurement limits of the PV scanner or analyser used in the system. Ideally, it is preferred to have one I-V scanner for each technology array. However, this would be very expensive; so, it is better to have one I-V scanner and a multiplexer which is an inexpensive option. But in such case measurement of individual PV module I-V within the PV array is curtailed. The embedded device collects all data from weather sensors, forms tables in the database using MySQL freeware database package. It is possible to create CSV files containing an individual table, as well as the entire database.

The data can be collected over large time and data for a specific period can be easily selectable for a specific period. The software also includes programs for I-V measurements of PV arrays and modules against time. This operates only during the sunny hours of the day. The heart of the data logging facility is the timestamp facility, which helps the user to view and compare I-V curves over the selected time period for different technology modules.

This is achieved by using the indexing feature of database tables so that the insertion and retrieval of data can be fast, even if the span of data is between years. It is estimated that for a day, about 230KB is required for weather data and about 3MB is required for storing PV monitoring data for one technology. The data acquisition system process is shown in Fig 3.13.

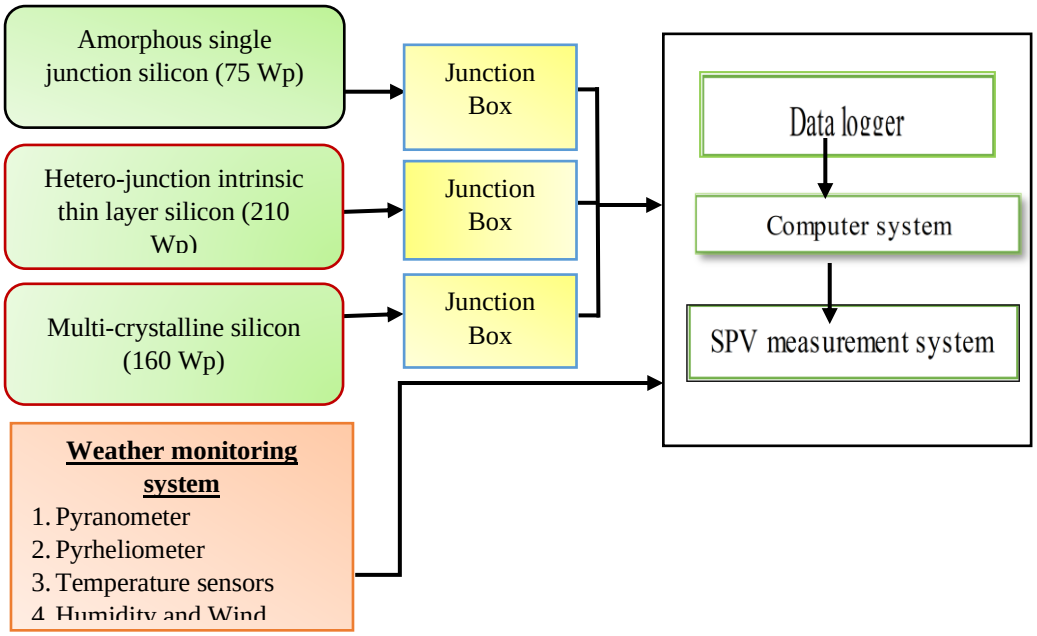

Fig 3.13. Experimental set-up for performance monitoring at NISE, Gurugram.

The data in the outdoor field is also taken for several experiments using the PVPM I-V scanner. The devices of type PVPM enable the measurement of the I-V-curve of photovoltaic modules as well as of strings. By a newly developed procedure, the device can measure and calculate the peak power Ppk, the Rs and Rp directly at the place of assembly of the PV system. Calculation results and the diagram can be displayed on the internal LCD-display. The PVPM is a mobile measuring device with integrated battery supply and charge controller in a durable metal housing shown in Fig 3.13.

The device has its own industrial miniature PC and a high-contrast LCD display and thus its function is independent of other devices. However, if desired a PC can be attached for data transfer and further analysis of the measured values over a standard interface. The PVPM is operated comfortably over a few keys and an on-screen menu. The functions are defined self-describing and the user is always led by the program. So, no long training activities for the operating staff are necessary. The PVPM automatically measures the I-Characteristic of the generator at a capacitive load. From the measured data, it calculates the effective solar cell characteristic, Ppk and Rs.

The I-V-characteristic can be shown directly on the LCD display. After the measurement, the data are stored automatically in non-volatile storage and so are available also. The device internally stores the data of several 1000 measurements. The following results are displayed. Peak Power PPk

- Internal Series Resistance Rs
- Internal Parallel Resistance Rp
- Current values, depending on irradiation and temperature.
- Vpmax, Ipmax, Pmax, Voc, Isc, FF, Tmod, and Eeff.

The PVPM is a mobile measuring device with integrated battery supply and battery charger in the durable aluminium housing. The device has its own industrial miniature PC and a high-contrast LCD display and thus its function is independent of other devices. However, if desired a PC can be attached for data transfer and further analysis of the measured values over a standard USB interface. The PVPM is operated comfortably over the front panel keys and an on-screen menu. The functions are defined self-describing and the user is always led by the program.

The performance ratio, thermal factor, spectrum factor and the efficiency in solar modules were studied by the data obtained by the about system using the mathematical modelling. Continuous data monitoring of the system has been done also the stability tests were performed for the various durations of time with specific intervals.

3.7.2 Optical Characterization

The field aged SPV modules have been investigated using Forward-Looking Infra-Red (FLIR) Camera and measurement of electrical parameters such as voltage and current as shown by the graphical representation of the experimental setup in Fig 3.14.

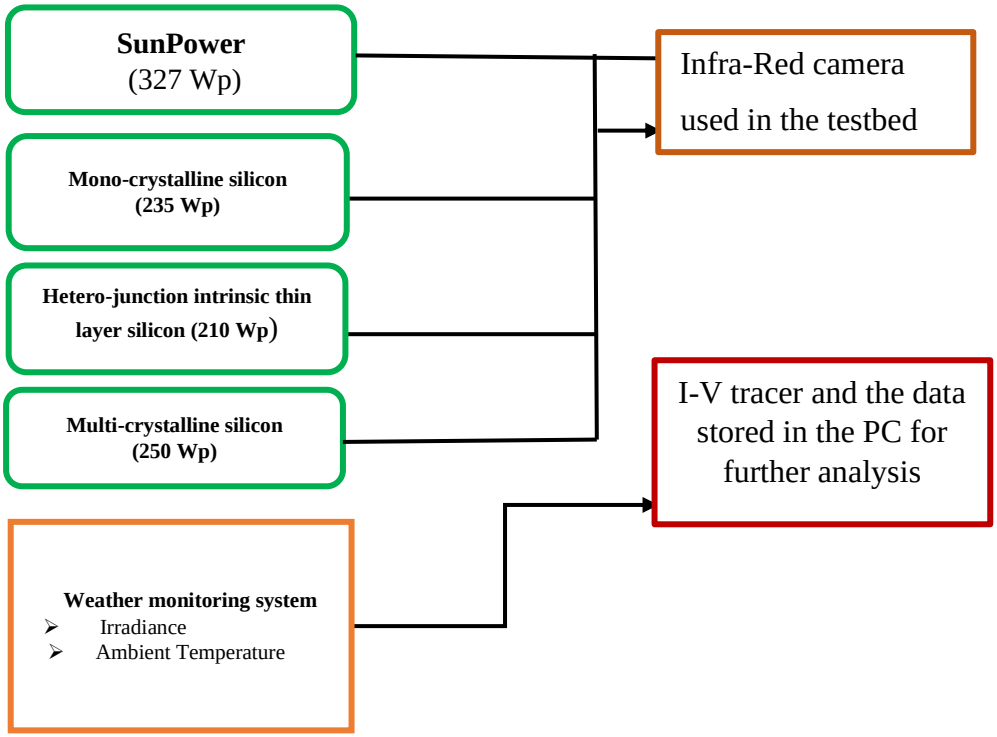

Fig 3.14. Experimental set-up for mapping thermal-stress monitoring at NISE, Gurugram.

The four solar module technologies are deployed in the outdoor field since 2014 working in a loaded condition. The I-V tracer and weather and weather monitoring station have been used for the measurement of current-voltage characteristics and environmental parameters respectively. The technical specifications of the FLIR camera are shown in Table 3.6.

Table 3.6. Specification of the Infra-Red camera used in the testbed

S. no	Specifications	Ranges
1	IR resolution	320 × 240 pixels
2	Thermal sensitivity/NETD	<45 mK @ +30°C (+86°F)
3	Object temperature range	–20°C to +120°C (–4°F to +248°F); 0°C to +650°C (+32°F to +1202°F)

4	Accuracy	±2°C (±3.6°F) or ±2% of reading, for ambient temperature; 10°C to 35°C (+50°F to 95°F)

The study aims to cover different temperature profiling configuration in the association of the solar cells in PV modules and monitor the thermal impact and its corresponding electrical parameters simultaneously. The experiment also focused on performing various shadow configuration, the utilization of the bypass diodes in the modules, usually three diodes placed in series connection

3.8 Conclusion

In conclusion, the chapter discussed the importance of quantitative and qualitative methods used in the study have been explored and explained, with detail given to choose of the method along with consideration to attain overall research quality. The chapter explains all the experimental aspects involved in this research work. The materials and the instruments used in this work are listed briefly. Basic steps followed for the performance monitoring are outlined along with their structural, electrical and optical characterization techniques. The steps involved in performance monitoring, reliability and degradation are described with the characterization tools for material's property and performance correlation.

CHAPTER 4

TO STUDY THE PERFORMANCE, RELIABILITY, AND DEGRADATION IN THE COMPOSITE CLIMATE OF INDIA

The performance of the SPV at real outdoor condition has been studied based on the filtering techniques, performance monitoring metrics and numerical methodologies. A set of nine SPV modules consisting multi-crystalline (m-si), Heterojunction with Intrinsic Thin layer (HIT) and amorphous silicon (a-si) each were characterized for a period of three years under the composite climate of India. The estimation of monthly average effective peak power (P_{eff}), performance ratio (PR) and temperature corrected performance ratio (PR_{CORR}) has been done.

4.1 Introduction: Performance. Reliability and degradation.

The different SPV technology module having different material properties, temperature coefficients, spectral capturing capacity, current and voltage as well as their reaction towards environmental parameters such as radiance, temperature, humidity, and wind speed also differ. Although it is a known factor that the efficiency and performance of the SPV modules change according to the climatic conditions like temperature, spectrum, radiation and wind speed, etc. determination of the true efficiency values in outdoor field condition is a major task [161]. The reliability and degradation studies on the crystalline-based SPV module is already available for many climatic zones but for the high-efficiency technologies like PERC, SunPower and HIT SPV technology, the study is utmost important for proper utilization of the technology in other climatic zones [93].

This chapter contains, comparative performance analysis of the different silicon-based module technologies under the composite climate based on monthly average effective peak power, monthly average performance ratio, monthly average temperature corrected performance ratio and monthly average efficiency; secondly to estimate the degradation rate based on the linear regression over the effective peak power, assessment of the series resistance by the procedure I provided in the IEC 60891 Edi. 2.0, its increment in the three years and its associated measurement uncertainty. The results and discussion are used for the evaluation of the effective peak power, performance ratio, efficiency, degradation rate and the estimate of series resistance. The paper ends with a conclusion.

4.2 Methodology

The detailed methodology and the experimental set-up used for the performance analysis has been presented in chapter 3 in the flowchart and discussed in the subsections. The sampling of the modules has been done as per the requirement. The sampling plan applied to each module make the correct decision and the bottom-line approach is to not consider visually observed defective modules, which would give a false interpretation of average plant performance.

The first step toward the analysis of the performance evaluation, analysis and degradation rate calculation was to extract and filter the outdoor measured experimental data set for each SPV system. The synchronization of the electrical data and the environmental data at10 minute average data has been done using the SQL programmed based on Microsoft Access. The raw data were collected and filtered for the night period and outage period.

The second step where the calculation of the performance parameters on the basis of the obtained data for each SPV module using the mathematical formulas. Then construct time series of the nine SPV modules based on the calculated monthly average effective peak power of the SPV modules, the performance ratio which is calculated on the basis of the raw data obtained from the outdoor measurements for a three-year period. The temperature corrected performance ratio has been calculated using the product of the performance ratio

and the thermal factor. Based on the time series on the monthly average effective peak power, the degradation rate has been calculated for nine SPV modules. All the constructed and calculated time series has been analyzed by employing the commonly used statically techniques of the linear regression to calculate the degradation rate of each PV module.

4.3 Results and Discussion

The composite climatic of the Gurugram has been analyzed in terms of the in-plane irradiance, ambient temperature, humidity, and wind-speed in chapter 3. The detailed discussion and the graphs are presented in the chapter-3.

4.3.1 Estimation of the monthly average effective peak power of the SPV modules

To calculate the monthly average effective peak power of nine SPV module technologies, the thermal factor of each module has been calculated using the Equations at chapter 3 over a period of three years presented in Fig 4.1 and 4.2. The impact of the seasonal variation is clearly evident over the thermal factor of the SPV modules has been observed for the representative SPV modules as they have similar results for the same technology module.

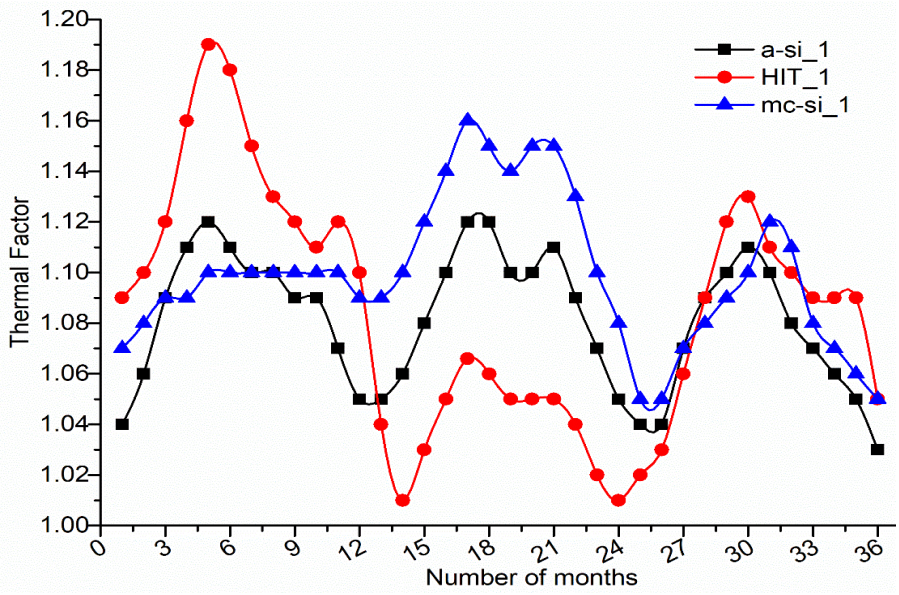

Fig 4.1. Thermal Factor of three silicon-based technologies above 800 W/m^2

The thermal factor has been utilized to estimate the effective peak power of the SPV module technologies. The maximum impact of the season is visible over HIT solar modules whereas the least impact is recorded for the a-si SPV module.

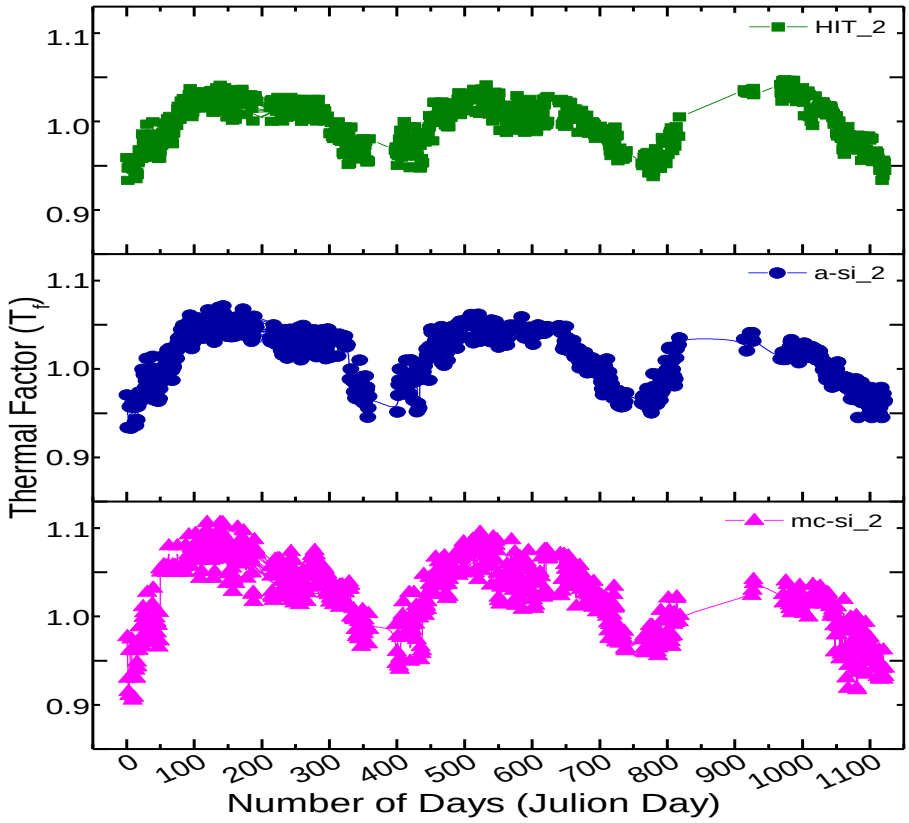

Fig 4.2. The time series of the thermal factor for HIT, a-si and mc-si technology modules for three years.

The estimation of the monthly average effective peak power of the nine SPV modules presented in Fig 4.3. The effective peak power (W) range for mc-si modules is 126-154, 121-152, 120-149 for mc-si_1, mc-si_2 and mc-si_3 respectively over a period of three years. The highest effective peak power is documented in January and November month. Similarly, the P_{eff} for HIT modules is in the range of 195.87-224, 196-224 and 199-224 (W) for HIT_1, HIT_2 and HIT_3 modules respectively. The highest effective power is documented in January month. For a-si modules, the range is 58.92-84, 58.71-

83.43 and 58.66-84.22 (W) for a-si_1, a-si_2 and a-si_3 respectively. The highest effective peak power is documented in the April month for a-si modules.

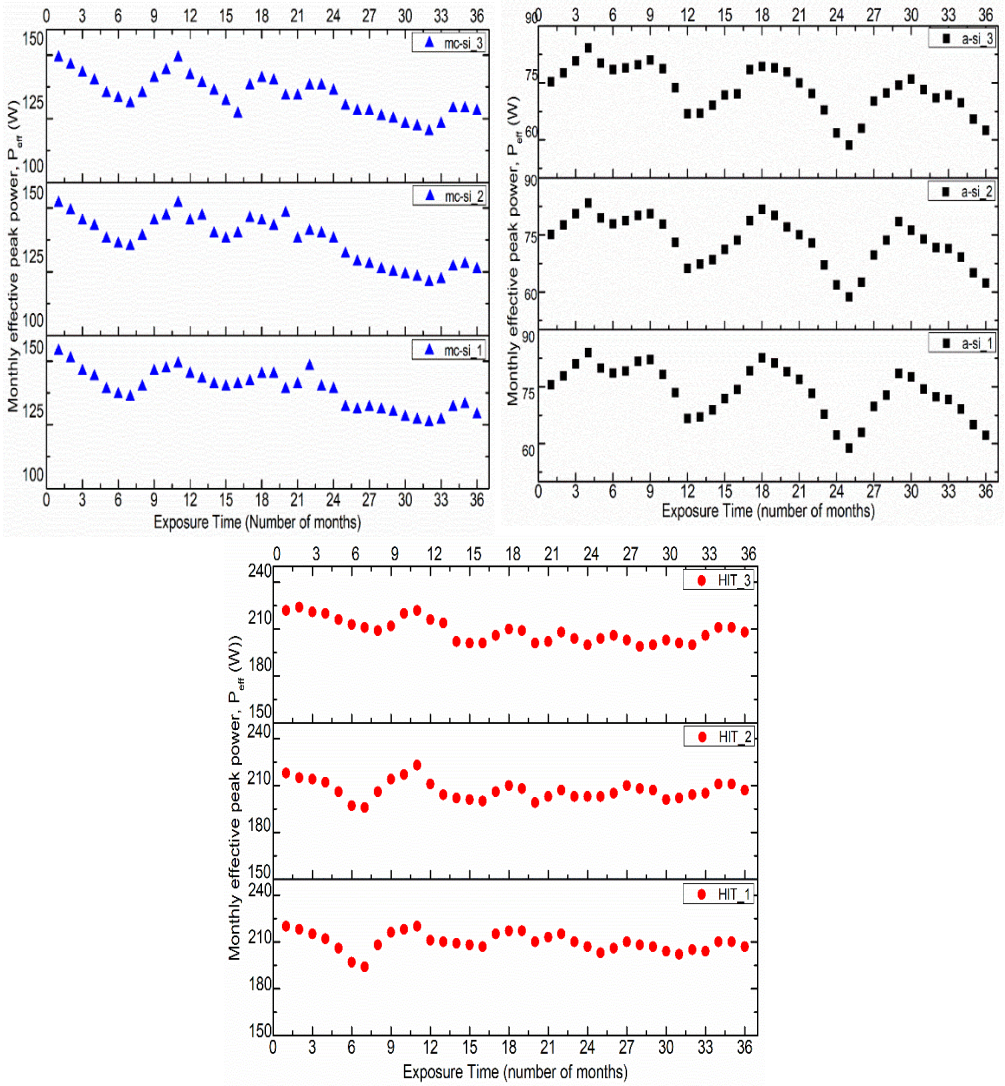

Fig 4.3. The monthly average effective peak power of the nine SPV modules over a period of three years

As it is clearly visible that the decreasing rate of the monthly effective peak power (P_{eff}) depends upon the environmental factor as well as material properties of different technologies of SPV module. The seasonal impact over effective power is visible for all nine SPV modules. The highest impact of the seasonal variation is visible over a-si modules and at least over the HIT modules. The effective peak power of the a-si modules significantly decreasing on the winter seasons i.e. in the month on November and December while the

highest effective peak power is observed in the warmer months. The effective peak power of the a-si module indicates that the SPV module is best suited for the hot climatic conditions. For HIT module technology, the effective peak power is least depending upon the seasonal variations. The effective peak power of the modules better in the winter months in comparison to the warmer months. The cooler ambient temperature helps to gain less module temperature and hence the performance improve by improving the open-circuit voltage. The m-si module shows the highest effective peak power decrement over a time period of three years among the other three technologies. The m-si module also exhibits the variation against the seasonal changes.

The estimation of the effective peak power has been done for three years and the percentage variation for a period of three has been done. The percentage variation is 16.22 %, 17.10 % and 14.09 % for mc-si_1, mc-si_2 and mc-si_3 respectively over a period of three years. The percentage variation is 17.71%, 17.04% and 16.96 % for a-si_1, a-si_2 and a-si_3 SPV module technologies. The percentage variation is 7.58 %, 7.58 % and 6.30 % for HIT_1, HIT_2 and HIT_3 modules respectively. The HIT module shows the least decrement of effective peak power for the three-year time period. The trend line over the monthly effective peak power later used to estimate the degradation rate of the nine SPV modules.

4.3.2 Estimation of the monthly average performance ratio, temperature corrected performance ratio

The monthly average performance ratio of the nine SPV modules of three silicon-based technologies has been calculated. The performance ratio of the mc-si, a-si and HIT modules are shown in Fig 4.4. The performance ratio is between the 0.65 to 0.88, 0.61 to 0.83 and 0.60 to 0.81 for mc-si_1, mc-si_2 and mc-si_3 modules respectively over a period of 36 months. The decrement in the performance ratio has been observed on time series of the mc-si modules technology. The performance ratio for a-si modules are 0. 72 to 0.90, 0.73 to 0.90 and 0.78 to 0.90 for a-si_1, a-si_2 and a-si_3 respectively. The monthly performance ratio for the HIT modules is in the range of 0.70 to 0.94, 0.74 to 0.95 and 0.75 to 0.93 for HIT_1, HIT_2, and HIT_3 respectively.

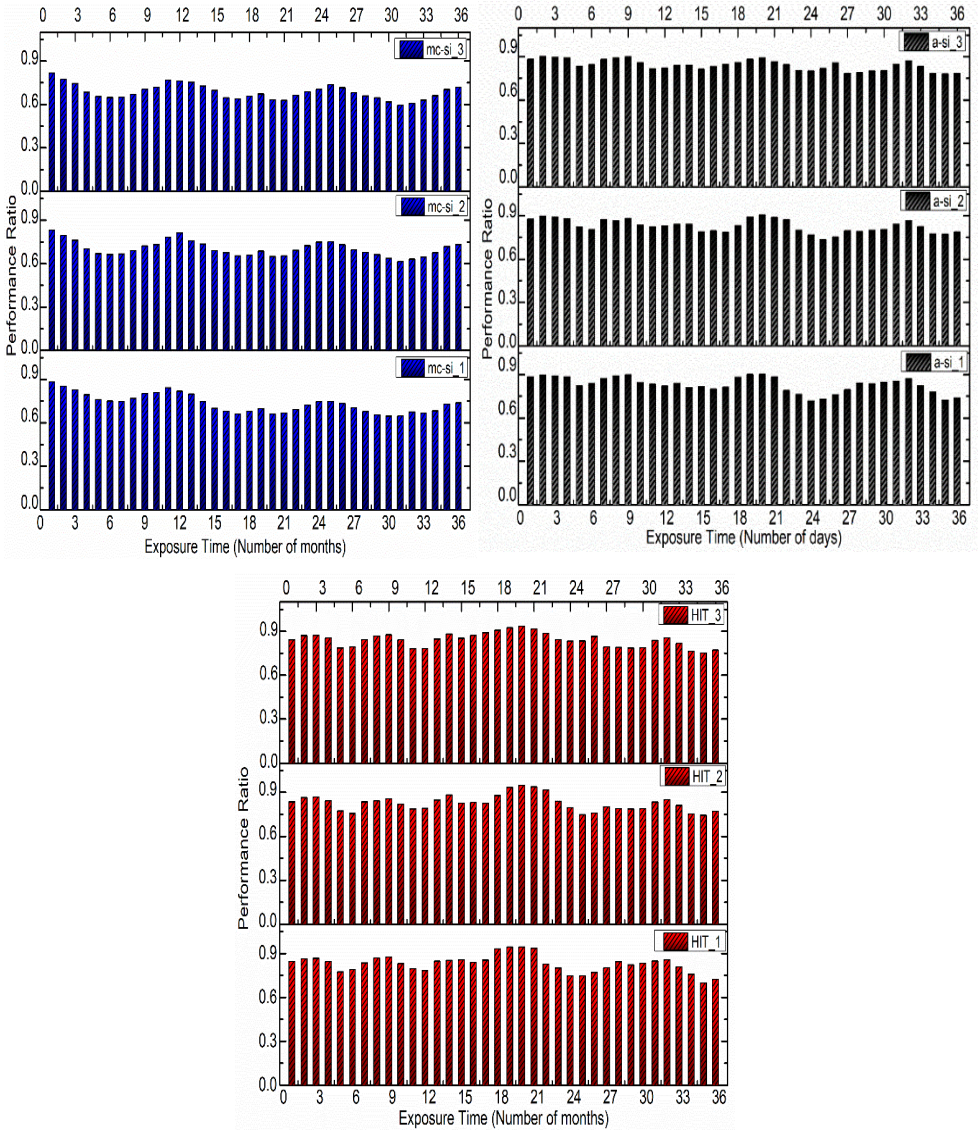

Fig 4.4. Monthly average Performance Ratio of the mc-si, a-si and HIT nine modules over a period of three years.

The S_F of the SPV modules is presented in Table 4.1. The spectrum factor is almost invariant for the year (around 1.0). It has been observed that the performance of the a-si modules is more affected through the solar spectrum, however, the impact is less in the mc-si modules. The performance of the SPV modules is graded on the basis of the performance ratio, normalized performance ratio, and efficiency.

The S_F of a-si modules shows the highest value of about 1.086 whereas mc-si modules are having 0.998 followed by HIT module technology 0.996.

Table 4.1. Spectrum Factor and a thermal factor of the three SPV technologies.

SPV technologies	Spectrum Factor	Thermal Factor
HIT	0.996	1.04
mc-si	0.988	1.06
a-si	1.086	1.05

From the results obtained from the thermal factor and the spectrum factor for nine modules of three silicon-based SPV technologies, the monthly temperature corrected performance ratio has been calculated.

The temperature corrected performance ratio of the mc-si, a-si and HIT technologies are shown in Fig 4.5. The temperature corrected performance ratio is between the 0.66 to 0.87, 0.68 to 0.88 and 0.71 to 0.94 for mc-si_1, mc-si_2 and mc-si_3 modules respectively over a period of 36 months. The highest temperature corrected performance ratio is during the winter seasons attributed to lower ambient as well as lower module temperature. The decrement in the performance ratio has been observed on time series of the mc-si modules technology.

The temperature corrected performance ratio for a-si modules are 0.81 to 0.99, 0.75 to 0.99 and 0.76 to 0.99 for a-si_1, a-si_2 and a-si_3 respectively. The highest performance has been observed during the summer seasons over a 36 months exposure time for a-si module technologies. The monthly temperature corrected performance ratio for the HIT modules is in the range of 0.81 to 0.99, 0.75 to 0.99 and 0.76 to 1 for HIT_1, HIT_2, and HIT_3 respectively.

The highest performance ratio for the composite climate of Gurugram has been recorded for the HIT modules thought out the exposure time of 36 months. Additionally, The HIT modules show minimum variation with the seasonal as well as minimum decrement throughout the 36 months. The temperature corrected performance ratio of a-si_2 is lower other nine SPV modules, whereas HIT_2 exhibits the highest performance

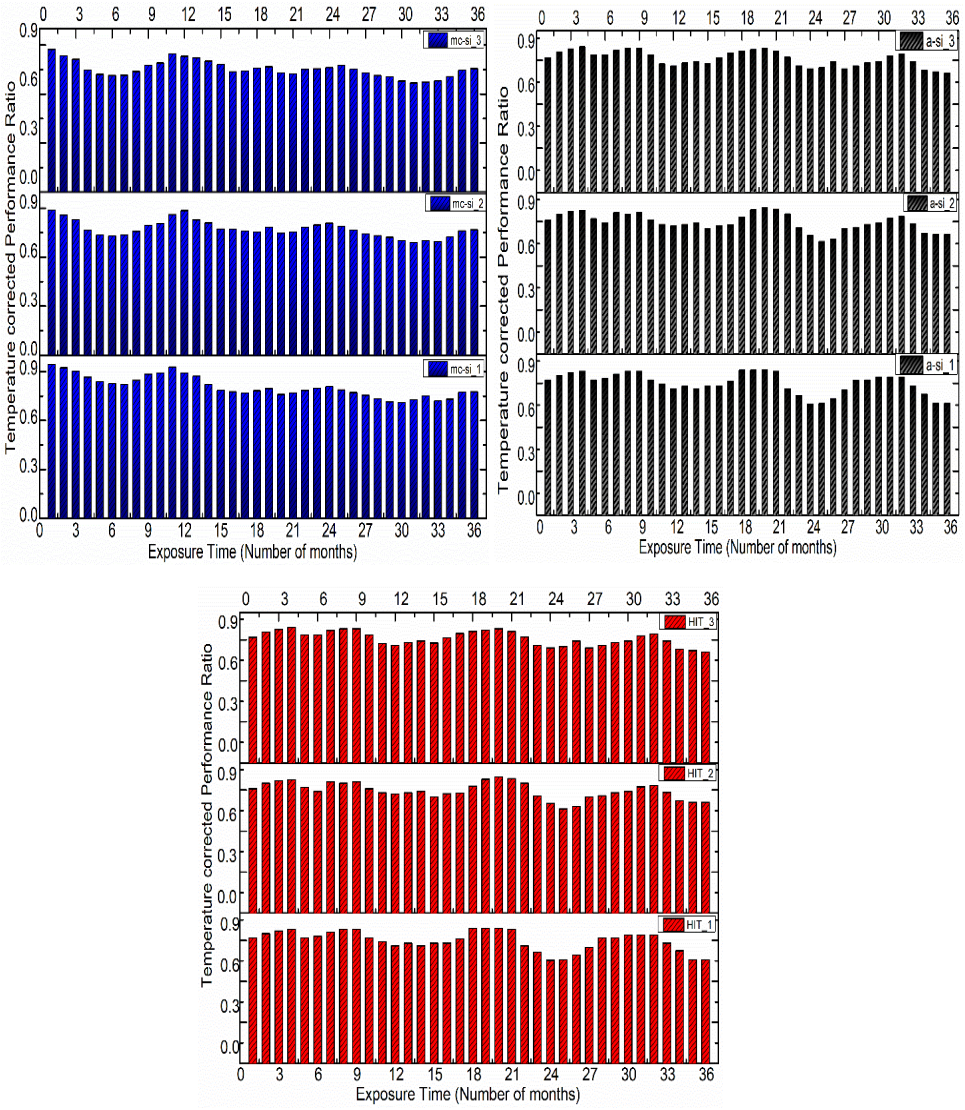

Fig 4.5. Monthly average temperature corrected Performance Ratio of the mc-si, a-si and HIT nine modules over a period of three years.

. The high impact of seasonal changes observed on PR_{NOR} of a-si modules and mc-si while slightly shows over HIT modules. T_F modifies the effect of module temperature on the performance of the solar modules. However, the performance of a-si modules are considered to be also influenced by both temperature of the module and solar irradiance received over the surface, that is annealed. The contours provide the real field conditions under which some specific technology PV modules will be operating at a specific site. This data will enable to estimate yield and PR for technology and site. Most useful in identifying appropriate PV technology suitable for the specific site.

The variation in the PR of three SPV technologies for three years, corresponding to different conditions (irradiance and module temperature) is given contour Fig. 4.6.

The description of the methodology is: (1) For SPV modules, in-plane irradiance is used as a column with an irradiance range from 50W/m^2 to 1200W/m^2 with a step of 50 W/m^2. T_M as a row with a range of 0 °C to 70 °C with a step of 5 °C to form a matrix. (2) The corresponding data of calculating performance ratio of three SPV module technologies have been added to each cell to complete the matrix. (3) The total integrated irradiation for each cell of the matrix was normalized with the highest integrated irradiation for the experimental period and plotted the contour graph.

From Fig. 4.6, it has been observed for a-si module that the PR range is spread between 0.79 to 1.08. The highest PR 1.08 has been observed in high module temperature and high irradiance which is 40 °C ± 5 °C at 850-900 W/m^2. The decrement in the PR over a period of three years is also evident from the graphs, the PR value is changed from 1.08 to 1.02. The highest performance ratio values contour scattered at high temperature and irradiance range for a-si module technology. The highest PR of HIT module is in the range of 1.01 to 1.05 at 20 °C ± 5 °C at 100-800 W/m^2 has been observed. During the second year, the PR is reduced to 0.97-1.02 and during the third-year value of PR is decreased to 0.96 - 1.

The high-performance ratio area is also decreased during an interval of three years. The highest PR value of the mc-si module has been observed at 15 ± 5 °C at 100-600 W/m^2 which is 0.96-1.02. The overall PR range of mc-si module is from 0.60 to1. 02 during the first year, which goes to 0.88-0.90 in the third year due to the various impact factors. From the contour graphs, it is also concluded that the a-si module technology is best suited for the hot environment condition like high temperature and high irradiance whereas the HIT required composite site condition for best performance (high PR). The mc-si technology is widespread technology, but from the graph, it is clear that this technology is

best suited for the low temperature and medium irradiance range for the best performance.

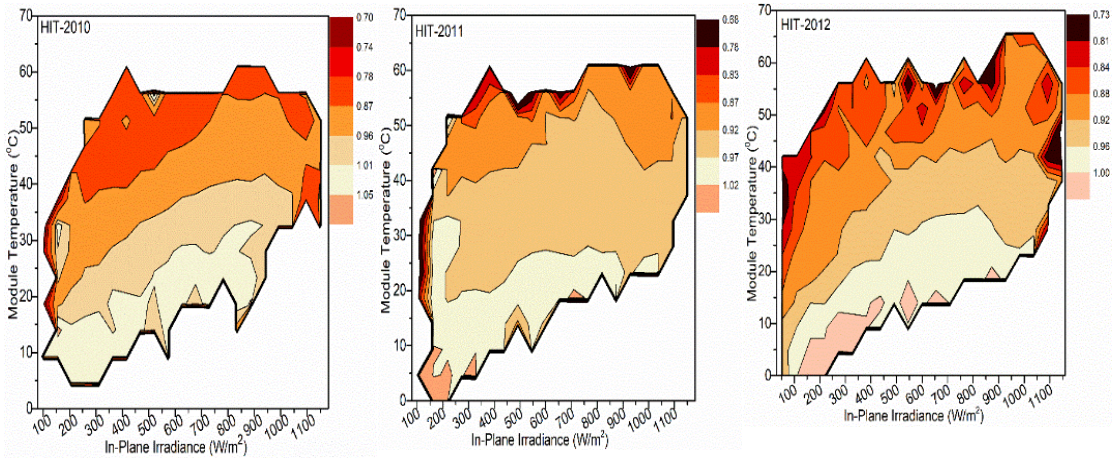

(a)

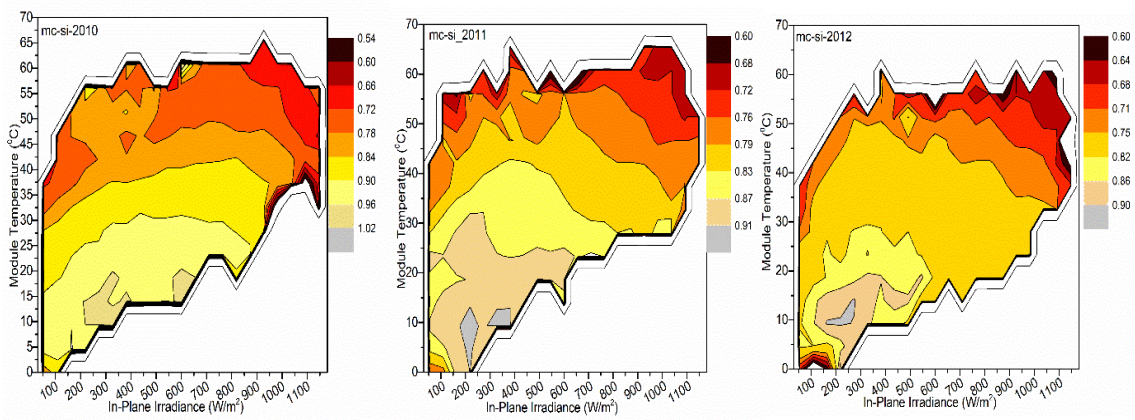

(b)

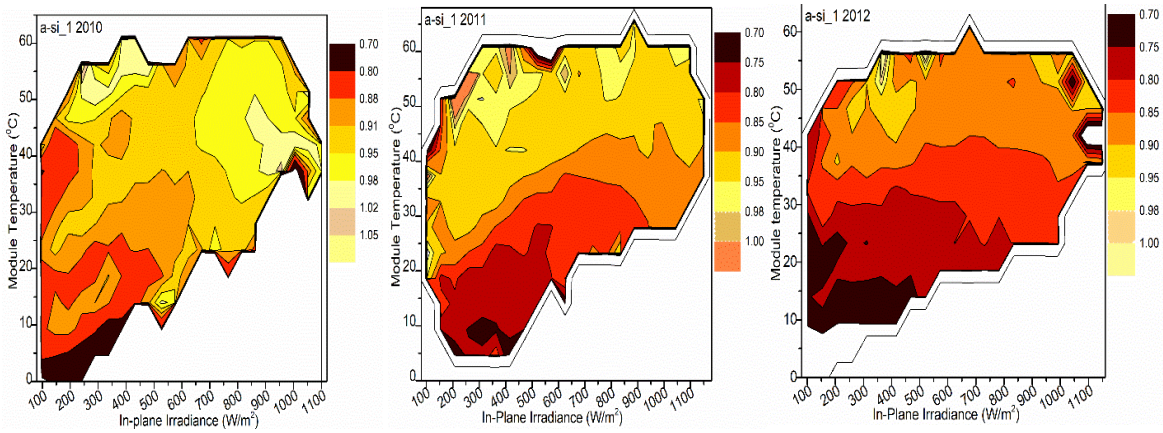

(c)

Fig. 4.6. Contour graphs of normalized performance ratio as a function of incident in-plane irradiation (W/m^2) and module temperature (°C) for (a) HIT, (b) mc-si and (c) a-si module for three years

Based on the results the performance modelling of different SPV technology based on the site and climatic condition is a very useful tool for proper optimization of energy.

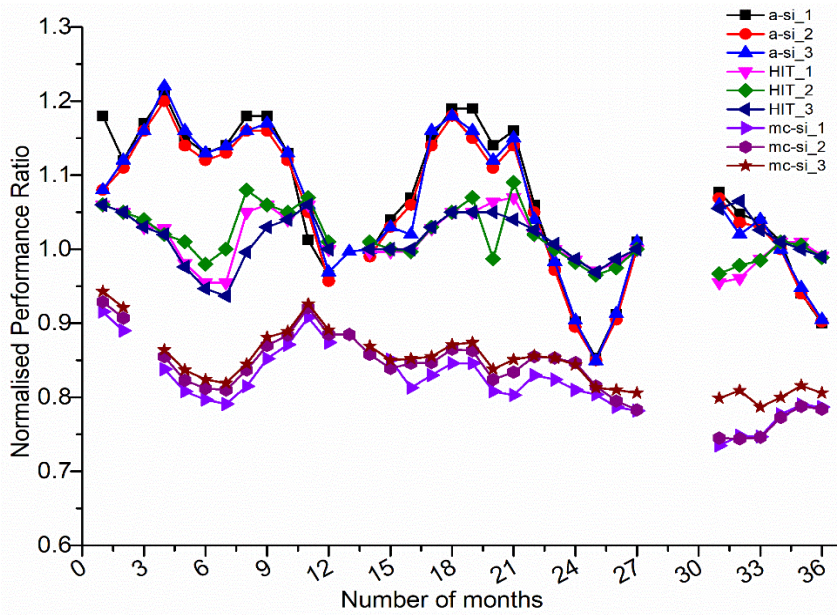

Fig. 4.7. Comparison of normalized performance ratio of nine SPV modules for three years.

The comparison of the three technologies has been done on the basis of normalized PR of the nine SPV modules of three different silicon-based technology over a period of three years. It has been observed in Fig. 4.7 that the similar SPV modules replicate the behaviour along the time with minor variations. The highest performance ratio has been observed for the a-si modules, however, the major variation along with the time is also observed in the same. The mc-si technology shows the lowest PR ratio having a decreasing trend line against the time series.

4.3.3. Effect on the seasonal normalized performance ratio over a period of three years

The percentage frequencies of temperature corrected PR of nine modules have been determined in the initial and final year of outdoor exposure to assess the season to season variation as shown in Fig. 4.8 for a-si, HIT and mc-si modules respectively over a period of three years. It shows a shift towards left with an increased spread for the three months in different seasons.

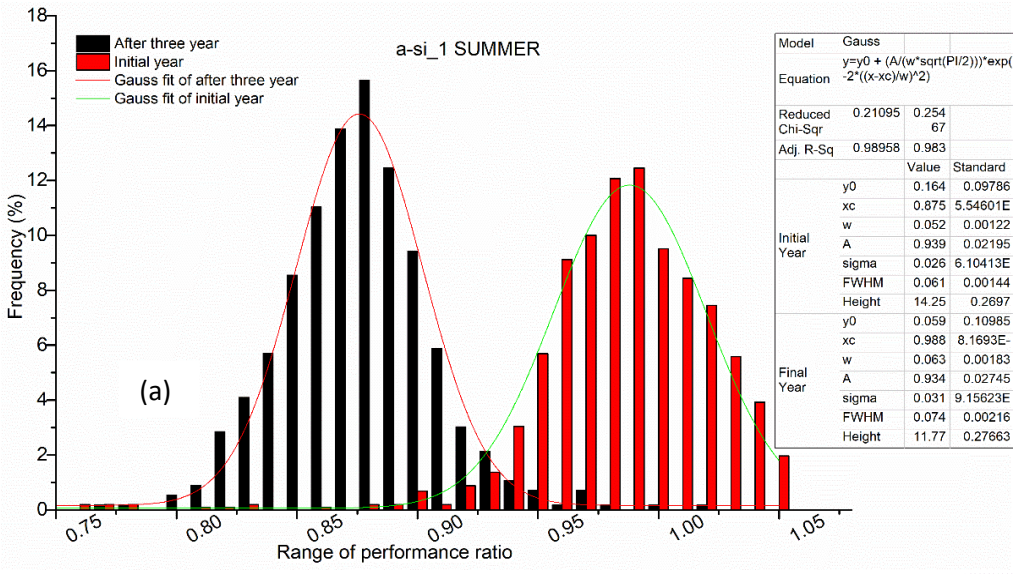

Model	Gauss		
Equation	y=y0 + (A/(w*sqrt(PI/2)))*exp(-2*((x-xc)/w)^2)		
Reduced Chi-Sqr	0.21095	0.25467	
Adj. R-Sq	0.98958	0.983	
		Value	Standard
Initial Year	y0	0.164	0.09786
	xc	0.875	5.54601E
	w	0.052	0.00122
	A	0.939	0.02195
	sigma	0.026	6.10413E
	FWHM	0.061	0.00144
	Height	14.25	0.2697
Final Year	y0	0.059	0.10985
	xc	0.988	8.1693E-
	w	0.063	0.00183
	A	0.934	0.02745
	sigma	0.031	9.15623E
	FWHM	0.074	0.00216
	Height	11.77	0.27663

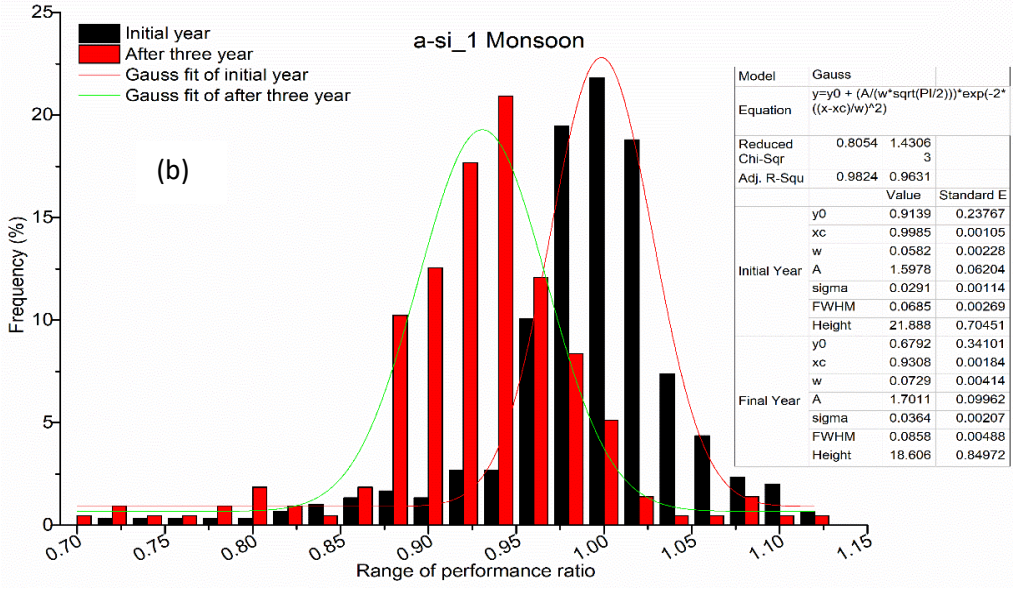

Model	Gauss		
Equation	y=y0 + (A/(w*sqrt(PI/2)))*exp(-2*((x-xc)/w)^2)		
Reduced Chi-Sqr	0.8054	1.43063	
Adj. R-Squ	0.9824	0.9631	
		Value	Standard E
Initial Year	y0	0.9139	0.23767
	xc	0.9985	0.00105
	w	0.0582	0.00228
	A	1.5978	0.06204
	sigma	0.0291	0.00114
	FWHM	0.0685	0.00269
	Height	21.888	0.70451
Final Year	y0	0.6792	0.34101
	xc	0.9308	0.00184
	w	0.0729	0.00414
	A	1.7011	0.09962
	sigma	0.0364	0.00207
	FWHM	0.0858	0.00488
	Height	18.606	0.84972

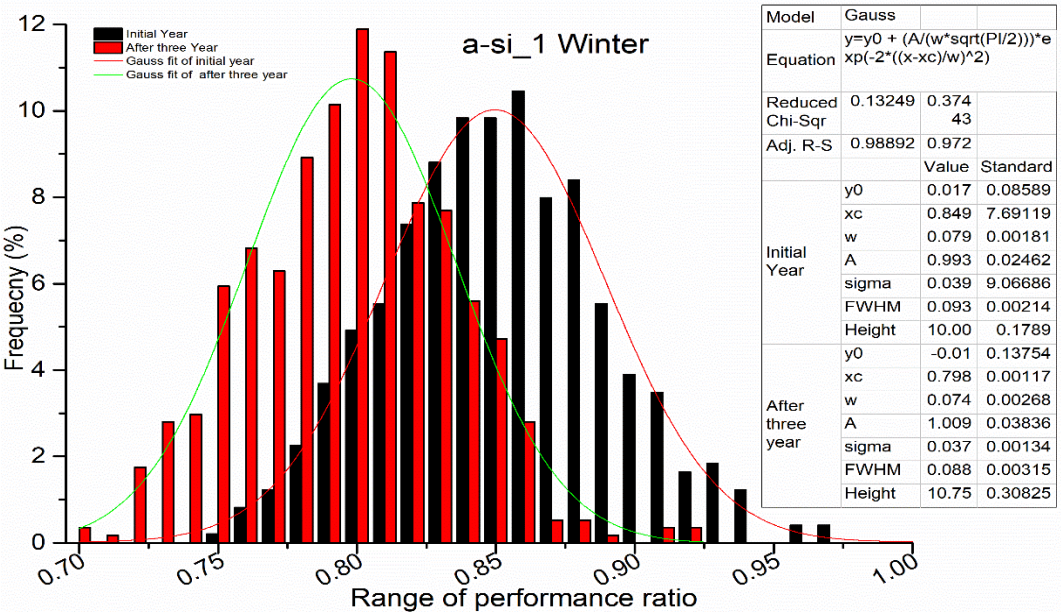

Model	Gauss		
Equation	y=y0 + (A/(w*sqrt(PI/2)))*exp(-2*((x-xc)/w)^2)		
Reduced Chi-Sqr	0.13249	0.37443	
Adj. R-S	0.98892	0.972	
		Value	Standard
Initial Year	y0	0.017	0.08589
	xc	0.849	7.69119
	w	0.079	0.00181
	A	0.993	0.02462
	sigma	0.039	9.06686
	FWHM	0.093	0.00214
	Height	10.00	0.1789
After three year	y0	-0.01	0.13754
	xc	0.798	0.00117
	w	0.074	0.00268
	A	1.009	0.03836
	sigma	0.037	0.00134
	FWHM	0.088	0.00315
	Height	10.75	0.30825

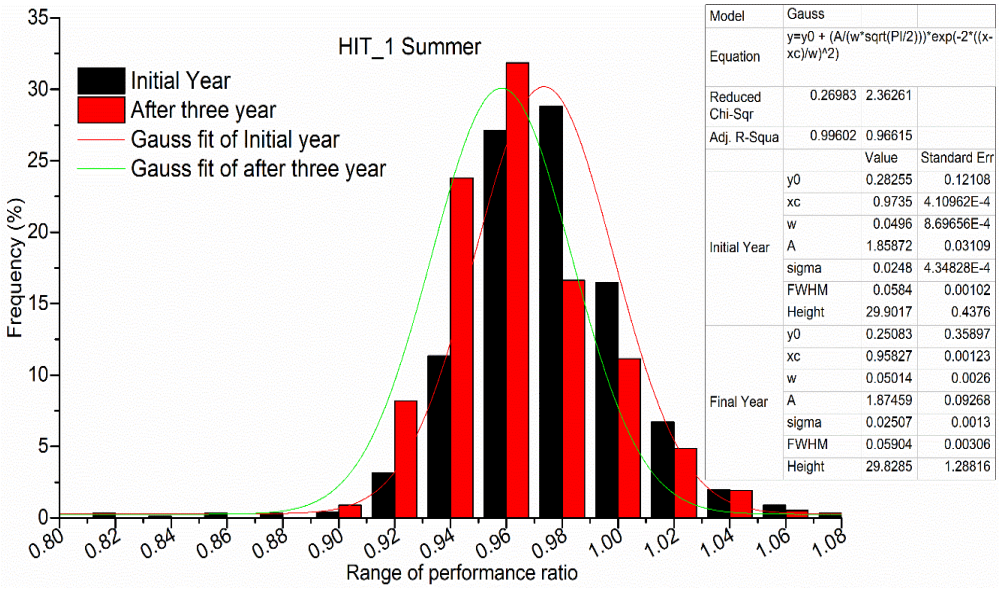

Model	Gauss		
Equation	y=y0 + (A/(w*sqrt(PI/2)))*exp(-2*((x-xc)/w)^2)		
Reduced Chi-Sqr	0.26983	2.36261	
Adj. R-Squa	0.99602	0.96615	
		Value	Standard Err
Initial Year	y0	0.28255	0.12108
	xc	0.9735	4.10962E-4
	w	0.0496	8.69656E-4
	A	1.85872	0.03109
	sigma	0.0248	4.34828E-4
	FWHM	0.0584	0.00102
	Height	29.9017	0.4376
Final Year	y0	0.25083	0.35897
	xc	0.95827	0.00123
	w	0.05014	0.0026
	A	1.87459	0.09268
	sigma	0.02507	0.0013
	FWHM	0.05904	0.00306
	Height	29.8285	1.28816

(a)

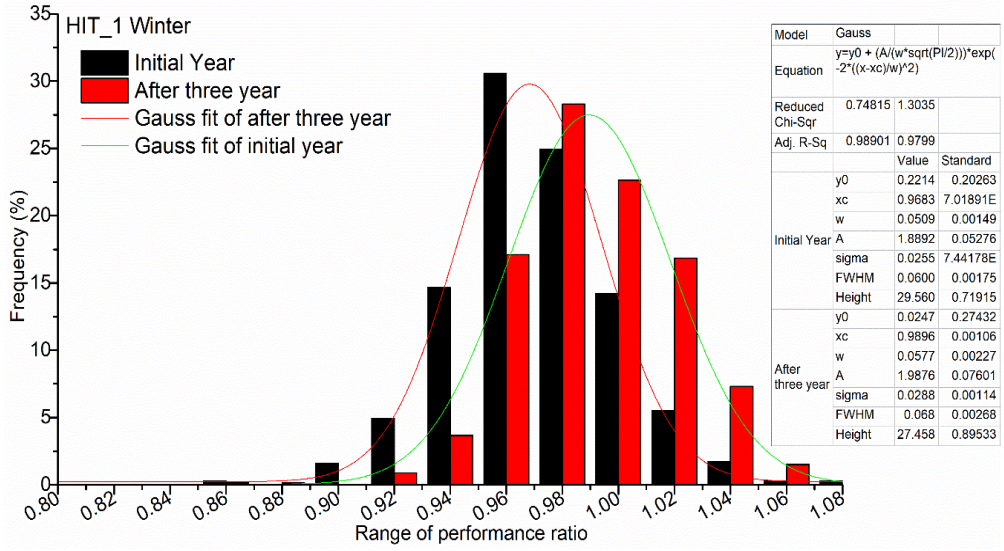

Model	Gauss		
Equation	y=y0 + (A/(w*sqrt(PI/2)))*exp(-2*((x-xc)/w)^2)		
Reduced Chi-Sqr	0.74815	1.3035	
Adj. R-Sq	0.98901	0.9799	
		Value	Standard
Initial Year	y0	0.2214	0.20263
	xc	0.9683	7.01891E
	w	0.0509	0.00149
	A	1.8892	0.05276
	sigma	0.0255	7.44178E
	FWHM	0.0600	0.00175
	Height	29.560	0.71915
After three year	y0	0.0247	0.27432
	xc	0.9896	0.00106
	w	0.0577	0.00227
	A	1.9876	0.07601
	sigma	0.0288	0.00114
	FWHM	0.068	0.00268
	Height	27.458	0.89533

(b)

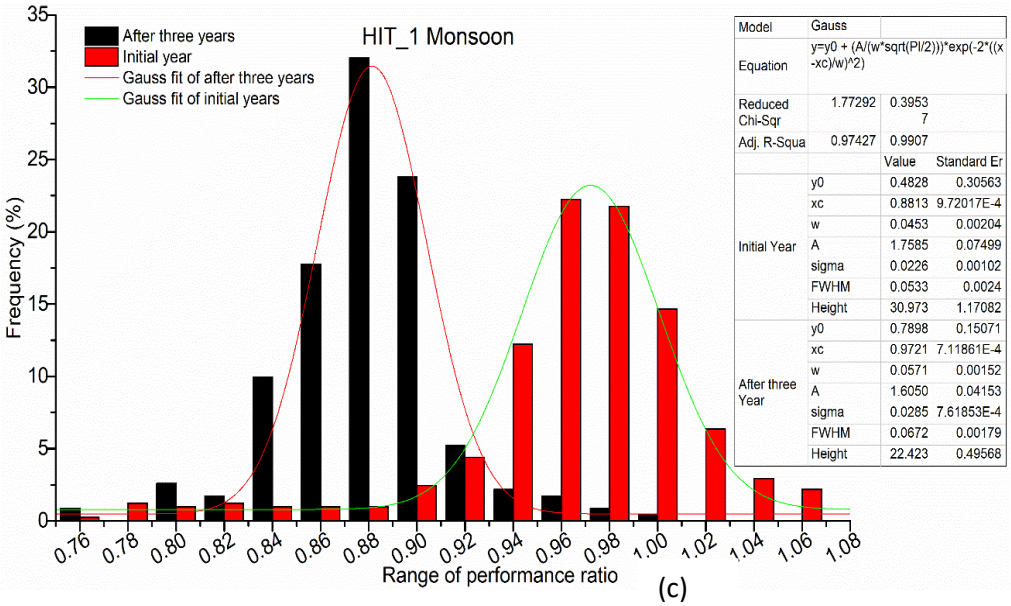

Model	Gauss		
Equation	y=y0 + (A/(w*sqrt(PI/2)))*exp(-2*((x-xc)/w)^2)		
Reduced Chi-Sqr	1.77292	0.3953 7	
Adj. R-Squa	0.97427	0.9907	
		Value	Standard Er
Initial Year	y0	0.4828	0.30563
	xc	0.8813	9.72017E-4
	w	0.0453	0.00204
	A	1.7585	0.07499
	sigma	0.0226	0.00102
	FWHM	0.0533	0.0024
	Height	30.973	1.17082
After three Year	y0	0.7898	0.15071
	xc	0.9721	7.11861E-4
	w	0.0571	0.00152
	A	1.6050	0.04153
	sigma	0.0285	7.61853E-4
	FWHM	0.0672	0.00179
	Height	22.423	0.49568

(c)

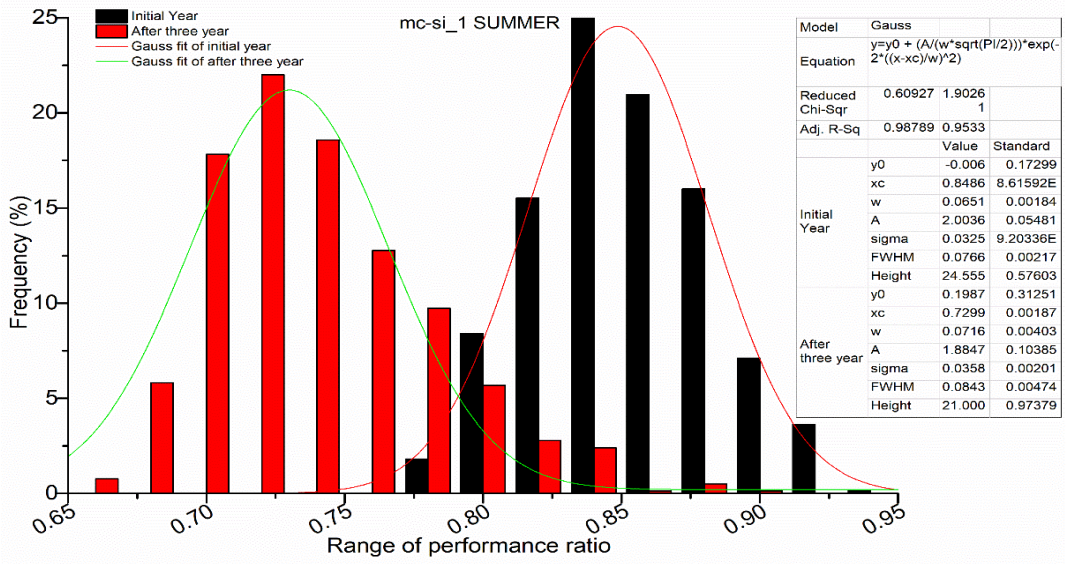

Model	Gauss		
Equation	y=y0 + (A/(w*sqrt(PI/2)))*exp(-2*((x-xc)/w)^2)		
Reduced Chi-Sqr	0.60927	1.90261	
Adj. R-Sq	0.98789	0.9533	
		Value	Standard
Initial Year	y0	-0.006	0.17299
	xc	0.8486	8.61592E
	w	0.0651	0.00184
	A	2.0036	0.05481
	sigma	0.0325	9.20336E
	FWHM	0.0766	0.00217
	Height	24.555	0.57603
After three year	y0	0.1987	0.31251
	xc	0.7299	0.00187
	w	0.0716	0.00403
	A	1.8847	0.10385
	sigma	0.0358	0.00201
	FWHM	0.0843	0.00474
	Height	21.000	0.97379

(a)

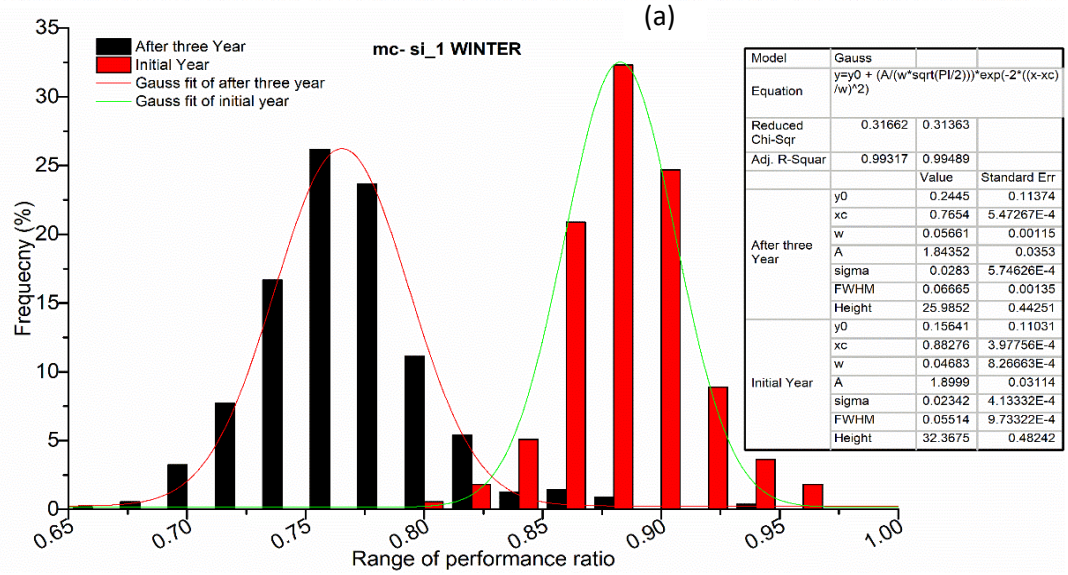

Model	Gauss		
Equation	y=y0 + (A/(w*sqrt(PI/2)))*exp(-2*((x-xc)/w)^2)		
Reduced Chi-Sqr	0.31662	0.31363	
Adj. R-Squar	0.99317	0.99489	
		Value	Standard Err
After three Year	y0	0.2445	0.11374
	xc	0.7654	5.47267E-4
	w	0.05661	0.00115
	A	1.84352	0.0353
	sigma	0.0283	5.74626E-4
	FWHM	0.06665	0.00135
	Height	25.9852	0.44251
Initial Year	y0	0.15641	0.11031
	xc	0.88276	3.97756E-4
	w	0.04683	8.26663E-4
	A	1.8999	0.03114
	sigma	0.02342	4.13332E-4
	FWHM	0.05514	9.73322E-4
	Height	32.3675	0.48242

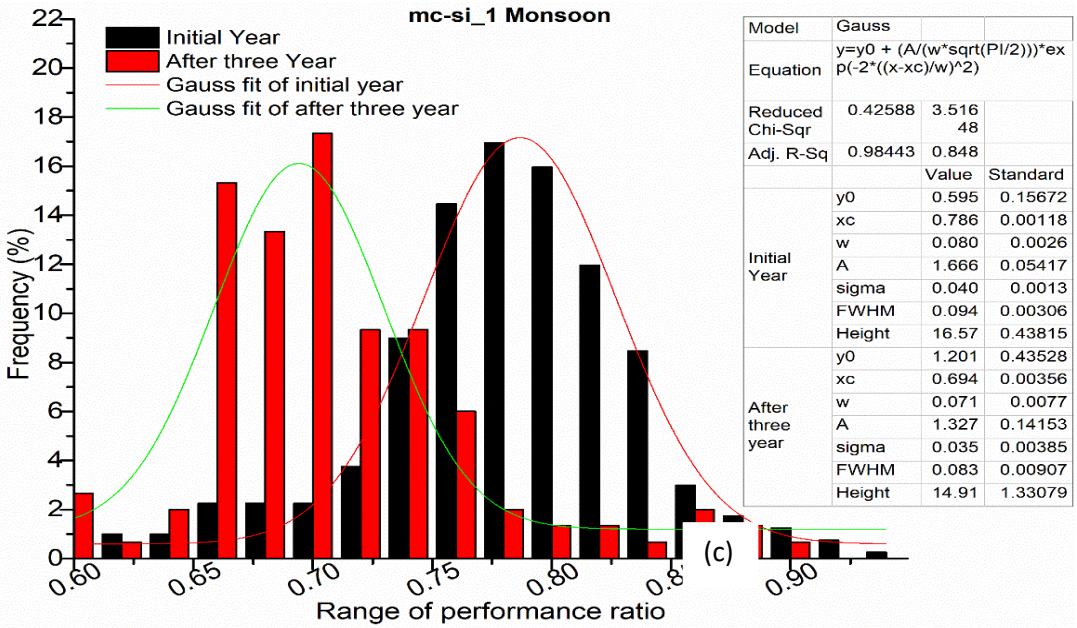

Model	Gauss		
Equation	y=y0 + (A/(w*sqrt(PI/2)))*exp(-2*((x-xc)/w)^2)		
Reduced Chi-Sqr	0.42588	3.51648	
Adj. R-Sq	0.98443	0.848	
		Value	Standard
Initial Year	y0	0.595	0.15672
	xc	0.786	0.00118
	w	0.080	0.0026
	A	1.666	0.05417
	sigma	0.040	0.0013
	FWHM	0.094	0.00306
	Height	16.57	0.43815
After three year	y0	1.201	0.43528
	xc	0.694	0.00356
	w	0.071	0.0077
	A	1.327	0.14153
	sigma	0.035	0.00385
	FWHM	0.083	0.00907
	Height	14.91	1.33079

(c)

Fig. 4.8. Frequency plot of the normalized performance ratio of the initial and final day of outdoor measurement of a-si, HIT and mc-si SPV module technologies for (a) summer (b) winter and (c) monsoon season.

From Fig.4.8, it has been observed that the full width at half maximum (FWHM) Gaussian function of a-si module the fit in the center shifted from 0.87 to 0.98 for the summer, from 0.84 to 0.79 for the winter and for monsoon, it is 0.99 to 0.93 whereas the FWHM width and area of the fittings increases from 0.05 to 0.06 and having a constant area 0.93 for summer, again constant width and increment in area 0.99 to 1.00 for winter and for monsoon 0.05 to 0.07 width and 1.59 to 1.70 area increases respectively. The HIT module, the FWHM Gaussian function the fit in the center shifted from 0.97 to 0.95, 0.96 to 0.98 and 0.88 to 0.97 for the summer, winter and monsoon season respectively, whereas the FWHM width and area of the fit increases from 0.04 to 0.05 and 1.05 to 1.87 for summer respectively, constant width 0.05 and increase area about 1.88 to 1.98 for winter and 0.04 to 0.05 increments and 1.75 to 1.68 decrement in the area for monsoon respectively. The FWHM Gaussian function the fit in the center shifted from 0.84 to 0.72 for the summer, from 0.76 to 0.88 for the winter and from 0.78 to 0.69 for the monsoon whereas the FWHM width and area of the fit increases from 0.06 to 0.07 and 2 to 1.88 for summer, for winter the width decreases from 0.05 to 0.04 and area increases from 1.84 to 1.89, for monsoon the width 0.08 to 0.07 decreases and area decreases 1.66 to 1.32 respectively for the mc-si module.

The frequency plot of the temperature corrected PR of the initial and final day at outdoor measurement shows that the highest center of the fit shifted for mc-si in summer season followed by mc-si in the winter season, whereas lowest shift has been observed for HIT modules for summer and winter followed by a-si module for summer season over a period of three years. It has been concluded that the HIT module is much more efficient than other technology in summer as well as in winter season however during monsoon the shift is again high.

4.3.4 Estimation of the monthly average normalized efficiency for the nine SPV module over a period of three years

The monthly normalized efficiency of the nine modules of three silicon-based technologies has been shown in Fig 4.9.

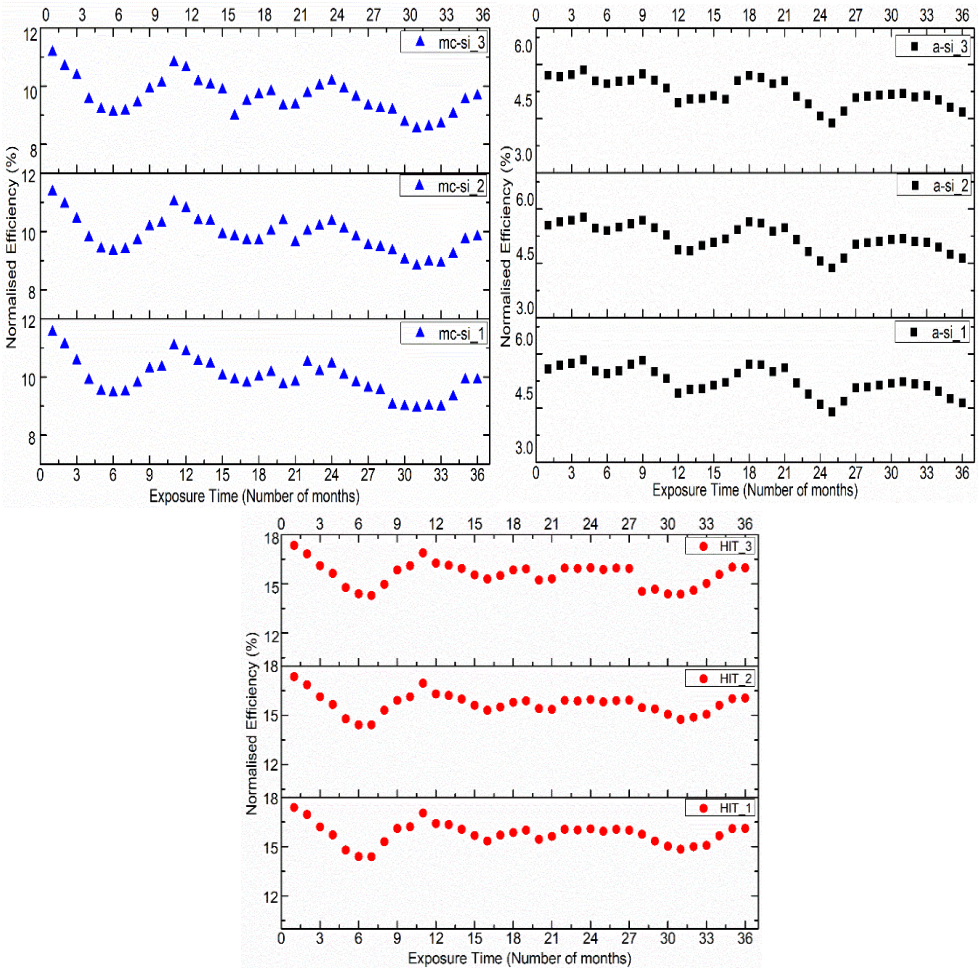

Fig 4.9. The monthly average normalized efficiency of the mc-si, a-si and HIT nine modules over a period of three years.

The monthly average efficiency of m-si modules technology is 8.93 to 11.54, 8.81 to 11.37 and 8.54 to 11.16 for mc-si_1, mc-si_2, and mc-si_3 PV modules respectively. The winter season is the more favourable season for the performance of the multi-crystalline module. The highest efficiency of the PV modules has been recorded in the November and January months having lower ambient as well as module temperature. The monthly average efficiency of the a-si modules is between the 4.39 to 5.83, 4.37 to 5.77 and 4.38 to 5.85 for a-si_1, a-si_2, and a-si_3 SPV modules respectively. In

contrast to mc-si technology, the a-si technology modules show a weak performance ratio in the winter seasons as a comparison to the summer season. The efficiency range is also low in comparison to m-si and HIT module technologies. The range of monthly average efficiency is 15.54 to 17.39, 15.81 to 17.35 and 15.87 to 17.34 respectively for HIT_1, HIT_2 and HIT_3 PV module technologies. Among the three silicon-based technologies the HIT modules exhibit the highest efficiency followed by mc-si modules whereas the a-si shows the lowest efficiency.

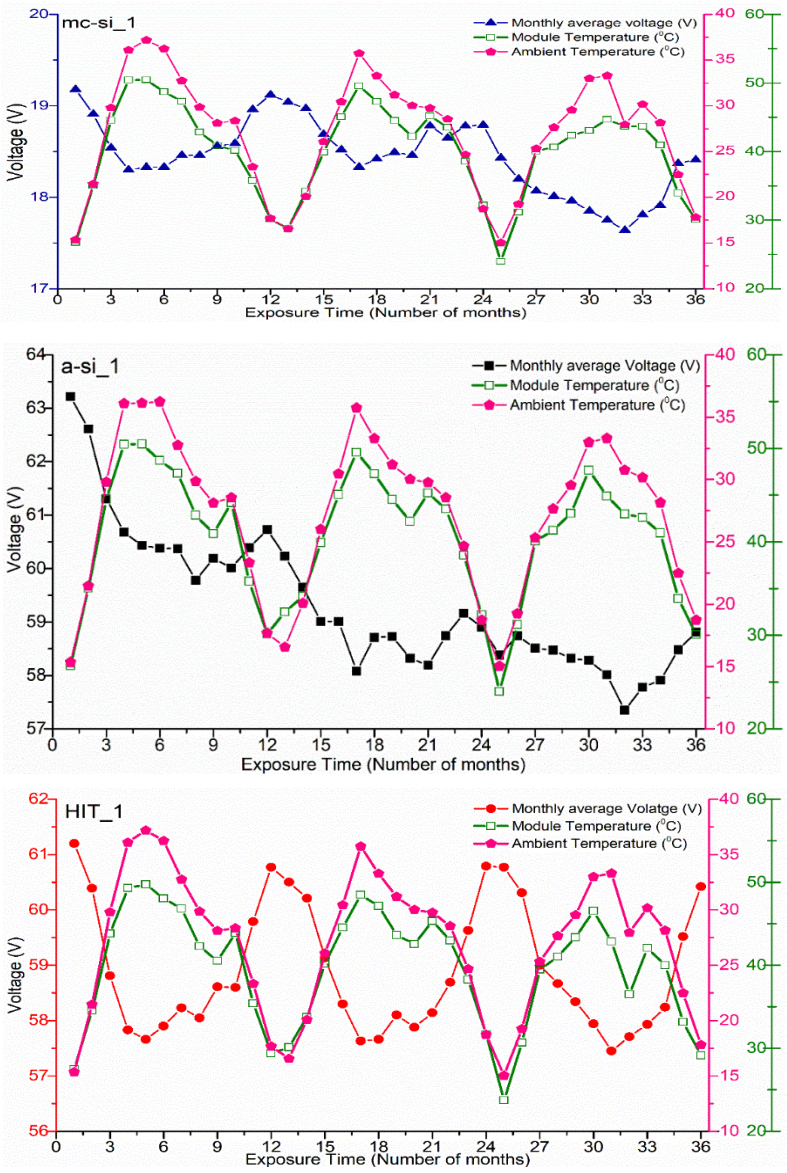

Fig 4.10. Monthly average values of ambient & module temperature and the output voltage of the representative mc-si, a-si and HIT SPV module technologies

. Fig 4.10 demonstrations the estimation of the monthly average output voltage at the maximum power point for the mc-si, a-si and HIT SPV technologies along with the ambient and module temperature for a period of 36 months. Highest reduction observed in the output voltage of the a-si modules technologies shows a similar trend as in the effective peak power provided in Fig 4.1. The least impact of the exposure time over the voltage has been observed for the HIT modules. Additionally, seasonal fluctuation of the output voltage has been observed for all the three technologies.

The seasonal fluctuation is clearly evident due to the ambient temperature variation over time. The estimation of the voltage is in accordance with the temperature profile and the percentage difference after the three years of exposure is about 40.14%, 69.75%, and 12.74 % form mc-si, a-si and HIT SPV module respectively The least variation over a period on the basis of percentage has been observed for HIT technology modules.

4.4 Estimation of the degradation rate based on the linear regression over the monthly average effective peak power of the SPV modules

The degradation rate of the nine SPV modules has been calculated over a field exposure of three years. The trend line over the time series of the monthly average effective peak power has been constructed and based on the linear regression the slope and intercept have been calculated for the 36-month period. The slope, intercept and the degradation rate of the nine modules are shown in Table 4.2.

Table 4.2. Slope, Intercept and Degradation rate of the three silicon-based SPV technologies over a period of three years.

Technology	Slope	Intercept	Degradation Rate
mc-si_1	-0.569	149.37	-4.58
mc-si_2	-0.692	150.07	-5.54
mc-si_3	-0.550	144.4	-4.57
HIT_1	-0.224	214.22	-1.26
HIT_2	-0.205	211.05	-1.17
HIT_3	-0.4852	217.75	-2.67
a-si_1	-0.338	80.20	-5.07

a-si_2	-0.327	79.44	-4.94
a-si_3	-0.349	79.83	-5.25

The highest rate of degradation which is about 4.5% degradation over a period of 36 months in outdoor field condition has been observed for a-si module whereas lowest is observed on the HIT modules technology which is about 1%. The annual degradation rate of the mc-si technologies is 1.5%, for a-si 1.6% and 0.39% for HIT technologies in the composite climate of India using the linear regression over the effective peak power. From all the three technologies considered in the study, the HIT shows the least degradation rate while the m-si and a-si show almost similar degradation rate over an exposure time of 36 months in the field aged condition.

4.4.1 Annual degradation rate using Linear Regression, LOESS and CSD over the three-year period

The annual degradation rate has been calculated on the normalized performance ratio using linear regression, CSD and LOESS over a period of initial three years for nine silicon-based PV modules. A decrement in the trend line over the performance parameters is termed as a positive degradation rate. The annual DC degradation rate of the nine modules obtained by applying the linear regression, CSD and LOESS are summarized in Table 4.3. For most of the case, the annual degradation rate calculated by applying linear regression to the time series was lower in comparison to the CSD calculated, results demonstrated clearly that the degradation rate has been affected by the opted analysis techniques and it's therefore noteworthy when carrying out such studies under real outdoor conditions. The fact that the CSD the annual degradation rate was evaluated from the deseasonalized time series seems to be the reason why the degradation is higher compared to the linear degradation results. For the a-si modules, the degradation rate is in the range of 3.67-3.76 for three years whereas 1.24%/year, for HIT modules 0.14 %/year, whereas the highest for mc-si modules 1.50 %/year using the linear regression methodology. The CSD techniques utilized, for estimation of degradation rate, the a-si modules the degradation rate is in the range of 3.12-3.96 for three years and 1.16%/year, for HIT modules 0.24-0.48 for three years and 0.56%/year, whereas the highest for mc-si modules 0.82%/year. Lastly, by using the LOESS methodology for estimation of degradation rate, the a-si modules the degradation rate is in the range of 2.11-2.83 having 1.16%/year, for HIT modules 1.33-1.87 having 011 %/year and highest for mc-si modules 2.32-2.70 having 1.46 %/year.

Table 4.3. Annual DC performance loss rate of SPV technologies calculated by applying linear regression, CSD and LOESS to monthly DC PR time series over a three-year period.

SPV Technology	Slope	Intercept	Annual DC performance loss rate by LR	Annual DC performance loss rate by CSD	Annual DC performance loss rate by LOESS
a-si_1	-0.003	0.96	3.76	3.96	2.83
a-si_2	-0.0029	0.95	3.67	3.36	2.11
a-si_3	-0.003	0.96	3.73	3.12	2.32
HIT_1	-0.0005	0.96	0.63	0.48	1.33
HIT_2	-0.0002	0.95	0.26	0.24	1.84
HIT_3	-0.0003	0.95	0.38	0.34	1.87
mc-si_1	-0.0038	0.89	5.12	5.04	2.70
mc-si_2	-0.0029	0.86	4.09	3.84	2.40
mc-si_3	-0.003	0.85	4.29	4.32	2.32

From Table 4.3, the degradation rate is higher for the mc-si modules using all the three techniques followed by the a-si modules technology. In contrast, the HIT modules show the least degradation rate using all the three methodologies. For most technologies, the annual degradation rates calculated by applying the linear regression and LOESS to the time series were lower in comparison to the CSD evaluated degradation rates except the one module of a-si modules. Due to the reason that the degradation rate has been calculated from the deseasonalized time series seems to be the reasons why the annual degradation rate is higher compared to other methodology.

Finally, the calculation of the performance analysis and the degradation rate of the high-efficiency PV technologies is not a simple method and there is yet no methodology to determine the accurate results based on the outdoor measurements.

4.5 Conclusion

The performance assessment of the nine modules of three different silicon-based technologies under outdoor long-term exposure in composite climate conditions has been analyzed for a period of three years. The monthly average effective peak power (P_{eff}), performance ratio (PR), temperature corrected performance ratio (PR_{CORR}) has been calculated over a period of three years. The estimation of the effective peak power of nine modules shows a reduction of around 15.80%, 17.23% and 7.15% for mc-si, a-si and HIT modules over an exposure time of 36 months. The impact of seasonal and temperature variability is highly observed over all the nine modules, however,

highest has been observed on a-si modules technologies and least on the HIT modules as a result of its higher temperature coefficient of power. The monthly average PR for mc-si, a-si and HIT modules were 0.70, 0.82 and 0.83 respectively. Also, the monthly average efficiency for the for mc-si is 9.82, for a-si is 5.22, and for a HIT is 15.68 modules respectively.

The degradation rate using the linear regression over the effective peak power for mc-si, a-si and HIT modules were 4.89%, 5.08% and 1.7% respectively over a period of three years. The highest degradation has been observed for the a-si followed by m-si modules whereas the HIT module shows the least degradation rate. The a-si module technologies are well suited for the hot and warm climatic zones whereas from the different performance indices the HIT module shows the best performance for the composite climate of India.

It has been observed that the impact of the observed variation in operating condition affects SPV modules very differently according to the module type (module material property). The annual DC degradation rate of the three-different silicon-based technology was calculated using the statistical methods of linear regression, LOESS, and the CSD over a period of three years. The tables clearly show that the selection of the assessment techniques affects the output and is important for the correctness of the results and study under field conditions. The compilation of the average performance ratio, efficiency and degradation rate of the three SPV technologies has been presented in Table 4.4.

Table 4.4. Compilation of the average performance ratio, efficiency and degradation rate of the three SPV technologies.

SPV Technology	Performance ratio			Efficiency			Degradation rate (%/Year)		
	I Year	II Year	III Year	I Year	II Year	III Year	LR	LOESS	CSD
a-si	0.94	0.91	0.86	5.48	5.27	4.78	1.24	0.81	1.16
HIT	0.95	0.94	0.92	15.59	15.46	15.16	0.14	0.56	0.11
mc-si	0.84	0.82	0.76	11.46	10.88	10.01	1.50	0.82	1.46

The HIT modules are less affected by the variation of the operating conditions like irradiance, temperature and spectrum factor. This module exhibited the least variation in all investigated parameters. The mc-si module has a negative impact of high temperature and irradiance, performance goes decreased by high operating temperature, performance is decreased during the summer. The result indicates that the significance of the outdoor performance of SPV technologies with reference to location specific climatic conditions. The location specific standards are needed to be used for the accurate and precise assessment and calculation of power output, energy yields and PR of the SPV technologies.

CHAPTER 5
METHODOLOGY FOR ASSESSING AND QUANTIFYING THE DISTRIBUTION AND EXTENT OF DEGRADATION

In this chapter, the series resistance of the high-efficiency silicon-based solar module has been estimated using the analytical, theoretical and light and dark I-V characteristics. The mapping of the series resistance has been done in between in-plane irradiance and module temperature. The uncertainty to estimate the series resistance has been calculated for three ranges of irradiance i.e. 1000 W/m^2, 900 W/m^2 and 800 W/m^2 for all the three technologies at outdoor field condition.

5.1 Introduction: Assessment of series resistance estimation techniques

Series resistance (Rs) is a significant electrical parameter of the solar photovoltaic module and is used for outdoor performance modelling, evaluation and degradation studies. An increase in series resistance leads to an increase in electrical losses and accordingly, reduces the efficiency. Therefore, a detailed analysis of series resistance is needed in order to assess the performance and degradation of the module in outdoor condition. The procedure I of the said IEC, i.e. simplified method, has been used because of the fact that it is being majorly used in the field and also due to the constraint of availability of additional data parameters required for another method.

5.2 Methodology

The detailed methodology to estimate the series resistance is described in the chapter-3 along with the graphical representation and material. The

arrangement for the estimation of series resistance using standard IEC 60891 Edi 2.0 is fulfilled using the mesh at outdoor conditions.

5.3 Results and Discussion

The comparative analysis of series resistance for the three solar PV technologies modules namely a-si, HIT and mc-si estimated using nine analytical methods and procedure based on standard IEC 60891 Edi 2.0 has been carried out.

5.3.1 Estimation of the series resistance by analytical methods

The series resistance for three technologies has been estimated using nine analytical methods at different irradiance level using outdoor measured data is presented in Fig 5.1.

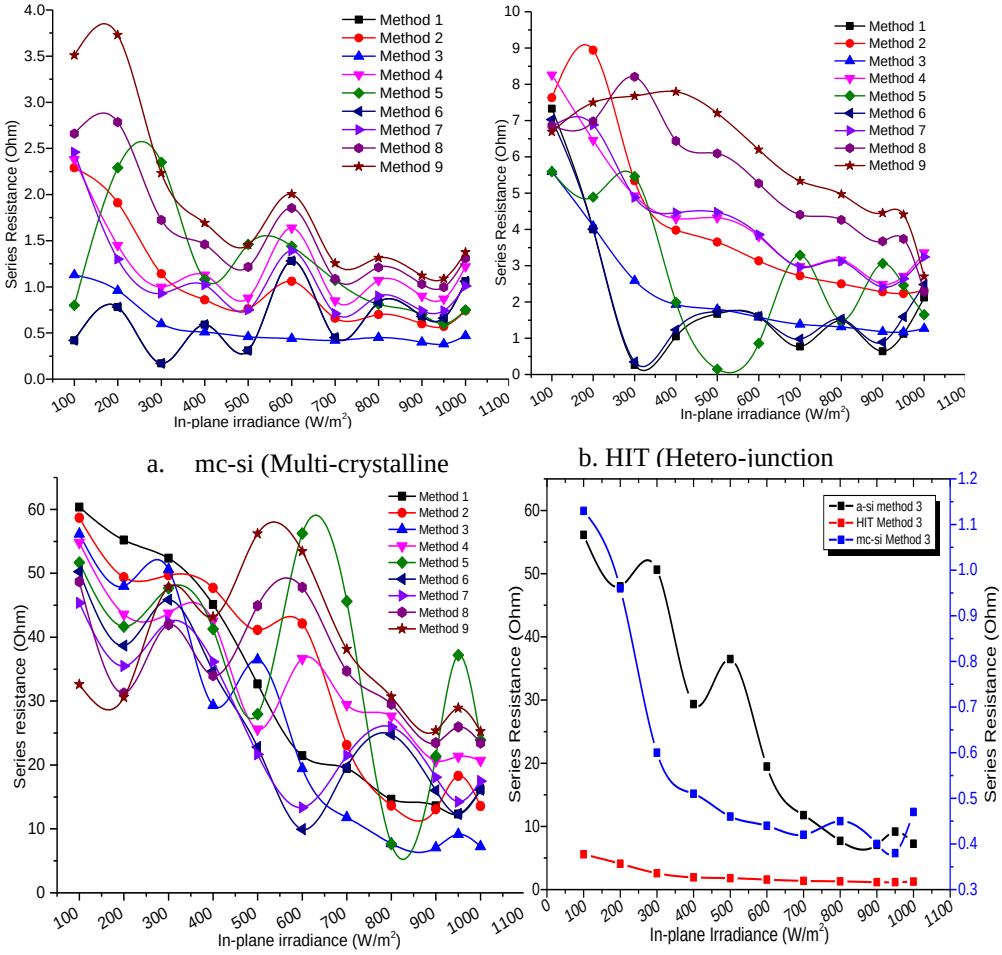

Fig 5.1. Estimated series resistance from nine methods for (a) Multi-crystalline module (b) Hetero-junction intrinsic thin layer and (c) Amorphous single-

junction silicon solar PV modules under different irradiance condition at 25 °C

(d) Method 3 for mc-si, HIT and a-si silicon

It has been observed that the series resistance of the solar PV modules decreases with the increase in solar irradiance. The estimated series resistance using analytical methods is found to more satisfactory and stable for the mc-si module as compared to HIT and a-si technology modules. The fluctuation in the results of different methods is higher for HIT and a-si technology, while the results follow a similar trend for mc-si technology. The methods have been developed for crystalline silicon technology and hence, well fitted to it. Method 3 shows a steadied series of resistance for all ranges of the irradiance for different technologies in PV modules.

The literature has also provided that method 3 is comparatively more accurate. The deviation in the estimated series resistances of mc-si using nine methods is higher for the low irradiance condition as compared to high irradiance. However, the variation is similar for a-si and HIT technology modules.

The standard deviation, means, maxima and minima of the estimated series resistance for three different technologies, i.e., mc-si, HIT and a-si for irradiance from 100 W/m^2 to 1000 w/m^2 at 25 °C is shown in Fig 5.2 (a)-(c). The deviation in the series resistance is found to be 3.09 Ω, 2.67 Ω and 27.77 Ω at 100 W/m^2 and 0.90 Ω, 2.09 Ω and 17.99 Ω at 1000 W/m^2 for mc-si, HIT and a-si solar PV modules respectively between maximum and minimum series resistance value. The mean series resistance for mc-si module varies from 1.78 Ω to 0.72 Ω for irradiance from 100 W/m^2 to 1000 W/m^2. For HIT module the estimated series resistance varies from 2.22 Ω to 0.61 Ω for irradiance from 100 W/m^2 to 1000 W/m^2. There is a continuous decrement in the series resistance for the a-si module whose series resistances varies from 50.95 Ω to 18.20 Ω between 100 W/m^2 to 1000 W/m^2. The slope of the declination of the series resistance by increasing the irradiance is -0.108, -0.063 and -3.348 for the mc-si, HIT and a-si solar PV module respectively. It has been observed that all minima lie in the same plane for mc-si module whereas some steady state of minima is also observed in the HIT SPV module for higher irradiance. However, there is no such pattern of minima has been observed for a-si module. The

smallest series resistance has been observed, i.e., 0.72 Ω at 1000 W/m^2 for the mc-si and highest series resistance, i.e., 50.95 Ω at 100 W/m^2 for the a-si solar technology module has been obtained from the analytic method.

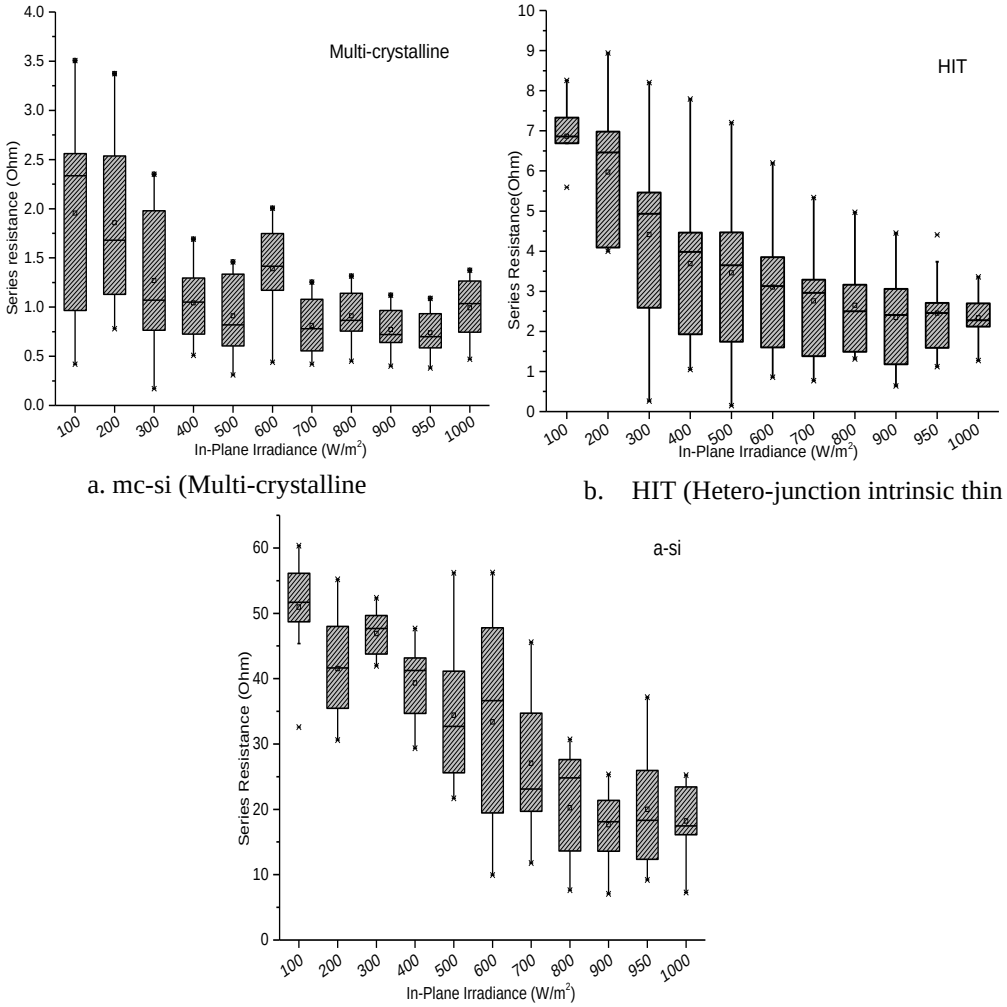

a. mc-si (Multi-crystalline

b. HIT (Hetero-junction intrinsic thin

c. a-si (Amorphous single junction

Fig 5.2. Standard deviation, mean, minima and maxima of (a) Multi-crystalline module (b) Hetero-junction intrinsic thin layer and (c) Amorphous single-junction silicon solar PV modules under different irradiance condition at 25 °C presented in the box chart

The estimated series resistance is in line with the possible series resistance as proposed in the literature for the mc-si technology. However, it is slightly high for other HIT and a-si modules. Some methods may be technology-specific, so it is not advisable to use these methods on each technology it may influence the result. It has been observed from this series of resistance that

choosing any Rs value from these may be leading the error in the translation procedure.

5.4. Estimation of the series resistance by IEC 60891 Edi.2.0

The electrical parameters measured at real operating condition by the PVPM instrument have been used to estimate two values of series resistance each for a-si, HIT and mc-si solar PV modules using procedure 1 of IEC 60891 Edi 2.0. The temperature of the SPV device should be alike for all irradiances at which the I-V characteristics curves are considered. However, as per standard allows a variation of ± 2 °C.

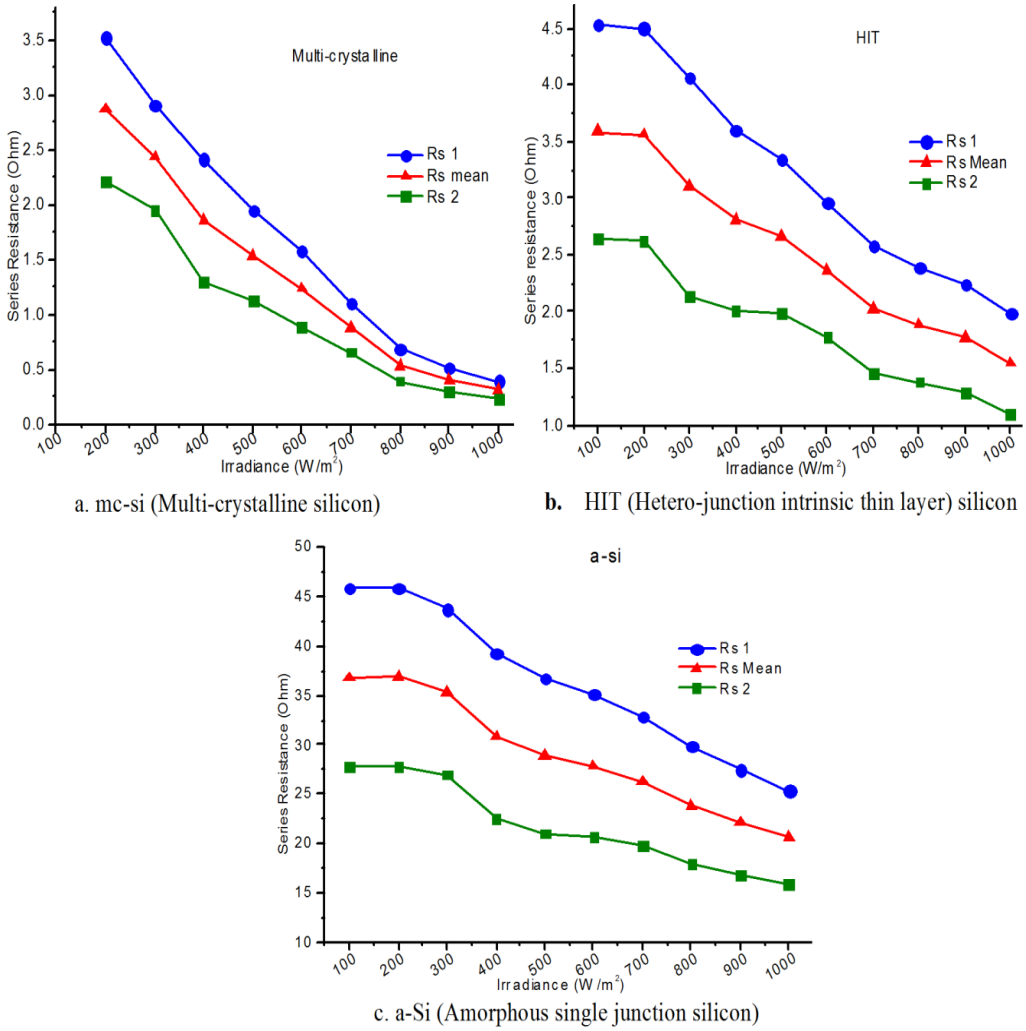

a. mc-si (Multi-crystalline silicon)

b. HIT (Hetero-junction intrinsic thin layer) silicon

c. a-Si (Amorphous single junction silicon)

Fig 5.3**.** The mean series resistance variation as per corrected irradiance for (a) Multi-crystalline module (b) Hetero-junction intrinsic thin layer and (c) Amorphous single-junction silicon solar PV modules under different irradiance condition at 25 °C

The outdoor data has been taken on different irradiance maintaining the same temperature and the spectrum using mesh. Then the measured data have been translated to 100 W/m^2, 200 W/m^2, 300 W/m^2, 400 W/m^2, 500 W/m^2, 600 W/m^2, 700 W/m^2, 800 W/m^2, 900 W/m^2 and 1000 W/m^2 respectively and at module temperature 25 °C, 35 °C and 50 °C. The closest measured data near to the desired irradiance has been used for the translation. The Rs_1 has been calculated by translating from measured data higher than the desired, whereas the Rs_2 has been calculated using the data lower than the desired data. The calculated Rs_1, Rs_2, and Rs_{mean} (i.e., The mean value of the Rs_1 and Rs_2) at 25 °C and different irradiance level is shown in Fig 5.3.

It has been found that the calculated mean series resistance varies from 0.310 Ω to 2.87 Ω for the mc-si module, 1.54 Ω to 3.57 Ω for HIT module and 20.62 Ω to 36.85 Ω for a-si solar PV module. Hence, the estimated series resistance of the mc-si, HIT, and a-si technology is found to be 0.310 Ω ± 25.806 %, 1.545 Ω ± 28.93 % and 20.628 Ω ± 22.93 % respectively at STC, i.e., 1000 W/m^2 and 25 °C. The mc-si modules (42 cells each) have a series resistance of 0.0142 Ω per cell, and HIT (110 cells each) have a series resistance of 0.019 Ω per cell which are typical values for these SPV technologies.

The series resistance of a-si cell (104 cells per modules) is found to be 0.289 Ω per cell, which is slightly higher than that of the value of series resistance available in the literature. The higher Rs is due to the stabilization period of the module. The mean series resistance value as a function of irradiance at different module temperature for (a) mc-si (b) HIT and (c) a-si are shown in Fig 5.4.

It has been observed that the series resistance is decreasing with increase in module temperature and the irradiance. The difference between the corresponding values of series resistance is very close to each other for different temperature. The series resistance for SPV modules is mainly a summation of lumped equivalent series resistance; the observed behaviour may be studied regarding various contributions to the Rs from different components.

The contact resistance of the solar cell's electrode and participation of base resistance is insignificant and lesser above 25 °C temperature. Accordingly, the base resistance decreases with increasing temperature. As a result, series resistance decreases rapidly with temperature.

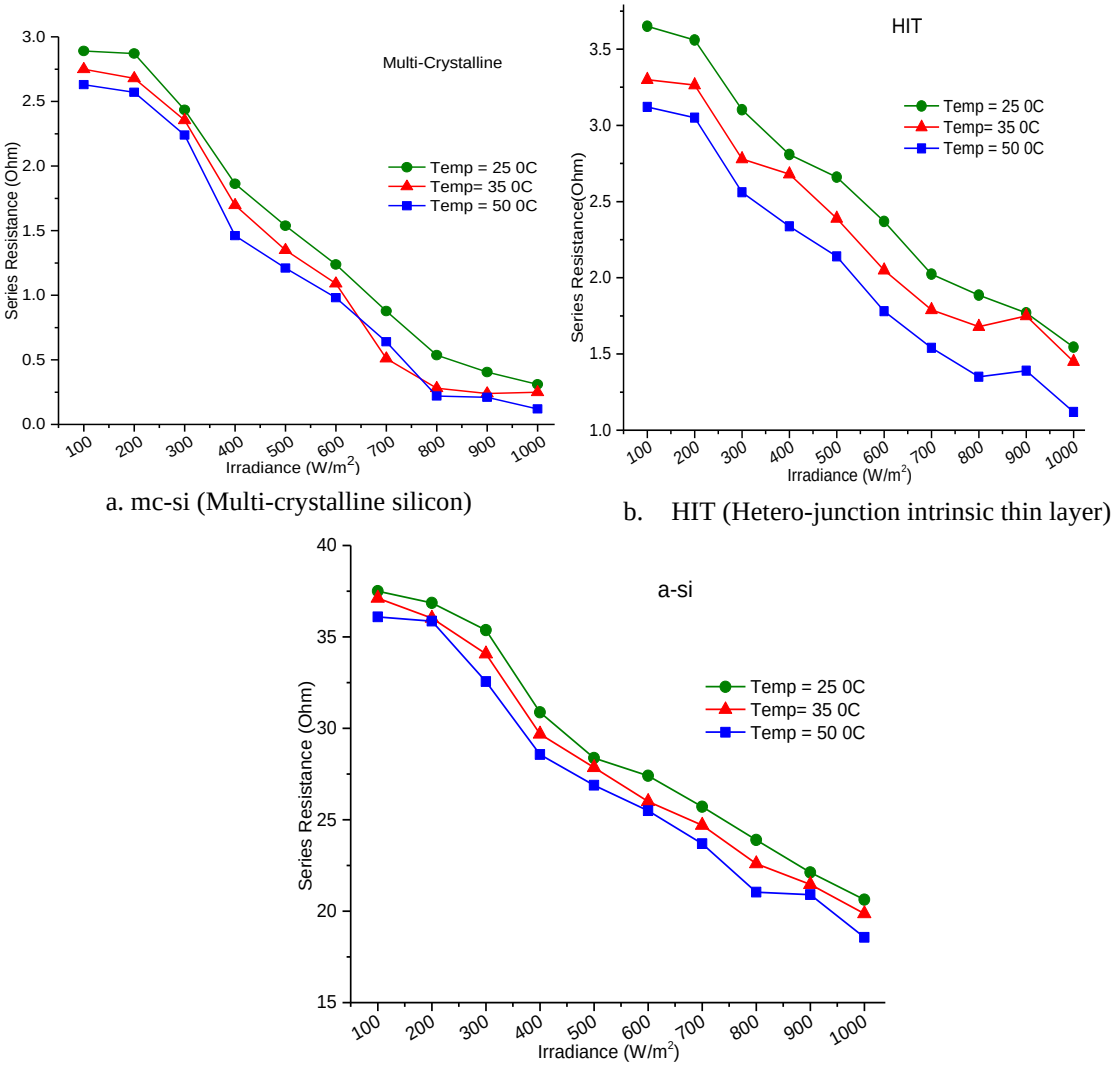

a. mc-si (Multi-crystalline silicon)

b. HIT (Hetero-junction intrinsic thin layer)

c. a-Si (Amorphous single junction silicon)

Fig 5.4. Mean series resistance value as a function of irradiance and temperature for (a) Multi-crystalline module (b) Hetero-junction intrinsic thin layer and (c) Amorphous single-junction silicon solar PV modules

At lower temperature ranges the internal resistance is dominated by the contact resistance of top and base resistance, so the Rs is high. The growth in the series resistance with decreasing irradiation may have an impingement of the

sheet resistance of the semiconductor, which is anticipated to break down with the increasing current due to high irradiance.

However, for thin film modules, resistance influences the resistivity of the semiconductor layer, which might change complexly with temperature.

5.5 Estimation of the series resistance using IEC 60891 Edi 2.0. and increment over a period of three year

The series resistance of the nine SPV modules has been calculated using the IEC 60891 edi.2.0 Procedure-I for the first year as shown in Fig 5.5. In the contour diagram, the series resistance for the nine modules has been presented against the module temperature (0^{o}C-70^{o}C) and the in-plane irradiance (100 W/m^2 -1000 W/m^2).

The range of series resistance are 0.59 Ω -2.31 Ω, 0.34 Ω -2.30 Ω and 0.30 Ω - 2.25 Ω for mc-si_1, mc-si_2 and mc-si_3 SPV modules respectively. Accordingly, the Rs ranges are 0.34 Ω - 45 Ω, 0.23 Ω - 48 Ω and 0.36 Ω - 47 Ω for a-si_1, a-si_2 and a-si_3 respectively. The Rs of HIT modules were 1.20 Ω - 4.79 Ω, 0.99 Ω - 4.43 Ω and 1.09 Ω - 4.59 Ω for HIT_1, HIT_2 and HIT_3 respectively. The highest Rs has been observed for the a-si modules followed by HIT modules whereas the lowest Rs has been observed for mc-si SPV modules.

It has been observed that by lowering the in-plane irradiance the value of the series resistance increases for all the SPV technology modules. There are basically two reasons behind this firstly due to low irradiance the lower generation of the photocurrent and hence high series resistance values, secondly the uncertainties in the assessment of the series resistance for lower ranges of the in-plane irradiance. It is clearly evident that in the low irradiance range the assessment of the series resistance causes a lot of uncertainties hence the high range of series resistance.

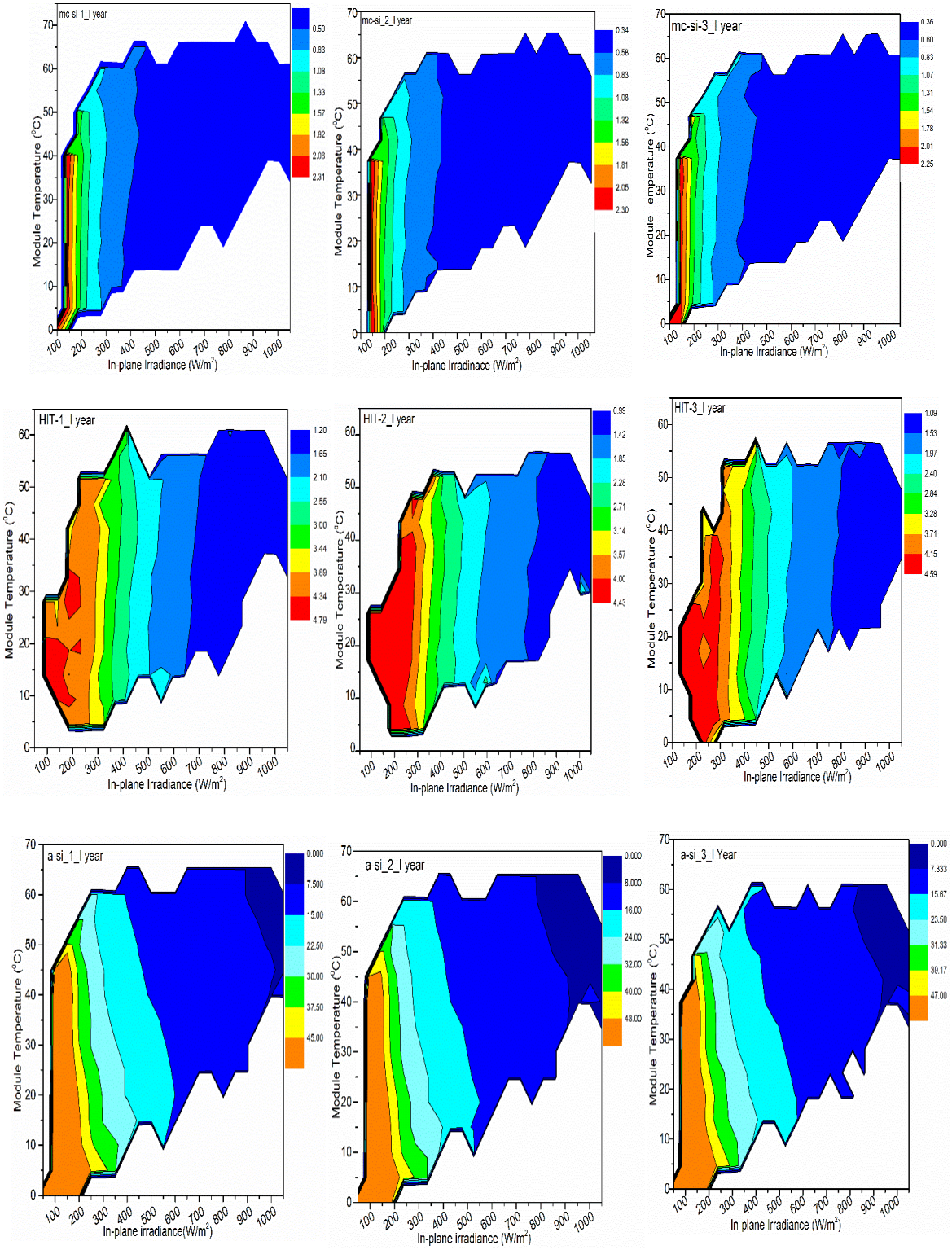

Fig 5.5. The series resistance of the nine modules of m-si, HIT and a-si technologies for I year of operation.

The degradation of the SPV modules in terms of increase in the series resistance has been estimated using the frequency distribution of the series resistance value for all the three years. The graph of the frequency distribution

of the three representative SPV modules, each from m-si, a-si and HIT has been presented in Fig 5.6.

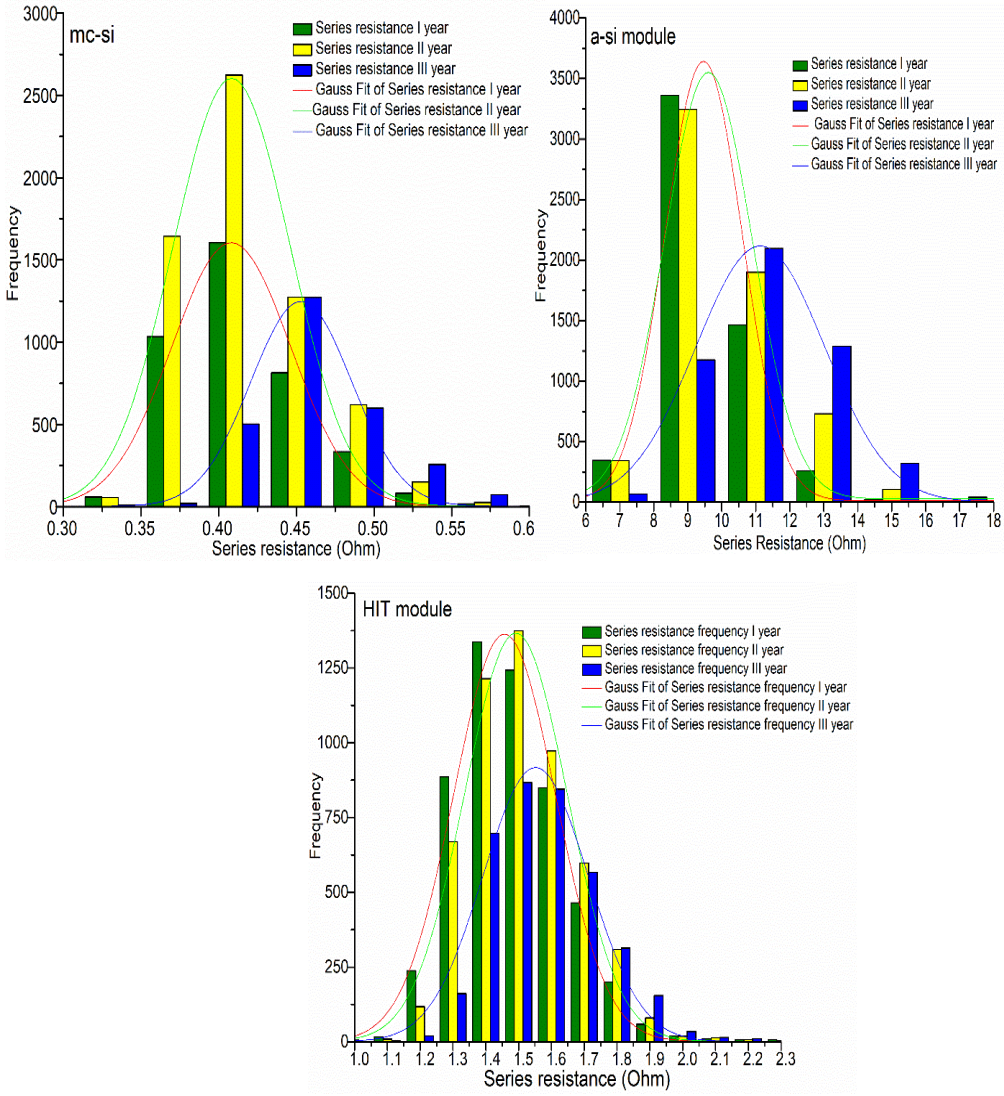

Fig 5.6. The Frequency Distribution of the series resistance for a period of three years

The Off-set (y0), Centre (xc), Width (w), Area (A), sigma (standard deviation), Full Width at Half Maximum (FWHM) is derived using Levenbergy-Marquardt iteration algorithm. The gauss fit for all the three years along with the standard error is done and summarized in Table 5.1. The xc of the mc-si module is increasing from 0.40 to 0.42 from one year to the second year and 0.45 in the third year. The shift in the center is about 12.5% over a period of three years. The percentage increment in the after the first year is 5%

whereas the increment is 7.14% for the final year. The FWHM width between the points on the y-axis is from 0.09 to 0.08 and then 0.07 for third last year. The width shows the spread of the series resistance value which is decreasing in the third year in comparison to the first and second year. The standard deviation is 0.03 constant for all three years.

Table 5.1. The frequency distribution of the series resistance for a period of three years using the Levenberg Marquardt algorithm.

Parameters	**mc-si module**			**a-si module**			**HIT module**		
Equation	y=y0 + (A/ (w*sqrt (PI/2))) *exp(-2*((x-xc)/w) ^2)								
Reduced Chi-Sqr.	852.64	3351.47	587.41	2504.02	20152.06	1162.01	960.35	1005.69	761.17
Adj. R-Square	0.98	0.97	0.97	0.99	0.96	0.99	0.98	0.99	0.98
	Parameter	**Value**	**Standard Error**	**Value**	**Standard Error**		**Value**	**Standard Error**	
Gauss Fit of the series resistance of Ist Year	y0	1.83	3.44	10.96	10.98		1.54	4.68	
	xc	0.40	7.58E-4	9.46	0.03		1.45	0.003	
	w	0.07	0.001	2.28	0.05		0.31	0.006	
	A	153.56	2.71	10377.95	194.29		529.26	9.70	
	Sigma	0.03	7.54E-4	1.14	0.02		0.15	0.003	
	FWHM	0.09	0.001	2.68	0.06		0.36	0.007	
Gauss Fit of the series resistance of IInd Year	y0	3.69	6.82	26.12	31.47		1.43	4.79	
	xc	0.42	9.22E-4	9.60	0.07		1.49	0.003	
	w	0.07	0.001	2.58	0.17		0.31	0.006	
	A	246.50	5.34	11417.79	588.83		535.53	9.98	
	Sigma	0.03	9.14E-4	1.29	0.08		0.15	0.003	
	FWHM	0.08	0.002	3.04	0.20		0.36	0.007	
Gauss Fit of the series resistance of IIIrd Year	y0	3.03	2.84	0.24	7.81		0.91	4.18	
	xc	0.45	7.58E-4	11.13	0.03		1.55	0.004	
	w	0.06	0.001	3.78	0.06		0.32	0.008	
	A	101.74	2.04	10053.99	171.31		367.54	8.79	
	Sigma	0.03	7.02E-4	1.89	0.03		0.16	0.004	
	FWHM	0.07	0.001	4.46	0.08		0.37	0.009	

The shift in the center of the a-si module is increasing from 9.46 to 9.60 from one year to the second year and 11.13 in the third year. The percentage increment in the shift of the center is about 17.65% over a period of three years. The percentage increment in the center after the first year is 1.47% whereas 15.93% after the final year. The FWHM width between the points on the y-axis is from 2.68 to 3.04 and then 4.46 for third last year. The width shows the spread of the series resistance value which is increasing every year. The standard

deviation is also increasing 1.14, 1.29 and 3.78 for I, II and III year respectively. The highest increment in the series resistance over a period of three years is observed for the a-si modules in correlation with the highest degradation rate of 1.69%/year. The increment in the series resistance of the modules with the exposure in the outdoor field is evident from the graphs and the Gaussian fit parameters.

Lastly, for the HIT module shift in the center is increasing from 1.45 to 1.49 from one year to the second year and 1.55 for the third year. The percentage increment in the shift of the center is about 6.89% over a period of three years. For the first year, the percentage increment in the center is 2.75% however for the final year the increment is 4.02%. The FWHM width between the points on the y-axis is constant for a first and second year about 0.36 then 0.37 for the third year. The width shows the spread of the series resistance value which is constant for I and II years and slightly increased in the third year. The standard deviation is constant for I and II years 0.15 and 0.16 for the third year. The lowest increment in the series resistance over a period of three years is observed for the HIT modules in correlation with the highest degradation rate of 0.39%/year.

It has been observed from the graphs and the extracted parameters that the power decrement and the increment in the series resistance has a strong correlation. The highest degradation rate has been documented for the a-si technologies also having the highest increment in the series resistance whereas the lowest degradation rate is observed for the HIT modules having the lowest degradation rate. The increment in series resistance may be caused due to the cell interconnect break, corrosion of the metal, busbar and electrical connections, lowering of the fill factors in the PV modules which leads to the degradation of the module.

5.6 Uncertainty estimation of the series resistance methodology

The uncertainty analysis of measurement and series resistance calculation has been carried out for three ranges of irradiance. The repeatability of the series resistance determination in terms of repeated I-V measurements at normally an identical condition have been taken and variation of series

resistance calculated from repeated I-V measurement at normally identical conditions for all the three technologies. Table 5.2 shows the mean series resistance, variance, standard deviation and uncertainty, including Type-A uncertainty, combined standard uncertainty and the expanded uncertainty at 1000 W/m^2, 900 W/m^2 and 800 W/m^2 irradiance level.

Table 5.2. The estimated percentage of uncertainty for each range of corrected irradiance

Solar Technology	Irradiance (W/m^2)	Variance	Standard Deviation	Type A (%)	Combined Standard Uncertainty (%)	Expanded Uncertainty (%)
Multi-crystalline silicon	**800**	0.001	0.013	0.138	1.963	3.926
	900	0.001	0.012	0.137	1.962	3.925
	1000	0.001	0.015	0.206	1.968	3.937
Hetero-junction intrinsic thin layer	**800**	0.003	0.033	0.134	1.962	3.925
	900	0.002	0.016	0.090	1.960	3.920
	1000	0.001	0.010	0.058	1.958	3.917
Amorphous single junction silicon	**800**	0.120	1.250	0.210	1.969	3.938
	900	0.156	1.404	0.290	1.979	3.958
	1000	0.159	1.456	0.293	1.980	3.965

It shows that the Type-A uncertainty for mc-si and a-si increases with the increasing irradiance however vice versa for HIT technology. The combined standard uncertainty and expanded uncertainty for all the three technologies are almost same for all the irradiance. Typical accuracy of the measurements taken through the device for the temperature, irradiance, voltage, and current is less than 1% for each. The variance is lowest for mc-si followed by HIT SPV module and highest for a-si solar module technology.

5.7 Conclusion

The ten different methodologies (i.e. Nine analytical and IEC procedure) for determining series resistance of three different technologies, i.e., Multi-crystalline, HIT and Amorphous Silicon, has been investigated and the effect of irradiance and module temperature on series resistance has also been assessed. The method three is found to be more stable among the nine analytical techniques of measuring series resistance.

The mean series resistances for mc-si, a-si and HIT modules are found to be 0.72 Ω, 18.20 Ω, and 0.61 Ω respectively using analytical techniques while 0.31 Ω, 20.62 Ω and 1.54 Ω respectively using IEC 60891 Edi. 2.0. The series resistance decreases with the increase in irradiance at the slope of -0.108, -0.063 and -3.348 for the mc-si, HIT and a-si solar PV module respectively. The effect of irradiance on series resistance is lowest on the HIT modules as compared to the other two technologies. From the results, it can be concluded that the variation in the results may be observed due to the input parameters, modelling equations and assumptions made during the calculations. The result shows that the modelling equations have been mainly derived for the mc-si technology and it is proposed that new modelling is required for the new emerging technologies like HIT and thin films modules. It has also been found that there is a need for a stable and standardized analytical method for calculating the series resistance.

The mapping of the series resistance has been done to the matrix of in-plane irradiance and module temperature. The uncertainty for estimation of the series resistance has been found out to be around 4% for three ranges of irradiance for all the modules. The work presented in this paper improves the knowledge of PV modules at the composite climate of India over a field exposure. Most of these characteristics are related to better performance assessment, which is very useful for developers, installers, financers, and clients in the scheduling of PV installations with a reduced level of uncertainty. This will eventually lead to lower cost of financing due to reduced risk and help in better valuation of mission feasibility. This is a very important feature to implement very large PV programs such as the National Solar Mission in India.

CHAPTER 6
THERMAL STRESS OVER HIGH-EFFICIENCY SOLAR PHOTOVOLTAIC MODULES

This chapter carried out a systematic compilation of a procedure to examine the thermal and the electrical stress analysis and fault detection in solar module technologies using Infra-Red thermography. The chapter covers the non-destructive performance monitoring of modules under various shading configurations to evaluate the impact of the partial shading on the thermal stress of the solar modules. This analysis also useful for manufacturers, solar field installer and solar power plant designer to set up a proper plant with safety standards along with long-term dependability and strength.

6.1 Introduction

The long-term monitoring and assessment of solar power plant over time provide the reliability and durability of the system at different climatic zones. The process of monitoring the condition of the solar modules in the field is considered as performance monitoring. It aims to check the current status of the plant, to deduct the early degradation, prevent the unexpected breakdown, maximize the plant life, and reduce the failure percentage in the field. Apart from the financial and economic losses it also leads to accidental damage to the society and the environment. The efficient performance monitoring aim is to monitor the solar module components, system designs, and faults, thereby enhancing the quality of the manufactured product and reduction in the maintenance cost.

Hot spots are a well-known phenomenon of defect and degradation occurring in the solar photovoltaics (SPV) modules. It happens when a solar cell

or group of solar cell operates in reverse-bias condition and starts dissipating power instead of generating it i.e., work as a load. Due to this phenomenon, the solar cell attains a higher temperature in comparison to other cells in the SPV modules. The cell exposed to higher temperature degrades at a higher rate and, if operation at high temperatures occurs for a prolonged time, make it operate permanently in reverse bias. Periodic Infra-Red thermography may be useful for the early identification and potential removal of the hotspot solar modules from the SPV power plants to mitigate future module mismatch issues at the string levels.

6.2 Methodology

There are two strategies (Case Study) are considered in the investigation of the thermal and electrical stress over the Solar PV modules having m-Si, mc-Si, HIT and SunPower IBC technology in outdoor condition at the composite climate of India. The four solar module technologies have been deployed in the outdoor field since 2014 working in a loaded condition. The I-V tracer and weather and weather monitoring station have been used for the measurement of current-voltage characteristics and environmental parameters respectively. The reading is carried on the Alternate test condition (ATC) which is irradiance 800 $W/m^2 \pm 50$ W/m^2 and the ambient temperature is 40 °C ±5 °C which is also the most frequent condition of the Gurugram for inter-comparison. The detailed experimental set-up and the opted methodologies for both case studies at the National Institute of Solar Energy, Gurugram are described in the chapter-3 along with the instrument's detail and range of accuracy.

6.2.1 Case Study-I

To study the thermal stress under arbitrary patterns of illumination, we developed a methodology of studying different Infra-Red images by short-circuiting the SPV modules for 10 mins continuously. The experiment is also extended by the short-circuiting the solar module up to 2 hours and the hotspot, so obtained can be regarded as the worst-case scenario.

Under normal operation of the solar module at maximum power points, the hotspots are expected to be much less severe (since the module at MPPT would not be dissipating the total input energy as heat as would happen in the

case of short-circuited modules). Infra-Red images have been used for mapping the temperature distribution over the module's surface, accordingly, the detection of the thermal stress is done.

6.2.2 Case Study-II

Infra-Red images have been used for mapping the temperature distribution under several partial shading conditions to determine the correlation between thermal imaging and electrical properties of the solar photovoltaic modules in the composite climate of India. The influence of the solar module technology, the number of cells per bypass diode, the position of the partial shading has also been studied. Further, the possibility of destructive hotspots has been forecasted. The function of bypass diode has also been considered under different shading conditions.

The methodology adopted in this work essentially entails exposing some of the modules to outdoor conditions and recording their electrical output parameters through a data logger on a continuous basis. Along with these, Infra-Red thermography techniques used for a definite time interval to identify the possible forms of defects and their progression in the solar modules.

6.3 Results and Discussion

The IR images and electrical measurements have been analyzed under several configurations, to assess the performance of the SPV module after three years of outdoor operations, about the identification of the hotspot defect. The results comprise of the thermal impact of the surrounding temperature over the PV modules, hotspot formation, impact of various shading configurations in the loaded state and analysis of the electrical behaviour of the field aged solar module technologies.

6.3.1 Case Study-I. Thermal impact over short-circuited configurations. Hotspot heating effect.

The temperature distribution mapping and histogram representation of temperature at the initial (i.e., the first measured after 10 minutes) and final condition (measurement after 2 hours) of field aged SunPower, Multi-

crystalline, HIT and Mono-crystalline SPV modules has been documented in below Figs.

The normalization of the measured temperature data has been done using the formula explained in the Chapter-3. Normalizing the temperature allows us to define a set of parameters that function well for a variety of Infra-Red images with varying temperature ranges. Deviations from the median temperature of several photovoltaic modules within an Infra-Red image are an indicator for such abnormalities. However, also overheating massively depends on the weather conditions, which can result in temperature fluctuations of 1°C to 10 °C. Using the median temperature, we can detect such faults. The data are extracted from the IR images and used to plot with the frequency they occur in the real operating condition. The severity of the hotspot formation will depend on the amount of power dissipated due to a high reverse bias voltage which causes the gain in the temperature of the cell region. The mode value of the histogram is taken as the representative temperature in the field aged PV module since it is the most frequently occurring temperatures in the module IR image. From the images the following requirements have been extracted;

1. The minimum and maximum temperature of the solar module, which helps to find the delta temperature of the module (ΔM).
2. The temperature value which is having the highest number of frequencies over the module upper surface.

The high-temperature cells, i.e., hotspots are shown as bright in the images. It has been observed that the temperature of modules and the number of hotspots increases with time, while the rate and range of temperature increment depend on the SPV module technology. The severity of the hotspot formation will depend on the amount of power dissipated due to a high reverse bias voltage which causes the gain in the temperature of the cell region. The mode value of the histogram is taken as the representative temperature in the field aged PV module since it is the most frequently occurring temperatures in the module IR image.

From Fig 6.1, the Infra-Red images of the initial and final periods, i.e. after 10 minutes of SunPower solar module technology with their occurrence frequencies in the histogram graph are presented. In case of SunPower module, the maximum frequency for temperature is found to be shifted from 44 °C to 46 °C with an increment of 4.54 % over a time period of 2 hours, while the range of temperature within a module varies from 40°C - 54 °C to 42°C-58°C. The initial median temperature of the SunPower technology is about 44 °C, and finally, after 10 minutes, the median of the temperature goes to 46 °C.

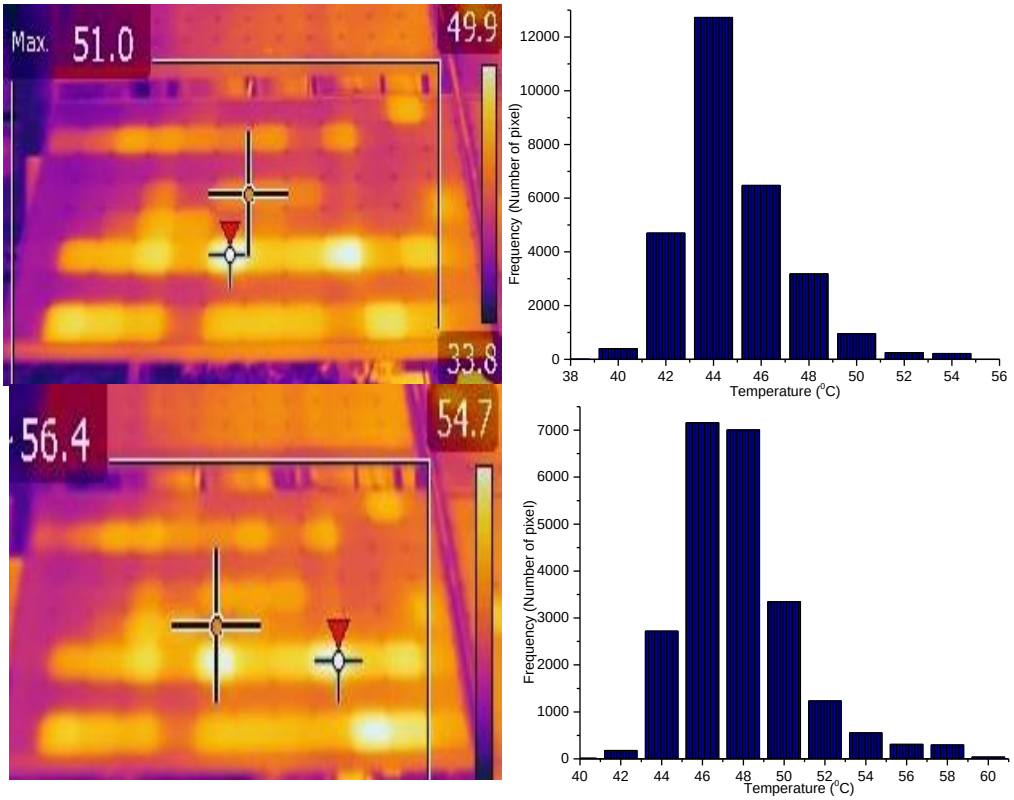

Fig 6.1. Infra-Red image of a SunPower PV module and its temperature histogram extracted from the IR images

The temperature coefficient of the SunPower technology for power is –0.29%/°C. C were to reach an extreme heat of 50 °C, it would reduce output by as much as 13.34 % (-0.29 % x 46). From this, by increasing per degree Celsius there is a -0.29% decrement of power output.

The initial mean temperature of the HIT solar module technology is about 38 °C, and after 10 minutes, the temperature goes to 50 °C shown in Fig 6.2. The mean temperature of the module also depends upon the short-circuiting

condition, its ranges in the initial values, i.e., 36°C to 56 °C. However, the temperature range is between 40 °C to 52 °C after 10 minutes. The percentage of increment in the temperature is around 24 %. The temperature coefficient of the HIT module is -0.30% / °C were to reach an extreme heat of 50 °C, it would reduce output by as much as 15 % (-0.3% x 50). Nevertheless, there is the impact of other parameters also than simply the coefficient value, and the equation is a little more complex.

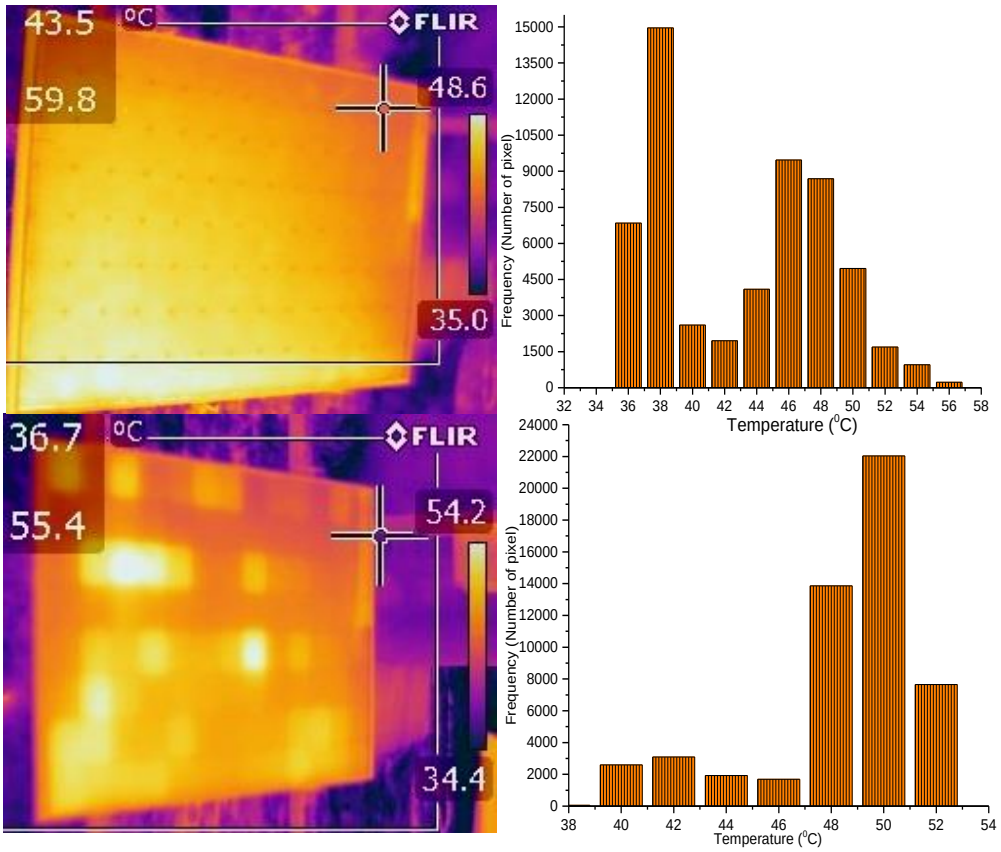

Fig 6.2. Infra-Red image of a HIT PV module and its temperature histogram extracted from the IR images

The temperature ranges of the mc-si solar modules in the initial time are between 40 °C to 50 °C but after 10 minutes it increases from 40 °C to 56 °C as presented in Fig 6.3. The initial median temperature of the mc-si module is about 48 °C, and finally, after 10 minutes, the median of the temperature goes to 52 °C. The percentage increments in the temperature of the PV module after 10 minutes is 7.69 %. The temperature coefficient of the mc-si technology for power is -0.42 % /°C were to reach an extreme heat of 52 °C, it would reduce output by as much as 21.84 % (-0.42% x 52).

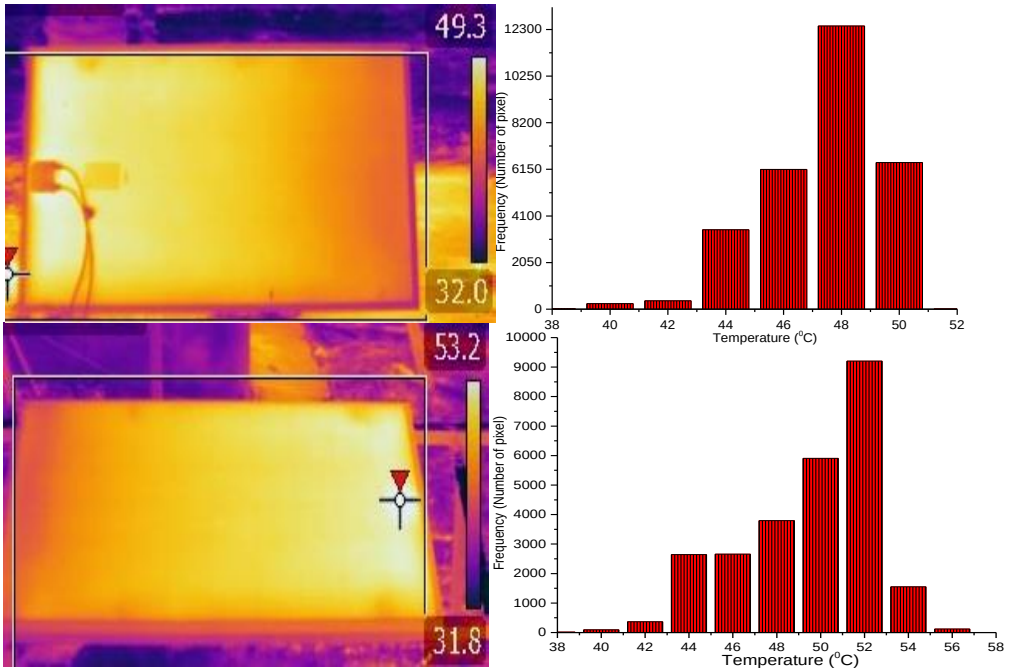

Fig 6.3. Infra-Red image of a multi-crystalline PV module and its temperature histogram extracted from the IR images

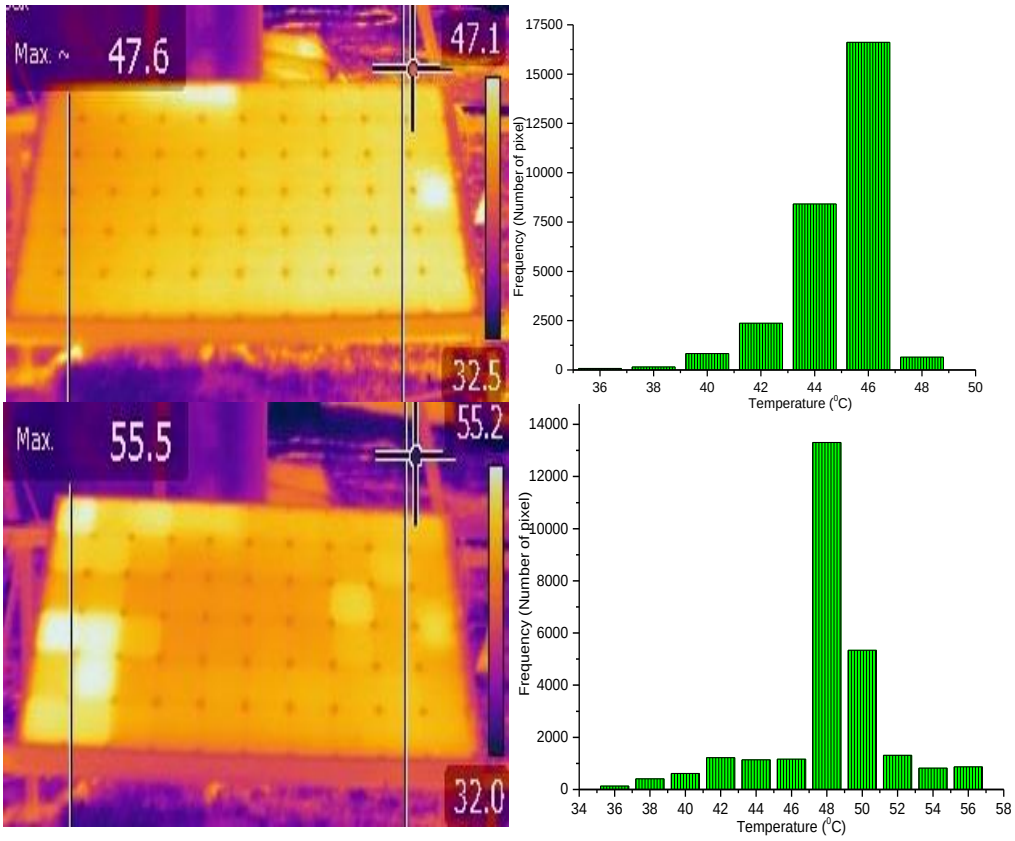

Fig 6.4. Infra-Red image of mono-si PV module and its temperature histogram extracted from the IR images

The initial and final period of the m-si module with their occurrence frequencies is shown in Fig 6.4 using the histogram. The temperature ranges of initial are 36 °C to 48 °C and after 10 minutes its increases from 36 °C to 56 °C. The initial median temperature of the m-si module is about 46 °C, and finally, after 10 minutes, the median goes to 48 °C. The percentage increments in the temperature of the SPV module after 10 minutes is 4.16 %. The temperature coefficient of the m-si PV technology for power is -0.42 % /°C were to reach an extreme heat of 48 °C, it would reduce output by as much as 20.16 % (-0.42% x 48).

The lowest output power decrement occurs in the SunPower technology followed by HIT modules. The temperature of the solar module is mainly affected by the ambient temperature (location), the temperature coefficient and the type of installation. First parameter, i.e. location in most cases cannot be changed as the ambient conditions are beyond the scope. The second parameter is the material-specific property and many types of research are going on to improve the temperature coefficients. Lastly, the type of panel installation also has an effect on the temperature of the panels. When solar panels are installed on a rooftop, they experience far greater temperatures than the current ambient temperature. Solar modules which are fixed parallel to the roof with no airflow between the rooftop and panel are the least efficient and experience the greatest rise in temperature.

It has also been observed that the temperature of hotspot also depends on the positioning of cell and bypass diode in the string due to heat dissipation. This temperature increases of a cell near to the junction box cause a variation in voltage (ΔV), which results in the mismatch between the solar cells equivalent to partial shadowing effect and leads to the reduction of power output (ΔP). If this effect is long and steady, the cell operating under increased temperature will eventually experience a slow physical degradation, leading to permanently reduce the power output of the solar modules.

6.3.2. Impact of partial shading over the temperature rise and electrical behaviour of the module

To investigate the impact of partial shading, the maximum temperature increment for various shading profiles over different solar module technologies

have been analysed and compared with electrical characterization. I-V curve was obtained for nine shading configurations using an opaque board by triggering each diode one by one for all the solar module technologies. The mono and multi-crystalline modules have 20 cells in each string, and the three strings are connected in series. In SunPower module, each string has 32 cells, and three strings are connected in series, while in HIT module, the four strings are connected in series, and each string has 26 cells. The modules have one diode for each string, i.e., 3 diodes for SunPower, Monocrystalline and multicrystalline modules while four diodes for HIT module, connected in a way, that each diode would bypass the respective string only.

The I-V curves are obtained under the various configurations i.e., activation of bypass diode and IR image for all diodes activated for the HIT, mono, and multi-crystalline SPV modules have been presented. Fig 6.5 shows the I-V characteristic curve which describes the triggering of all the four diodes in the HIT solar module by various shading patterns and Infra-Red image of the worst condition. The temperature has been rising up to 63 °C maximum in worst shading configuration of the module. The range of the temperature of the entire modules is in between the 40 °C to 63 °C. From Fig 6.6, the m-si solar module has an increment of the 48 °C to the 56.4 °C. The highest temperature peak goes to 60 °C in the Infra-Red imaging. The mc-si solar module has been raised in the temperature from 40 °C to 58.6 °C. The maximum temperature of the solar module is about 60 °C.

The temperature increment above the junction box is the hottest cell compare to the rest of the module in all the cases. In general, the maximum temperature is obtained when a significant dimension of the modules was shaded. It is imperative to note that the increase in temperature depends on factors that the modules which are in shaded behave as a power dissipation device (like a resistor) which is called reverse bias, starts consuming power and hence produced heat. This increment in the temperature affects the voltage series resistance of the modules. If these states occur for a more extended period, it may cause the hotspot or the permanent degradation of the module material.

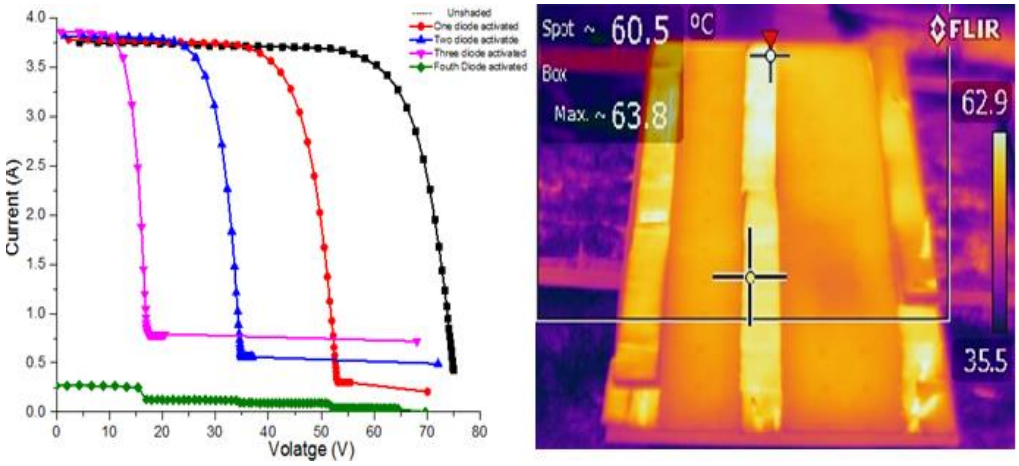

Fig 6.5. I-V Characteristics curve of HIT module in all shading configuration and IR image in the worst case (all three diodes activated)

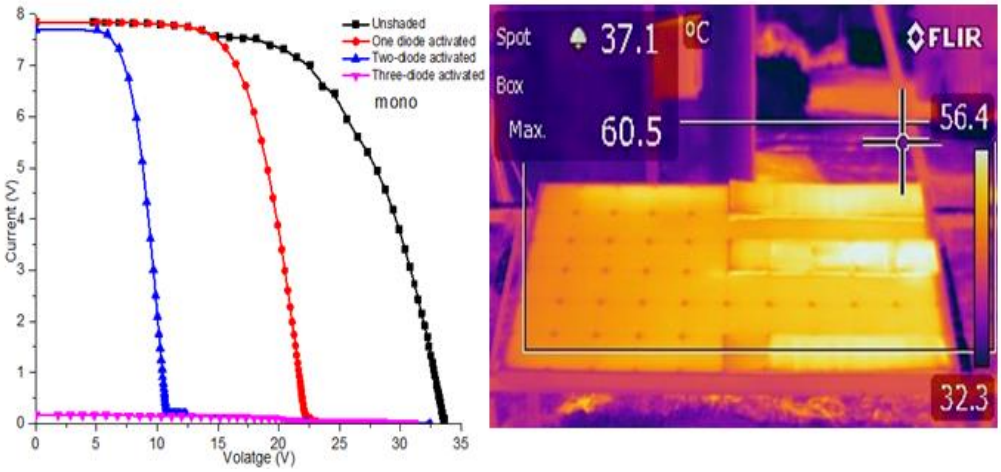

Fig 6.6. I-V Characteristics curve of the m-si module in all shading configuration and IR image in the worst case (all three diodes activated)

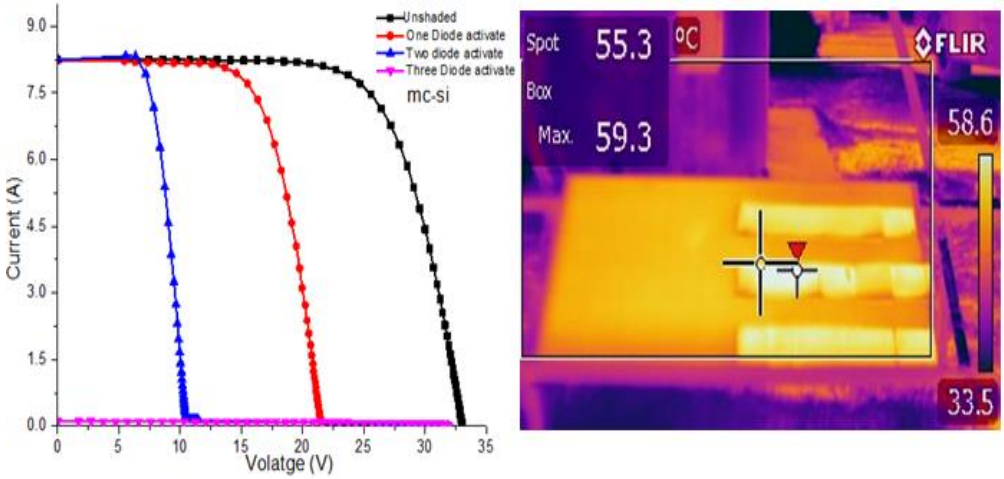

Fig 6.7. I-V Characteristics curve of an mc-si module in all shading configuration and IR image in the worst case (all three diodes activated)

The number of cells serially connected does not affect the point at which the bypass diodes, but it is crucial to maximum temperature reached by the shaded cell. The various shading configurations help to correlate all the possible combinations of the shading and triggering the bypass diodes. The I-V characteristic curve of the solar modules shows that the deterioration in SPV performance is mainly due to high resistance to various shading conditions. The parasitic series resistance for different SPV module technologies is given in Table 6.1.

Table 6.1. The series resistance of various partial shading configurations over different technology modules

S.no.	Configuration of the solar modules	Series Resistance (Ohm) Ω			
		m-si	mc-si	HIT	SunPower
1	Unshaded solar module	0.722	0.470	1.897	0.986
2	10% of one string in the solar modules	1.472	1.106	6.123	1.12
3	50% of one string in the solar modules	1.291	1.100	6.250	1.190
4	100% of one string in the solar modules	1.272	1.085	6.016	1.25
5	10% of two string in the solar modules	2.885	2.087	7.023	2.560
6	50% of two string in the solar modules	2.368	1.931	7.322	2.68
7	100% of two string in the solar modules	2.459	1.986	7.56	2.65
8	10% of three string in the solar modules	5.000	6.000	9.630	3.450
9	50% of three string in the solar modules	85.00	96.00	11.898	9.56

It has been observed from the Table 6.1, that the partial shading of a string is more hazardous than full shading, as the series resistance of a module with 50% shaded string is higher than that of the 100% shaded strings. The series resistance of the SPV modules is increased by increasing the shading fraction over the modules. This will impact on the modules if modules remain in the same states. Periodic Infra-Red thermography may be useful for the early identification and potential removal of the hotspot solar modules from the SPV power plants to mitigate future module mismatch issues at the string levels.

Electrical degradation can cause severe failures at all levels of the PV system, PV cell, modules and array. Some common field aged electrical deterioration is the micro cracks, snail trails, delamination, Back sheet tearing or cracking, faulty solder joints, etc. These types of defects cause an increase in

the series resistance which leads to the generation of the more thermal stress cause non-uniform temperature profiling which can be easily detected through the IR methods. During the partial shading effect, the series resistance for each profile is also measured. The series resistance of all the four technology shows increasing behaviour with an appositive value of the slope. From the I-V curve of all the modules, the decreased slope of Open circuit voltage proves the existence of a high series resistance due to the shading. Improvements to the IR modelling approaches could be made by considering the different source of IR losses in the image and further the image processing. For monitoring the largest solar power plants through the IR images could be an important tool to save time and labour.

6.4 Conclusion

In this chapter, an overview has been provided on the uses of different approaches of Infra-Red thermography for monitoring, detection, and characterization of different field aged solar modules. A comprehensive evaluation of the thermal and electrical effects caused by the partial shading has been carried out for four different SPV module technologies. The increment in maximum frequency, the temperature of an SPV module is observed to be highest in mc-si PV modules.

The effect of the ambient temperature of the solar modules has been examined in the present study. The increase in the range of module temperature is an indication of non-uniformity of the temperature of each cell within the module, which, in turn, is either prone to or occurrence of the hotspot. The range of temperature is found to be increased significantly in the SunPower and Mono-crystalline modules as compared to others, and therefore, the hotspots are apparently visible in the IR images. The relative temperature differences measured within the solar cell may assist in the diagnosis of early degradation in the solar module. The partial shading of a string or cell within an SPV module is more severe than that of full shading and causes more degradation.

CHAPTER-7
FEASIBILITY STUDY OF THE HIGH-EFFICIENCY PV MODULES

This thesis addresses the economic assessment of high-efficiency modules in the composite climate of India (Gurugram).

7.1. Introduction

With the growing demand for harnessing renewable energy in the world instead of traditional energies in electricity generation, a diverse assessment of the performance of PV solar power plant has become necessary to make the most of them everywhere in the world.

7.2 Methodology

The PVSYST V6.79 software has been used for the feasibility study of the three silicon-based PV modules for the location Dhera-Mandi (National Institute of Solar Energy, Gurugram). The location is having Latitude 28.42° N and Longitude 77.15° E on an altitude of 246 m. Two cases have been adopted for the feasibility study of the High-Efficiency PV modules.

Case 1: For installation of the 100 KWp plant, the total requirement of the land for each technology having other things constant (location and climatic condition).

Case 2: For technical and cost comparison the compilation of the performance matrices has been done. Four performance matrices are used.

7.3 Results and Discussion

The results and discussion are divided into two parts for two cases. In Case-1, the results of the case-1 are summarized in below Figures 7.1, 7.2 and Figure 7.3 using the PVSYST V6.79 Software. The HIT, mc-si and SunPower power plant of 100 kWp have used for the area requirement. The yearly PR calculation for three-silicon based technology has been estimated using the software.

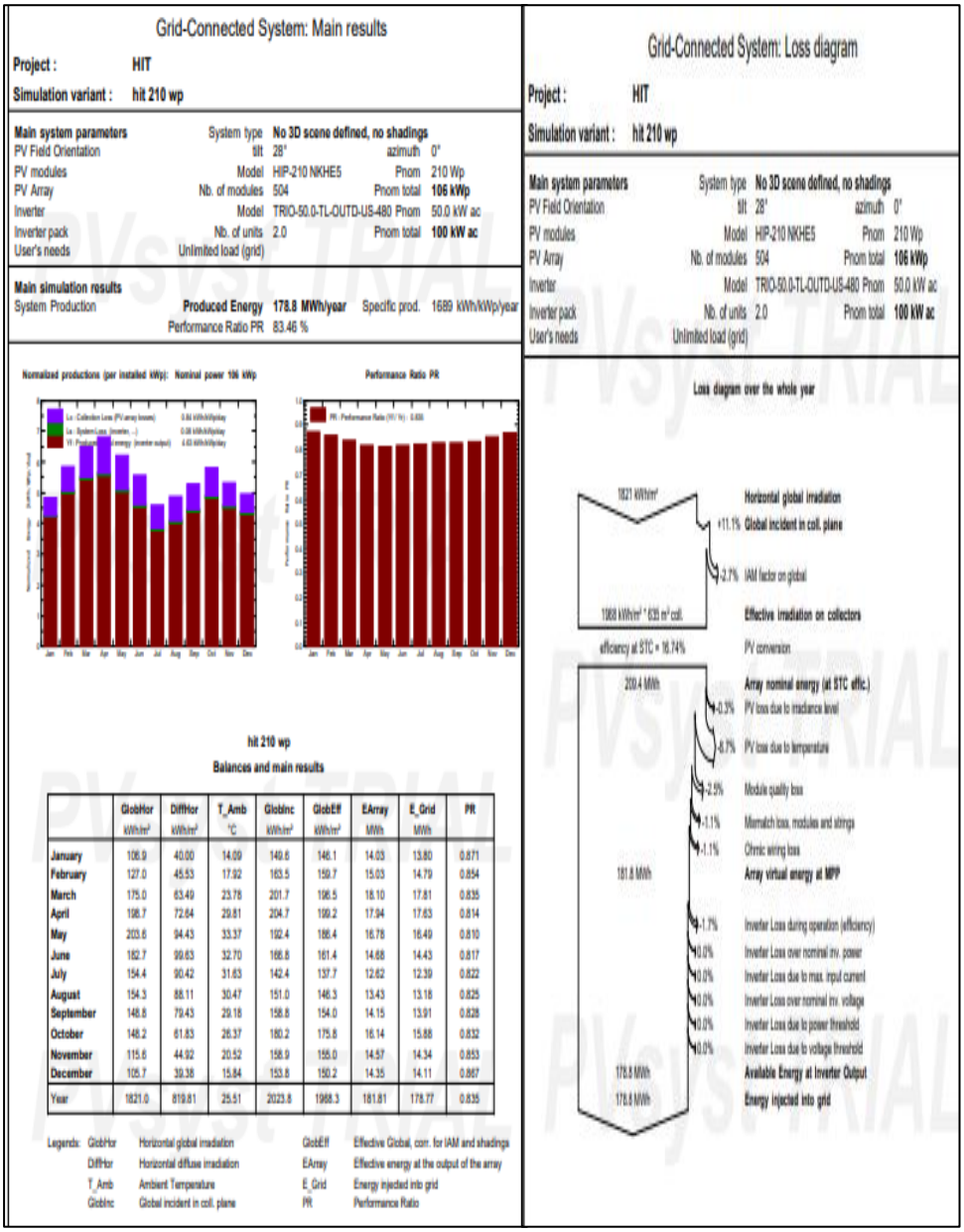

Grid-Connected System: Main results

Project : HIT

Simulation variant : hit 210 wp

Main system parameters — System type: No 3D scene defined, no shadings
PV Field Orientation — tilt 28° — azimuth 0°
PV modules — Model HIP-210 NKHE5 — Pnom 210 Wp
PV Array — Nb. of modules 504 — Pnom total 106 kWp
Inverter — Model TRIO-50.0-TL-OUTD-US-480 — Pnom 50.0 kW ac
Inverter pack — Nb. of units 2.0 — Pnom total 100 kW ac
User's needs — Unlimited load (grid)

Main simulation results
System Production — Produced Energy 178.8 MWh/year — Specific prod. 1689 kWh/kWp/year
Performance Ratio PR 83.46 %

Normalized productions (per installed kWp): Nominal power 106 kWp

Performance Ratio PR

hit 210 wp

Balances and main results

	GlobHor kWh/m²	DiffHor kWh/m²	T_Amb °C	GlobInc kWh/m²	GlobEff kWh/m²	EArray MWh	E_Grid MWh	PR
January	106.9	40.00	14.09	149.6	146.1	14.03	13.80	0.871
February	127.0	46.53	17.92	163.5	159.7	15.03	14.79	0.854
March	175.0	63.49	23.78	201.7	196.5	18.10	17.81	0.835
April	198.7	72.64	29.81	204.7	199.2	17.94	17.63	0.814
May	203.6	94.43	33.37	192.4	186.4	16.78	16.49	0.810
June	182.7	99.63	32.70	166.8	161.4	14.68	14.43	0.817
July	154.4	90.42	31.63	142.4	137.7	12.62	12.39	0.822
August	154.3	88.11	30.47	151.0	146.3	13.43	13.18	0.825
September	148.8	79.43	29.18	156.8	154.0	14.15	13.91	0.828
October	148.2	61.83	26.37	180.2	175.8	16.14	15.88	0.832
November	115.6	44.92	20.52	156.9	155.0	14.57	14.34	0.853
December	105.7	39.38	15.84	153.6	150.2	14.35	14.11	0.867
Year	1821.0	819.81	25.51	2023.8	1968.3	181.81	178.77	0.835

Legends: GlobHor Horizontal global irradiation; GlobEff Effective Global, corr. for IAM and shadings; DiffHor Horizontal diffuse irradiation; EArray Effective energy at the output of the array; T_Amb Ambient Temperature; E_Grid Energy injected into grid; GlobInc Global incident in coll. plane; PR Performance Ratio

Grid-Connected System: Loss diagram

Project : HIT

Simulation variant : hit 210 wp

Main system parameters — System type: No 3D scene defined, no shadings
PV Field Orientation — tilt 28° — azimuth 0°
PV modules — Model HIP-210 NKHE5 — Pnom 210 Wp
PV Array — Nb. of modules 504 — Pnom total 106 kWp
Inverter — Model TRIO-50.0-TL-OUTD-US-480 — Pnom 50.0 kW ac
Inverter pack — Nb. of units 2.0 — Pnom total 100 kW ac
User's needs — Unlimited load (grid)

Loss diagram over the whole year

1821 kWh/m² Horizontal global irradiation
+11.1% Global incident in coll. plane
-2.7% IAM factor on global
1968 kWh/m² * 635 m² coll. Effective irradiation on collectors
efficiency at STC = 16.74% PV conversion
209.4 MWh Array nominal energy (at STC effic.)
-0.3% PV loss due to irradiance level
-8.7% PV loss due to temperature
-2.5% Module quality loss
-1.1% Mismatch loss, modules and strings
-1.1% Ohmic wiring loss
181.8 MWh Array virtual energy at MPP
-1.7% Inverter Loss during operation (efficiency)
0.0% Inverter Loss over nominal inv. power
0.0% Inverter Loss due to max. input current
0.0% Inverter Loss over nominal inv. voltage
0.0% Inverter Loss due to power threshold
0.0% Inverter Loss due to voltage threshold
178.8 MWh Available Energy at Inverter Output
178.8 MWh Energy injected into grid

Fig. 7.1 Software report of the feasibility study of the HIT power plant using the PVSYST 4.67 version software.

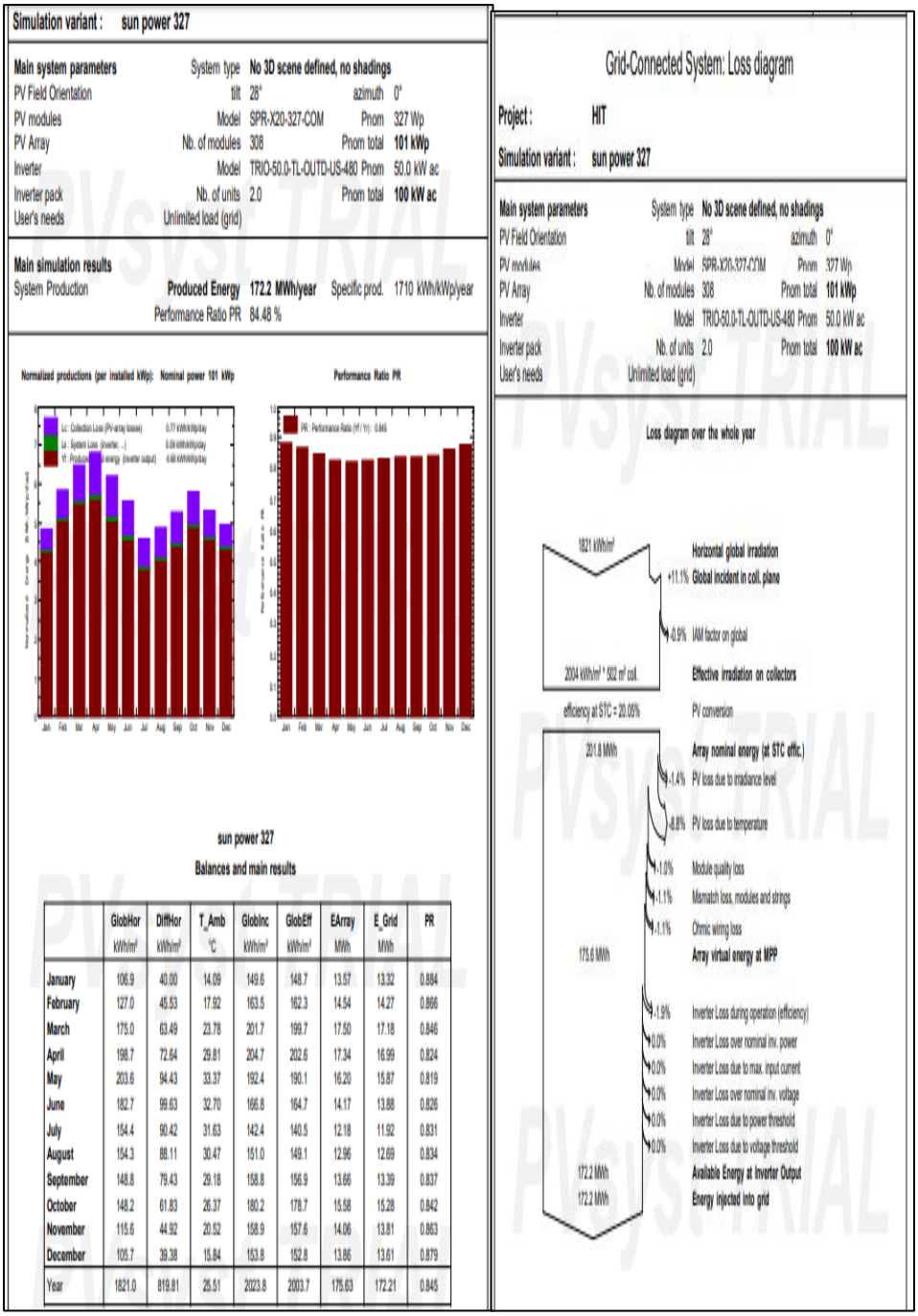

Fig 7.2. Software report of the feasibility study of the SunPower power plant using the PVSYST 4.67 version software

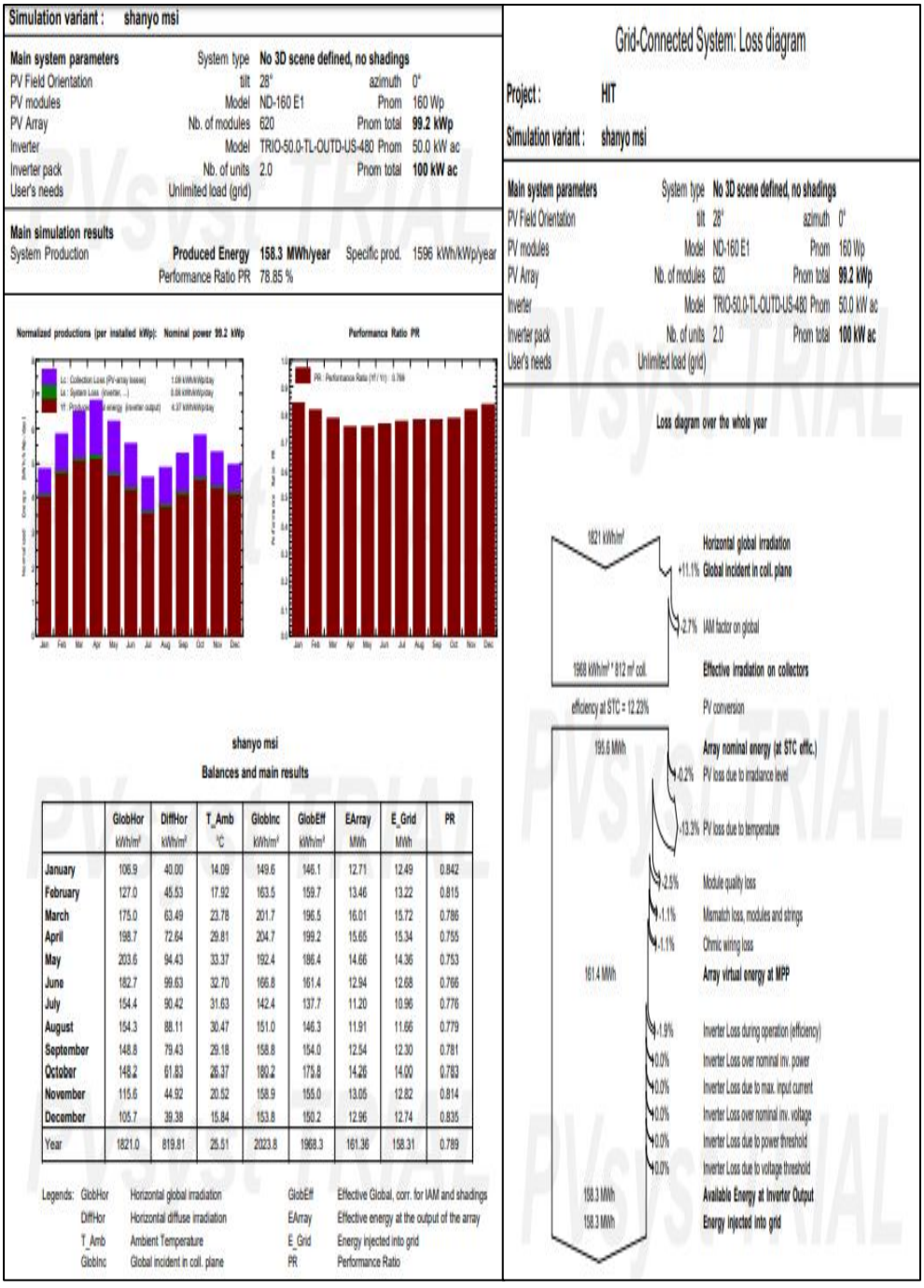

7.3. Software report of the feasibility study of the mc-si power plant using the PVSYST 4.67 version software

Different technology along with their yield (mWh/Year), area requirement and the PR is described in Table 7.1.

The highest PR is represented by the SunPower power plant which is around 85% followed by the PERC PV modules around 85%. The HIT is having a PR of around 84%.

Table 7.1. The area requirement of the PV modules technologies.

Technology	Yield (MWh/Year)	Area Required (m^2)	PR
HIT	178.8	635	83.46
SUNPOWER	172.2	502	84.48
PERC	176.4	698	84.12
mc-si	158.3	812	78.85
a-si	145.8	1582	72.10

These all are coming under high-efficiency solar module technologies. the highest PR in minimum area requirement is attained by the SunPower power plant followed by HIT then PERC. The highest area is required by the a-si modules.

Case-2, For technical and cost comparison, the compilation of the performance matrices of four different technologies (mc-si, HIT, SunPower and PERC) has been done. Four performance matrices are used which is the efficiency, temperature coefficient, years of warranties and the price per watt.

Table 7.2. Technical and cost comparison, the compilation of the performance matrices of four different technologies (mc-si, HIT, SunPower and PERC).

Technology	Efficiency	Temperature Coefficient	Warranties	Price (Rs. /Watt)
mc-si	14% -18%	-0.43%/^{O}C	10 Yrs.	Rs. 18 -Rs.22
HIT	18.5%- 20.3%	-0.29%/^{O}C-0.26%/^{O}C	25 Yrs.	Rs. 33-38
SunPower	16% -22.8%	-0.38%/^{O}C -0.29%/^{O}C	25 Yrs.	Rs. 35 To Rs. 40.
PERC	18%-24.06%	-0.39%/^{O}C	25 Yrs.	Rs. 32-35

The HIT, PERC and SunPower technologies having a better temperature coefficient and efficiency range. Accordingly, the price per watt is also higher in comparison to the mc-si modules.

7.4 Conclusion

The results demonstrated that HIT, PERC and SunPower PV modules have excellent and diverse qualities among other commercially available PV modules. All through the country, where the PV power system is the best system to overcome the fluctuating weather, raising the reliability, and increasing efficiency of the system. Finally, the results showed the ability of the high-efficiency modules to achieve the optimal solution with high precision and fastness.

CHAPTER-8
CONCLUSION

The main conclusions of the thesis are underlined in this chapter along with several recommendations for future work regarding areas that could be further investigated.

8.1 Thesis Summary

This thesis investigated diagnostic methods for characterizing and performance monitoring of the silicon-based crystalline silicon PV modules and arrays and was focused on. (i) PV module characterization and diagnostic methods based on the module performance monitoring, reliability studies and degradation studies, investigated in Chapter 4, Chapter 5, Chapter-6 and Chapter 7; Chapter 2 provide a literature review of all the aspects based on performance metrics of solar photovoltaic modules and the array is put together. A detailed literature survey has been carried out in order to compile information regarding the earlier research conducted in the field of performance of solar photovoltaics and described in the subsequent section. Chapter 3 discusses the research methodology and experimental setup used for the analysis of the issues revealed by the literature survey.

The SPV technologies modules, data logger system and the scientific instruments used are discussed briefly in the provided sections. In this chapter, a snapshot of the whole research methodologies formulation on the solar photovoltaics modules i.e. a-Si (amorphous single-junction silicon), HIT (Hetero-junction intrinsic thin layer silicon), mc-si (multi-crystalline silicon), m-si (mono-crystalline), SunPower and PERC (Passivated Emitter and Rear

Contact) modules are presented. Also, steps involved in characterization and degradation analysis based on mathematical modelling are explained in the form of schematic diagrams with a short description.

Chapter 4 discuss the performance of the SPV at real outdoor condition has been studied based on the filtering techniques, performance monitoring metrics and numerical methodologies. A set of nine SPV modules consisting multi-crystalline (m-si), Heterojunction with Intrinsic Thin layer (HIT) and amorphous silicon (a-si) each were characterized for a period of three years under the composite climate of India. The estimation of monthly average effective peak power (P_{eff}), performance ratio (PR) and temperature corrected performance ratio (PR_{CORR}) has been done. The performance assessment of the nine modules of three different silicon-based technologies under outdoor long-term exposure in composite climate conditions has been analyzed for a period of three years. The monthly average effective peak power (P_{eff}), performance ratio (PR), temperature corrected performance ratio (PR_{CORR}) has been calculated over a period of three years. The estimation of the effective peak power of nine modules shows a reduction of around 15.80%, 17.23% and 7.15% for m-si, a-si and HIT modules over an exposure time of 36 months. The impact of seasonal and temperature variability is highly observed over all the nine modules, however, highest has been observed on a-si modules technologies and least on the HIT modules as a result of its higher temperature coefficient of power. The monthly average PR for m-si, a-si and HIT modules were 0.70, 0.82 and 0.83 respectively. Also, the monthly average efficiency for the for m-si is 9.82, for a-si is 5.22, and for a HIT is 15.68 modules respectively.

The degradation rate using the linear regression over the effective peak power for m-si, a-si and HIT modules were 4.89%, 5.08% and 1.7% respectively. The highest degradation has been observed for the a-si followed by m-si modules whereas the HIT module shows the least degradation rate. The a-si module technologies are well suited for the hot and warm climatic zones whereas from the different performance indices the HIT module shows the best performance for the composite climate of India.

In Chapter 5, the series resistance of the high-efficiency silicon-based solar module has been estimated using the analytical, theoretical and light and dark I-V characteristics. The mapping of the series resistance has been done in between in-plane irradiance and module temperature. The uncertainty to estimate the series resistance has been calculated for three ranges of irradiance i.e. 1000 W/m^2, 900 W/m^2 and 800 W/m^2 for all the three technologies at outdoor field condition.

The ten different methodologies (i.e. Nine analytical and IEC procedure) for determining series resistance of three different technologies, i.e., Multi-crystalline, HIT and Amorphous Silicon, has been investigated and the effect of irradiance and module temperature on series resistance has also been assessed. The method three is found to be more stable among the nine analytical techniques of measuring series resistance.

The mean series resistances for mc-si, a-si and HIT modules are found to be 0.72 Ω, 18.20 Ω, and 0.61 Ω respectively using analytical techniques while 0.31 Ω, 20.62 Ω and 1.54 Ω respectively using IEC 60891 Edi. 2.0. The series resistance decreases with the increase in irradiance at the slope of -0.108, -0.063 and -3.348 for the mc-si, HIT and a-si solar PV module respectively. The effect of irradiance on series resistance is lowest on the HIT modules as compared to the other two technologies. From the results, it can be concluded that the variation in the results may be observed due to the input parameters, modelling equations and assumptions made during the calculations. The result shows that the modelling equations have been mainly derived for the mc-si technology and it is proposed that new modelling is required for the new emerging technologies like HIT and thin films modules. It has also been found that there is a need for a stable and standardized analytical method for calculating the series resistance. For further research, a study on the effect of various environmental parameters on the series resistance and comparative analysis of two procedures of estimating series resistance laid down by IEC may be carried out.

The mapping of the series resistance has been done to the matrix of in-plane irradiance and module temperature. The uncertainty for estimation of the series resistance has been found out to be around 4% for three ranges of irradiance for all the modules.

In Chapter 6, a systematic compilation of a procedure to examine the thermal and the electrical stress analysis and fault detection in solar module technologies using Infra-Red thermography. The chapter covers the non-destructive performance monitoring of modules under various shading configurations to evaluate the impact of the partial shading on the thermal stress of the solar modules. This analysis also useful for manufacturers, solar field installer and solar power plant designer to set up a proper plant with safety standards along with long-term dependability and strength. An overview has been provided on the uses of different approaches of Infra-Red thermography for monitoring, detection, and characterization of different field aged solar modules. A comprehensive evaluation of the thermal and electrical effects caused by the partial shading has been carried out for four different SPV module technologies. The increment in maximum frequency, the temperature of an SPV module is observed to be highest in mc-si PV modules.

The effect of the ambient temperature of the solar modules has been examined in the present study. The increase in the range of module temperature is an indication of non-uniformity of the temperature of each cell within the module, which, in turn, is either prone to or occurrence of the hotspot. The range of temperature is found to be increased significantly in the SunPower and Mono-crystalline modules as compared to others, and therefore, the hotspots are apparently visible in the IR images. The relative temperature differences measured within the solar cell may assist in the diagnosis of early degradation in the solar module. The partial shading of a string or cell within an SPV module is more severe than that of full shading and causes more degradation.

8.2 Main contributions To PV industry

The studied work also is useful for the PV module manufacturers, PV installer and PV system designers. Various filtering techniques, performance monitoring metrics and numerical methodologies have been used for the performance monitoring and characterization of the Silicon-based PV modules. The efforts have been done to derived equations relating the I-V curve parameters such as the series resistance. Knowing the values of the series resistance helps to identify the electrical losses during the installations. The silicon-based PV module technologies have been technically established and are being installed on a large scale, whereas several high-efficiency solar technologies are in the progressive state. The performance of commercially deployed PV modules is vital for the financial viability of the project. The understanding of fundamental mathematical models of solar cells and their assumptions helps to estimate and assess the electrical behaviour of the solar cell and to develop new solar cell structures/configuration by tuning the different parameters. The efficiency of the solar cell is not only a quality criterion yet whenever accomplished the correct way it can firmly lessen the expense of the solar module and in the end for generating solar energy.

The thermal stress study is useful for deciding parameter like the type of installation and height of structures for the technology-specific implementation based on a particular location. It is also a useful tool for detecting the safety issues are also the prime concern; it should not damage the structures nor harm the residents. The advanced structures of the new modules coming into the market are having the advantage to reduce the impact of partial shading or mismatch conditions. The power dissipation is not the, most pertinent issue instead of the maximum heat density that can occur since high heat will damage the solar cell, module encapsulates and the back tail. The non-uniformity of the power also occurs in the modules, especially over the weakest solar cells.

These findings may benefit PV makers and system designers since they show a path to maximizing the energy yield.

8.3 Future Work

The possibility for future work remains and can advance in several directions. The following are some points which needed to be done in future work;

1. The Potential Induced Degradation (PID), based characterization of the commercially available module technologies using the accelerated lifetime testing needed to study. Based upon the outcome, modelling other PID stress factors such as humidity, temperature and the voltage with the associated failure mechanisms.

2. Develop a real field experimental setup efficient for the tracing both the light I-V and dark I-V characteristics of solar modules, and use it to test and improve performance evaluation methodology.

3. Different modelling and topologies for the estimation of the distribution of series resistance, diode voltage, and other diode model parameters, within the module.

4. Improve the fault detection method based on performance modelling by employing a lookup table of performance model parameters, corresponding to different time periods of the year, to remove the effect of seasonal variations.

CHAPTER-9

REFERENCES

[1] Yadav K, Kumar A, Sastry OS, Wandhare R. An assessment for the selection of weather pro fi les for performance testing of SPV pumps in Indian climate. Sol Energy 2019;179:11–23. doi:10.1016/j.solener.2018.12.021.

[2] IRENA Statistics. Renewable Energy Capacity Statistics 2019. 2019.

[3] Alim MA, Tao Z, Hassan MK, Rahman A, Wang B, Zhang C, et al. Is it time to embrace building integrated Photovoltaics? A review with particular focus on Australia. Sol Energy 2019;188:1118–33. doi:10.1016/j.solener.2019.07.002.

[4] Hacke P, Lokanath S, Williams P, Vasan A, Sochor P, TamizhMani GS, et al. A status review of photovoltaic power conversion equipment reliability, safety, and quality assurance protocols. Renew Sustain Energy Rev 2018;82:1097–112. doi:10.1016/j.rser.2017.07.043.

[5] Karin T, Jones CB, Jain A. Photovoltaic Degradation Climate Zones. Conf Rec IEEE Photovolt Spec Conf 2019:687–94. doi:10.1109/PVSC40753.2019.8980831.

[6] Dash PK, Gupta NC, Rawat R, Pant PC. A novel climate classification criterion based on the performance of solar photovoltaic technologies. Sol Energy 2017;144:392–8. doi:10.1016/j.solener.2017.01.046.

[7] Rao Golive Y, Zacharaiah S, Bhaduri S, Dubey R. All-India Survey of Photovoltaic Module Reliability : 2018 Executive Summary 2017:217.

[8] Geisemeyer I, Tucher N, Muller B, Steinkemper H, Hohl-Ebinger J, Schubert MC, et al. Angle dependence of solar cells and modules: The role of cell texturization. IEEE J Photovoltaics 2017;7:19–24. doi:10.1109/JPHOTOV.2016.2614120.

[9] Walsh TM, Xiong Z, Khoo YS, Tay AAO, Aberle AG. Singapore modules-optimised PV modules for the tropics. Energy Procedia 2012;15:388–95. doi:10.1016/j.egypro.2012.02.047.

[10] Moretón R, Lorenzo E, Narvarte L. Experimental observations on hot-spots and derived acceptance/rejection criteria. Sol Energy 2015;118:28–40. doi:10.1016/j.solener.2015.05.009.

[11] Sen C, Chan C, Hamer P, Wright M, Varshney U, Liu S, et al. Annealing prior to contact firing: A potential new approach to suppress LeTID. Sol Energy Mater Sol Cells 2019;200:109938. doi:10.1016/j.solmat.2019.109938.

[12] Dubey R, Chattopadhyay S, Kuthanazhi V, John J, Ansari F, Rambabu S, et al. All-India Survey of Photovoltaic Module Reliability: 2014 2016:1–164.

[13] Ibn-Mohammed T, Koh SCL, Reaney IM, Acquaye A, Schileo G, Mustapha KB, et al. Perovskite solar cells: An integrated hybrid lifecycle assessment and review in comparison with other photovoltaic technologies. Renew Sustain Energy Rev 2017;80:1321–44. doi:10.1016/j.rser.2017.05.095.

[14] Chatzisideris MD, Ohms PK, Espinosa N, Krebs FC, Laurent A. Economic and environmental performances of organic photovoltaics with battery storage for residential self-consumption. Appl Energy 2019;256:113977. doi:10.1016/j.apenergy.2019.113977.

[15] Monokroussos C, Salis E, Etienne D, Zhang X, Dittmann S, Friesen G, et al. Electrical characterization intercomparison of high-efficiency c-Si modules within Asian and European laboratories. Prog Photovoltaics Res Appl 2019:pip.3134. doi:10.1002/pip.3134.

[16] Schulte-Huxel H, Witteck R, Holst H, Vogt MR, Blankemeyer S, Hinken D, et al. High-Efficiency modules with passivated emitter and rear solar Cells-An analysis of electrical and optical losses. IEEE J Photovoltaics 2017;7:25–31. doi:10.1109/JPHOTOV.2016.2614121.

[17] Terrestrial photovoltaic (PV) modules – Design qualification and type approval – Part 2: Test procedures. INTERNATIONAL STANDARD-IEC 61215-2. 2016.

[18] Kumar NM, Sudhakar K, Samykano M, Micheli L, Fernandez EF, Caballero JA, et al. Statistical evaluation of PV system performance and failure data among different climate zones Statistical evaluation of PV system performance and failure data among different climate zones. Renew Energy 2019;139:1040–60. doi:10.1016/j.renene.2019.02.135.

[19] Djordjevic S, Parlevliet D, Jennings P. Detectable faults on recently installed solar modules in Western Australia. Renew Energy 2014;67:215–21. doi:10.1016/j.renene.2013.11.036.

[20] Tossa AK, Soro YM, Thiaw L, Azoumah Y, Sicot L, Yamegueu D, et al. Energy performance of different silicon photovoltaic technologies under hot and harsh climate. Energy 2016;103:261–70. doi:10.1016/j.energy.2016.02.133.

[21] Muñoz J V., Nofuentes G, Fuentes M, de la Casa J, Aguilera J. DC energy yield prediction in large monocrystalline and polycrystalline PV plants: Time-domain integration of Osterwald's model. Energy 2016;114:951–60. doi:10.1016/j.energy.2016.07.064.

[22] Balaska A, Tahri A, Tahri F, Stambouli AB. Performance assessment of five different photovoltaic module technologies under outdoor conditions in Algeria. Renew Energy 2017;107:53–60. doi:10.1016/j.renene.2017.01.057.

[23] Makrides G, Theristis M, Bratcher J, Georghiou GE. Five-year performance and reliability analysis of monocrystalline photovoltaic modules with different backsheet materials Five-year performance and reliability analysis of monocrystalline photovoltaic modules with di ff erent backsheet materials. Sol Energy 2018;171:491–9. doi:10.1016/j.solener.2018.06.110.

[24] Kichou S, Wolf P, Silvestre S, Chouder A. Analysis of the behaviour of cadmium telluride and crystalline silicon photovoltaic modules deployed outdoor under humid continental climate conditions. Sol Energy 2018;171:681–91. doi:10.1016/j.solener.2018.07.028.

[25] Berardone I, Lopez Garcia J, Paggi M. Analysis of electroluminescence and infrared thermal images of monocrystalline silicon photovoltaic modules after 20 years of outdoor use in a solar vehicle. Sol Energy

2018;173:478–86. doi:10.1016/J.SOLENER.2018.07.055.

[26] Wang H, Muñoz-García MA, Moreda GP, Alonso-García MC. Seasonal performance comparison of three grid connected photovoltaic systems based on different technologies operating under the same conditions. Sol Energy 2017;144:798–807. doi:10.1016/j.solener.2017.02.006.

[27] Elibol E, Özmen ÖT, Tutkun N, Köysal O. Outdoor performance analysis of different PV panel types. Renew Sustain Energy Rev 2017;67:651–61. doi:10.1016/j.rser.2016.09.051.

[28] Shravanth Vasisht M, Srinivasan J, Ramasesha SK. Performance of solar photovoltaic installations: Effect of seasonal variations. Sol Energy 2016;131:39–46. doi:10.1016/j.solener.2016.02.013.

[29] Sastry OS, Saurabh S, Shil SK, Pant PC, Kumar R, Kumar A, et al. Performance analysis of field exposed single crystalline silicon modules. Sol Energy Mater Sol Cells 2010;94:1463–8. doi:10.1016/j.solmat.2010.03.035.

[30] Pillai DS, Rajasekar N, Ram JP, Chinnaiyan VK. Design and testing of two phase array reconfiguration procedure for maximizing power in solar PV systems under partial shade conditions (PSC). Energy Convers Manag 2018;178:92–110. doi:10.1016/j.enconman.2018.10.020.

[31] Macalpine S, Deceglie M, Kurtz S, Bora B, Sastry OS, Singh YK, et al. Analysis of a Single Year of Performance Data for Thin Film Modules Deployed at NREL and NISE 2016.

[32] Gottschalg R, Betts TR, Infield DG, Kearney MJ. The effect of spectral variations on the performance parameters of single and double junction amorphous silicon solar cells n.d.:1–29.

[33] Alonso-Abella M, Chenlo F, Nofuentes G, Torres-Ramírez M. Analysis of spectral effects on the energy yield of different PV (photovoltaic) technologies: The case of four specific sites. Energy 2014;67:435–43. doi:10.1016/j.energy.2014.01.024.

[34] Gaglia AG, Lykoudis S, Argiriou AA, Balaras CA, Dialynas E. Energy efficiency of PV panels under real outdoor conditions–An experimental assessment in Athens, Greece. Renew Energy 2017;101:236–43. doi:10.1016/j.renene.2016.08.051.

[35] Silvestre S, Tahri A, Tahri F, Benlebna S, Chouder A. Evaluation of the performance and degradation of crystalline silicon-based photovoltaic modules in the Saharan environment. Energy 2018;152:57–63. doi:10.1016/j.energy.2018.03.135.

[36] Hosseini S, Taheri S, Farzaneh M, Taheri H, Narimani M. Determination of Photovoltaic Characteristics in Real Field Conditions. IEEE J Photovoltaics 2018;8:572–80. doi:10.1109/JPHOTOV.2018.2797974.

[37] Fairbrother A, Boyd M, Lyu Y, Avenet J, Illich P, Wang Y, et al. Differential degradation patterns of photovoltaic backsheets at the array level. Sol Energy 2018;163:62–9. doi:10.1016/j.solener.2018.01.072.

[38] Purohit I, Purohit P. Performance assessment of grid-interactive solar photovoltaic projects under India's national solar mission. Appl Energy 2018;222:25–41. doi:10.1016/j.apenergy.2018.03.135.

[39] Appiah AY, Zhang X, Ayawli BBK, Kyeremeh F. Review and performance evaluation of photovoltaic array fault detection and diagnosis techniques. Int J Photoenergy 2019;2019. doi:10.1155/2019/6953530.

[40] Phinikarides A, Philippou N, Makrides G, Georghiou GE. Performance loss rates of different photovoltaic technologies after eight years of operation under warm climate conditions. 29th EU-PVSEC 2014:2664–8. doi:10.4229/EUPVSEC20142014-5BV.1.27.

[41] Dhere NG, Pethe SA, Kaul A. Methods for high-voltage bias testing of PV modules in hot and humid climate 2011;8112:81120O. doi:10.1117/12.894035.

[42] Gxasheka AR, Van Dyk EE, Meyer EL. Evaluation of performance parameters of PV modules deployed outdoors. Renew Energy 2005;30:611–20. doi:10.1016/j.renene.2004.06.005.

[43] Dunlop ED, Halton D. The performance of crystalline silicon photovoltaic solar modules after 22 years of continuous outdoor exposure. Prog Photovoltaics Res Appl 2006;14:53–64. doi:10.1002/pip.627.

[44] Rawat R, Kaushik SC, Sastry OS, Singh YK, Bora B. Energetic and exergetic performance analysis of CdS/CdTe based photovoltaic

technology in real operating conditions of composite climate. Energy Convers Manag 2016;110:42–50. doi:10.1016/j.enconman.2015.11.069.

[45] Takashima T, Yamaguchi J, Otani K, Oozeki T, Kato K, Ishida M. Experimental studies of fault location in PV module strings. Sol Energy Mater Sol Cells 2009;93:1079–82. doi:10.1016/j.solmat.2008.11.060.

[46] Sastry OS, Bora B, Singh YK, Bangar M, Singh R, Renu, et al. RPN analysis of field exposed mono crystalline silicon PV modules under composite climate of India. 2015 IEEE 42nd Photovolt Spec Conf PVSC 2015 2015:13–5. doi:10.1109/PVSC.2015.7356128.

[47] Khan J, Arsalan MH. Solar power technologies for sustainable electricity generation - A review. Renew Sustain Energy Rev 2016;55:414–25. doi:10.1016/j.rser.2015.10.135.

[48] Woodhouse M, Jones-Albertus R, Feldman D, Fu R, Horowitz K, Chung D, et al. On the Path to SunShot: The Role of Advancements in Solar Photovoltaic Efficiency, Reliability, and Costs. Natl Renew Energy Lab 2016:44. doi:NREL/TP-6A20-65872.

[49] Rawat R, Singh R, Sastry OS, Kaushik SC. Performance evaluation of micromorph based thin film photovoltaic modules in real operating conditions of composite climate. Energy 2017;120:537–48. doi:10.1016/j.energy.2016.11.105.

[50] Rodrigues S, Torabikalaki R, Faria F, Cafôfo N, Chen X, Ivaki AR, et al. Economic feasibility analysis of small scale PV systems in different countries. Sol Energy 2016;131:81–95. doi:10.1016/j.solener.2016.02.019.

[51] Chen Y, Liu Y, Chen Y, Wang D, Wang X, Lacarrière B, et al. A risk-based multi-criteria spatial decision analysis for solar power plant site selection in different climates : A case study in Iran. Renew Energy 2019;143:483–9. doi:10.1016/j.egypro.2019.01.139.

[52] Magare DB, Sastry OS, Gupta R, Betts TR, Gottschalg R, Kumar A, et al. Effect of seasonal spectral variations on performance of three different photovoltaic technologies in India. Int J Energy Environ Eng 2016;7:93–103. doi:10.1007/s40095-015-0190-0.

[53] Rajput P, Sastry OS, Tiwari GN. Effect of irradiance, temperature

exposure and an Arrhenius approach to estimating weathering acceleration factor of Glass, EVA and Tedlar in a composite climate of India. Sol Energy 2017;144:267–77. doi:10.1016/j.solener.2017.01.027.

[54] Nikolaeva-Dimitrova M, Kenny RP, Dunlop ED, Pravettoni M. Seasonal variations on energy yield of a-Si, hybrid, and crystalline Si PV modules. Prog Photovoltaics Res Appl 2010;18:311–20. doi:10.1002/pip.918.

[55] Chang M, Gangwar P, Manoj N, Kumar A, Zaimi M, Achouby H El, et al. HOT SPOT PERFORMANCE COMPARISON OF FIELD AND LAB FOR P-TYPE C-SI l : n : e : . Sol Energy 2019;191:341–59. doi:10.4229/EUPVSEC20152015-5CV.2.42.

[56] Gholami A, Khazaee I, Eslami S, Zandi M, Akrami E. Experimental investigation of dust deposition e ff ects on photo-voltaic output performance. Sol Energy 2018;159:346–52. doi:10.1016/j.solener.2017.11.010.

[57] Dubey R, Chattopadhyay S, Kuthanazhi V, John JJ, Solanki CS, Kottantharayil A, et al. Correlation of electrical and visual degradation seen in field survey in India. Conf Rec IEEE Photovolt Spec Conf 2016;2016-Novem:1692–6. doi:10.1109/PVSC.2016.7749912.

[58] Rajput P, Tiwari GN, Bora B, Sastry OS. Visual and electrical degradation of 22 years field age monocrystalline silicon PV module in composite climate of India. 2015 IEEE 42nd Photovolt Spec Conf PVSC 2015 2015. doi:10.1109/PVSC.2015.7355702.

[59] García M, Marroyo L, Lorenzo E, Marcos J, Pérez M. Observed degradation in photovoltaic plants affected by hot-spots. Prog Photovoltaics Res Appl 2014;22:1292–301. doi:10.1002/pip.2393.

[60] Mohammed S, Boumediene B, Miloud B. Assessment of PV modules degradation based on performances and visual inspection in Algerian Sahara. Int J Renew Energy Res 2016;6:106–16.

[61] Rajput P, Tiwari GN, Sastry OS, Bora B, Sharma V. Degradation of mono-crystalline photovoltaic modules after 22 years of outdoor exposure in the composite climate of India. Sol Energy 2016;135:786–95. doi:10.1016/j.solener.2016.06.047.

[62] Hepp J, Machui F, Egelhaaf H-J, Brabec CJ, Vetter A. Automatized

analysis of IR-images of photovoltaic modules and its use for quality control of solar cells. Energy Sci Eng 2016;4:363–71. doi:10.1002/ese3.140.

[63] Kampwerth H, Trupke T, Weber JW, Augarten Y. Advanced luminescence based effective series resistance imaging of silicon solar cells. Appl Phys Lett 2008;93:91–4. doi:10.1063/1.2982588.

[64] Davis a. P, Lettington a. H. Principle of Thermal Imaging. Appl Therm Imaging 1988:275–86.

[65] Kaplani E. Detection of degradation effects in field-aged c-Si solar cells through IR thermography and digital image processing. Int J Photoenergy 2012;2012. doi:10.1155/2012/396792.

[66] Sharma V, Sastry OSS, Kumar A, Bora B, Chandel SSS. Degradation analysis of a-Si, (HIT) hetro-junction intrinsic thin layer silicon and m-C-Si solar photovoltaic technologies under outdoor conditions. Energy 2014;72:536–46. doi:10.1016/j.energy.2014.05.078.

[67] Breitenstein O, Schmidt C. Thermal failure analysis by IR lock-in thermography. … Fail Anal Desk … 2004:330–9.

[68] Abdul Majid J, Sulaiman M, Zailani S, Shaharudin MR, Saw B, Wu CL, et al. Proceedings of the 1st International Conference on Electronic Engineering and Renewable Energy. Sol Energy 2018;8:1–8. doi:10.1007/978-981-13-1405-6.

[69] Kaplani E. Detection of Degradation Effects in Field-Aged c-Si Solar Cells through IR Thermography and Digital Image Processing 2012;2012. doi:10.1155/2012/396792.

[70] Zhang C, Zhang J, Hao Y, Lin Z, Zhu C. A simple and efficient solar cell parameter extraction method from a single current-voltage curve. J Appl Phys 2011;110. doi:10.1063/1.3632971.

[71] Aubry V, Meyer F. Schottky diodes with high series resistance: Limitations of forward I-V methods. J Appl Phys 1994;76:7973–84. doi:10.1063/1.357909.

[72] Merten J, Andreu J. Clear separation of seasonal effects on the performance of amorphous silicon solar modules by outdoor I /V - measurements. Sol Energy Mater Sol Cells 1998;52:11–25.

doi:10.1016/S0927-0248(97)00263-8.

[73] Garrido-Alzar CL. Algorithm for extraction of solar cell parameters from I–V curve using double exponential model. Renew Energy 1997;10:125–8. doi:10.1016/0960-1481(96)00049-3.

[74] Khan F, Singh SN, Husain M. Determination of diode parameters of a silicon solar cell from variation of slopes of the I-V curve at open circuit and short circuit conditions with the intensity of illumination. Semicond Sci Technol 2010;25. doi:10.1088/0268-1242/25/1/015002.

[75] Hong L, Lim I, Ye Z, Ye J, Yang D, Du H. A linear method to extract diode model parameters of solar panels from a single I e V curve. Renew Energy 2015;76:135–42. doi:10.1016/j.renene.2014.11.018.

[76] Singh VN, Singh RP. A method for the measurement of solar cell series resistance. J Phys D Appl Phys 1983;16:1823–5. doi:10.1088/0022-3727/16/10/007.

[77] Khan F, Singh SN, Husain M. Effect of illumination intensity on cell parameters of a silicon solar cell. Sol Energy Mater Sol Cells 2010;94:1473–6. doi:10.1016/j.solmat.2010.03.018.

[78] Hacke P, Spataru S, Johnston S, Terwilliger K, Vansant K, Kempe M, et al. Elucidating PID Degradation Mechanisms and in Situ Dark I-V Monitoring for Modeling Degradation Rate in CdTe Thin-Film Modules. IEEE J Photovoltaics 2016;6:1635–40. doi:10.1109/JPHOTOV.2016.2598269.

[79] Humada AM, Hamada HM, Hojabri M, Mekhilef S, Hamada HM. Solar cell parameters extraction based on single and double-diode models : A review. Renew Sustain Energy Rev 2017;56:494–509. doi:10.1016/j.rser.2015.11.051.

[80] Ahmad T, Sobhan S, Nayan F. Comparative Analysis between Single Diode and Double Diode Model of PV Cell: Concentrate Different Parameters Effect on Its Efficiency. J Power Energy Eng 2016;4:31–46. doi:10.4236/jpee.2016.43004.

[81] Humada AM, Hamada H. Solar cell parameters extraction based on single and double-diode models : A review. Renew Sustain Energy Rev 2017;56:494–509. doi:10.1016/j.rser.2015.11.051.

[82] Singh R, Sharma M, Rawat R, Banerjee C. An assessment of series resistance estimation techniques for different silicon based SPV modules. Renew Sustain Energy Rev 2018;98:199–216. doi:10.1016/j.rser.2018.09.020.

[83] Phinikarides A, Makrides G, Zinsser B, Schubert M, Georghiou GE. Analysis of photovoltaic system performance time series: Seasonality and performance loss. Renew Energy 2015;77:51–63. doi:10.1016/j.renene.2014.11.091.

[84] Makrides G, Zinsser B, Schubert M, Georghiou GE. Performance loss rate of twelve photovoltaic technologies under field conditions using statistical techniques. Sol Energy 2014;103:28–42. doi:10.1016/j.solener.2014.02.011.

[85] Kichou S, Silvestre S, Nofuentes G, Torres-Ramírez M, Chouder A, Guasch D. Behavioral data of thin-film single junction amorphous silicon (a-Si) photovoltaic modules under outdoor long term exposure. Data Br 2016;7:366–71. doi:10.1016/j.dib.2016.02.055.

[86] Alexander Phinikarides, George Makrides and GEG. INITIAL PERFORMANCE DEGRADATION OF AN A-SI/A-SI TANDEM PV ARRAY. 27th Eur Photovolt Sol Energy Conf Exhib 2015;1:3267–70.

[87] Makrides G, Zinsser B, Schubert M, Georghiou GE. Seasonal performance comparison of different photovoltaic technologies installed in Cyprus and Germany. Int J Sustain Energy 2013;32:466–88. doi:10.1080/14786451.2012.759572.

[88] Singh R, Bora B, Sastry OS, Rai S, Bangar M. Uncertainty analysis in the power rating measurement of solar cell as per IEC 61853-1 Uncertainty analysis in the power rating measurement of solar cell as per IEC 61853-1 2016.

[89] Sabry M, Ghitas AE. Influence of Temperature on Methods for Determining Silicon Solar Cell Series Resistance. J Sol Energy Eng 2007;129:331. doi:10.1115/1.2735350.

[90] Jordehi AR. Parameter estimation of solar photovoltaic (PV) cells: A review. Renew Sustain Energy Rev 2016;61:354–71. doi:10.1016/j.rser.2016.03.049.

[91] Nituca C, Chiriac G, Cuciureanu D, Zhang G, Han D, Plesca A. Numerical Analysis of a Real Photovoltaic Module with Various Parameters 2018;2018.

[92] Singh R, Sharma M, Os S. Non-destructive in-situ performance monitoring of high-efficiency SPV modules using infrared thermography in composite climate of India 2018;2:54–60. doi:10.15406/mojsp.2018.02.00024.

[93] Singh R, Bora B, Yadav K, Sastry OS, Kumar M, Kumar A, et al. Effect of series resistance on degradation of isc, power output and fill factor of HIT technology. 2015 IEEE 42nd Photovolt Spec Conf PVSC 2015 2015:1–5. doi:10.1109/PVSC.2015.7356032.

[94] Wolf M, Rauschenbach H. Series resistance effects measurements. Adv Energy Convers 1963;3:455–79. doi:10.1016/0365-1789(63)90063-8.

[95] Ortiz-Conde A, Lugo-Muñoz D, García-Sánchez FJ. An explicit multiexponential model as an alternative to traditional solar cell models with series and shunt resistances. IEEE J Photovoltaics 2012;2:261–8. doi:10.1109/JPHOTOV.2012.2190265.

[96] Bissels GMMW, Schermer JJ, Asselbergs MAH, Haverkamp EJ, Mulder P, Bauhuis GJ, et al. Theoretical review of series resistance determination methods for solar cells. Sol Energy Mater Sol Cells 2014;130:605–14. doi:10.1016/j.solmat.2014.08.003.

[97] Ortiz-Conde A, Lugo-Muñoz D, García-sánchez FJ, Kim YS, Kang SM, Johnston B, et al. Theory for voltage dependent series resistance in silicon solar cells. Sol Energy Mater Sol Cells 2014;2:135–42. doi:10.1002/pip.

[98] Bartolomeo A Di, Giubileo F, Luongo G, Cataldo E, Lieto A Di, Maccarrone F. On a rapidly converging iterative algorithm for diode parameter extraction from a single IV curve On a rapidly converging iterative algorithm for diode parameter extraction from a single IV curve n.d.

[99] Singh R, Bora B, Sastry OS, Yadav K, Rai S, Kumar Y, et al. ICAER 2015 Estimation of Dynamic resistance of HIT technology module in dark and illuminated condition 2015:1–6.

[100] Lee M-KK, Wang J-CC, Horng S-FF, Meng H-FF. Extraction of solar cell series resistance without presumed current–voltage functional form. Sol Energy Mater Sol Cells 2010;94:578–82. doi:10.1016/j.solmat.2009.11.026.

[101] Ghani F, Duke M, Carson J. Numerical calculation of series and shunt resistances and diode quality factor of a photovoltaic cell using the Lambert W -function. Sol Energy 2013;91:422–31. doi:10.1016/j.solener.2012.09.005.

[102] Chin VJ, Salam Z, Ishaque K. Cell modelling and model parameters estimation techniques for photovoltaic simulator application: A review. Appl Energy 2015;154:500–19. doi:10.1016/j.apenergy.2015.05.035.

[103] Silvestre S, Kichou S, Chouder A, Nofuentes G, Karatepe E. Analysis of current and voltage indicators in grid connected PV (photovoltaic) systems working in faulty and partial shading conditions. Energy 2015;86:42–50. doi:10.1016/j.energy.2015.03.123.

[104] Piciano WT. Determination of the solar cell equation parameters, including series resistance, from empirical data. Energy Convers 1969;9:1–6. doi:http://dx.doi.org/10.1016/0013-7480(69)90077-1.

[105] Charles JP, Abdelkrim M, Muoy YH, Physique D De, Sciences F, Mialhe P, et al. A PRACTICAL METHOD OF ANALYSIS OF THE C U R R E N T - VOLTAGE CHARACTERISTICS OF S O L A R CELLS B - AkT 1981;4:169–78.

[106] Chan DSH, Phillips JR, Phang JCH, Ridge K. A c o m p a r a t i v e study of e x t r a c t i o n m e t h o d s f o r solar cell m o d e l p a r a m e t e r s 1986;29:329–37.

[107] Jia Q, Anderson WA, Liu E, Zhang S. A novel approach for evaluating the series resistance of solar cells. Sol Cells 1988;25:311–8. doi:10.1016/0379-6787(88)90069-5.

[108] DIBa' S, *, M. DE LA BARDONNIEb, A. KHOURYa FPelanchon and PMialhe. a New Method for the Extraction of Diode Parameters Using a Single Exponential Model. Ctive AndPassive Elec Comp, 1999, Vol 22, Pp 157-163 1999;22:157–63.

[109] Kiran E, İnan D. Technical note An approximation to solar cell equation

for determination of solar cell parameters. Renew Energy 1999;17:235–41. doi:10.1016/S0960-1481(98)00118-9.

[110] El-Adawi MK, Al-Nuaim IA. A method to determine the solar cell series resistance from a single I-V. Characteristic curve considering its shunt resistance - New approach. Vacuum 2001;64:33–6. doi:10.1016/S0042-207X(01)00370-0.

[111] Tivanov M, Patryn a., Drozdov N, Fedotov a., Mazanik a. Determination of solar cell parameters from its current–voltage and spectral characteristics. Sol Energy Mater Sol Cells 2005;87:457–65. doi:10.1016/j.solmat.2004.07.033.

[112] Priyanka, Lal M, Singh SN. A new method of determination of series and shunt resistances of silicon solar cells. Sol Energy Mater Sol Cells 2007;91:137–42. doi:10.1016/j.solmat.2006.07.008.

[113] Cotfas D, Cotfas P, Kaplanis S, Ursutiu D. Results on series and shunt resistances in a c-Si PV cell . Comparison using existing methods and a new one 2008;10:3124–30.

[114] Lo Brano V, Orioli A, Ciulla G, Di Gangi A. An improved five-parameter model for photovoltaic modules. Sol Energy Mater Sol Cells 2010;94:1358–70. doi:10.1016/j.solmat.2010.04.003.

[115] Bencherif M, Chermitti A. New Method to Assess the Losses Parameters of the Photovoltaic Modules 2012:215–24.

[116] Yang J, Sun Y, Xu Y. Modeling impact of environmental factors on photovoltaic array performance. Int J Energy Environ 2013;4:955–68.

[117] Chaffin RJ, Osbourn GC. Measurement of concentrator solar cell series resistance by flash testing 2014;637:2012–5. doi:10.1063/1.92004.

[118] Kumar M, Kumar A. An efficient parameters extraction technique of photovoltaic models for performance assessment. Sol Energy 2017;158:192–206. doi:10.1016/j.solener.2017.09.046.

[119] Khan F, Baek S, Kim JH. Intensity dependency of photovoltaic cell parameters under high illumination conditions : An analysis. Appl Energy 2014;133:356–62. doi:10.1016/j.apenergy.2014.07.107.

[120] Carrero C, Rodríguez J, Ramírez D, Platero C. Simple estimation of PV modules loss resistances for low error modelling. Renew Energy

2010;35:1103–8. doi:10.1016/j.renene.2009.10.025.

[121] Shockley W. The Theory of p-n Junctions in Semiconductors and p-n Junction Transistors 1948.

[122] Kaminski A, Marchand JJ, Laugier A. I-V methods to extract junction parameters with special emphasis on low series resistance. Solid State Electron 1999;43:741–5. doi:10.1016/S0038-1101(98)00338-4.

[123] Khanna V, Das BK, Vandana, Singh PK, Sharma P, Jain SK. Statistical analysis and engineering fit models for two-diode model parameters of large area silicon solar cells. Sol Energy 2016;136:401–11. doi:10.1016/j.solener.2016.07.018.

[124] Cabestany J, Castaner L. A simple solar cell series resistance measurement method. Rev … 1983;18:565–7. doi:10.1051/rphysap:01983001809056500.

[125] A. POLMAN, W. G. J. H. M. VAN SARK WS and FWS. A new method for the evaluation of solar cell parameters. 1986;17:241–51.

[126] Bühler AJ, Krenzinger A. Method for photovoltaic parameter extraction according to a modi fi ed double-diode model 2012. doi:10.1002/pip.

[127] Stutenbaeumer U, Mes B. Equivalent model of monocrystalline , polycrystalline and amorphous silicon solar cells 1999;18:501–12.

[128] Enebish N, Agchbayar D, Dorjkhand S, Baatar D, Ylemj I. Numerical analysis of solar cell current-voltage characteristics. Sol Energy Mater Sol Cells 1993;29:201–8. doi:10.1016/0927-0248(93)90035-2.

[129] Jain A, Kapoor A. Exact analytical solutions of the parameters of real solar cells using Lambert W-function. Sol Energy Mater Sol Cells 2004;81:269–77. doi:10.1016/j.solmat.2003.11.018.

[130] Jain A, Kapoor A. A new approach to study organic solar cell using Lambert W-function. Sol Energy Mater Sol Cells 2005;86:197–205. doi:10.1016/j.solmat.2004.07.004.

[131] Ghani F, Rosengarten G, Duke M, Carson JK. The numerical calculation of single-diode solar-cell modelling parameters. Renew Energy 2014;72:105–12. doi:10.1016/j.renene.2014.06.035.

[132] Cubas J, Pindado S, De Manuel C. Explicit expressions for solar panel equivalent circuit parameters based on analytical formulation and the

lambert W-function. Energies 2014;7:4098–115. doi:10.3390/en7074098.

[133] Polverini D, Tzamalis G, Müllejans H. A validation study of photovoltaic module series resistance determination under various operating conditions according to IEC 60891 2012:650–60. doi:10.1002/pip.

[134] Trentadue G, Pavanello D, Salis E, Field M, Müllejans H. Determination of internal series resistance of PV devices: Repeatability and uncertainty. Meas Sci Technol 2016;27. doi:10.1088/0957-0233/27/5/055005.

[135] Service SC. Photovoltaic devices – Procedures for temperature and irradiance corrections to measured I-V characteristics IEC 60891 Edi 2.0. Communication 2003:1–8.

[136] Priya SS, Sastry OS, Bora B, Kumar A. Comparison of curve correction procedure of current and voltage as per IEC 60891 for thin film technology. 2015 IEEE 42nd Photovolt Spec Conf PVSC 2015 2015:2–5. doi:10.1109/PVSC.2015.7355843.

[137] Rawat R. Measurement and comparative analysis of series resistance of different silicon based PV technologies : Effect of irradiance and temperature 2017.

[138] Jordan DC, Deceglie MG, Kurtz SR, Renewable N, Parkway DW. PV Degradation Methodology Comparison – a Basis for a Standard 2016:273–8.

[139] Jordan DC, Silverman TJ, Sekulic B, Kurtz SR. PV degradation curves: non-linearities and failure modes. Prog Photovoltaics Res Appl 2017;25:583–91. doi:10.1002/pip.2835.

[140] Dolara A, Lazaroiu GC, Leva S, Manzolini G. Experimental investigation of partial shading scenarios on PV (photovoltaic) modules. Energy 2013;55:466–75. doi:10.1016/j.energy.2013.04.009.

[141] Emery K. Nondestructive Performance Characterization Techniques for Module Reliability 2003.

[142] García M, Marroyo L, Lorenzo E, Marcos J, Pérez M. Observed degradation in photovoltaic plants affected by hot-spots. Prog Photovoltaics Res Appl 2014;22:1292–301. doi:10.1002/pip.2393.

[143] TamizhMani G, Sharma S. Hot spot evaluation of photovoltaic modules

2008;7048:70480K. doi:10.1117/12.794237.

[144] Timothy P, Silverman J, Deceglie MG, Deline C, Kurtz S, Silverman TJ. Partial Shade Stress Test for Thin-Film Photovoltaic Modules: Preprint 2015;18302. doi:10.1117/12.2188774.

[145] Silverman TJ, Wohlgemuth J, Miller DC, Kempe M, McNutt P. Review of observed degradation modes and mechanisms from fielded modules. Pvmrw 2015 2015.

[146] IEC 61215-2:2016. INTERNATIONAL STANDARD-IEC 61215-2. 2016.

[147] Gallon J, Horner GS, Hudson JE, Vasilyev LA, Lu K. PV Module Hotspot Detection. Tau Sci Corp n.d.:99.

[148] Dubey R, Chattopadhyay S, Kuthanazhi V, Kottantharayil A, Singh Solanki C, Arora BM, et al. Comprehensive study of performance degradation of field-mounted photovoltaic modules in India. Energy Sci Eng 2017;5:51–64. doi:10.1002/ese3.150.

[149] Tsanakas JA, Botsaris PN. Non-destructive in situ evaluation of a PV module performance using infrared thermography 2009. doi:10.13140/2.1.4742.1441.

[150] Tsanakas JA, Chrysostomou D, Botsaris PN, Gasteratos A. Fault diagnosis of photovoltaic modules through image processing and Canny edge detection on field thermographic measurements. Int J Sustain Energy 2015;34:351–72. doi:10.1080/14786451.2013.826223.

[151] Sinha A, Sastry OS, Gupta R. Nondestructive characterization of encapsulant discoloration effects in crystalline-silicon PV modules. Sol Energy Mater Sol Cells 2016;155:234–42. doi:10.1016/j.solmat.2016.06.019.

[152] Dotenco S, Dalsass M, Winkler L, Wurzner T, Brabec C, Maier A, et al. Automatic detection and analysis of photovoltaic modules in aerial infrared imagery. 2016 IEEE Winter Conf Appl Comput Vis 2016:1–9. doi:10.1109/WACV.2016.7477658.

[153] Sinha A, Sastry OS, Gupta R. Detection and characterisation of delamination in PV modules by active infrared thermography. Nondestruct Test Eval 2016;31:1–16.

doi:10.1080/10589759.2015.1034717.

[154] Kaseman M, Kwapil W, Walter B, Giesecke J, Michl B, The M, et al. Progress in Silicon Solar Cell Characterization With Infrared Imaging Methods. 23rd Eur Photovolt Sol Energy Conf 2008:1–5.

[155] Nofuentes G, Chenlo F. Renewable Energy in the Service of Mankind Vol II 2016;II:477–81. doi:10.1007/978-3-319-18215-5.

[156] Alonso-García MC, Herrmann W, Böhmer W, Proisy B. Thermal and electrical effects caused by outdoor hot-spot testing in associations of photovoltaic cells. Prog Photovoltaics Res Appl 2003;11:293–307. doi:10.1002/pip.490.

[157] Ebner R, Kubicek B, Ujvari G, Novalin S, Rennhofer M, Halwachs M. Optical characterization of different thin film module technologies. Int J Photoenergy 2015;2015. doi:10.1155/2015/159458.

[158] Bashahu M, Habyarimana A. Review and test of methods for determination of the solar cell series resistance. Renew Energy 1995;6:129–38. doi:10.1016/0960-1481(94)E0021-V.

[159] Cotfas DT, Cotfas P a., Kaplanis S. Methods to determine the dc parameters of solar cells: A critical review. Renew Sustain Energy Rev 2013;28:588–96. doi:10.1016/j.rser.2013.08.017.

[160] Bora B, Sastry OS, Singh R, Bangar M, Rai S. Series Resistance measurement of Solar PV Modules using Mesh in Real Outdoor condition. Energy Procedia 2016;90:503–8. doi:10.1016/j.egypro.2016.11.217.

[161] Humada AM, Hojabri M, Mekhilef S, Hamada HM. Solar cell parameters extraction based on single and double-diode models : A review. Renew Sustain Energy Rev 2016;56:494–509. doi:10.1016/j.rser.2015.11.051.

List of Publications:

Journals

1. Field Analysis of three different silicon-based Technologies in Composite Climate Condition-Part II-Seasonal assessment and performance degradation rates using statistical tools, Rashmi Singh, Madhu Sharma, Rahul Rawat, Chandan Banerjee, Renewable Energy 147 (2020) 2102-2117.
   DOI: https://doi.org/10.1016/j.renene.2019.10.015.
2. Field Analysis of three different Silicon-based Technologies in Composite Climatic Condition, Rashmi Singh, Madhu Sharma, Chandan Banerjee, Solar Energy 182 (2019) 102-116.
   DOI: https://doi.org/10.1016/j.solener.2019.02.045.
3. An assessment of series resistance estimation techniques for different silicon-based SPV modules Rashmi Singh, Madhu Sharma, Rahul Rawat, Chandan Banerjee, Renewable and Sustainable Energy Reviews 98 (2018) 199–216.
   DOI: 10.1016/j.rser.2018.09.020.
4. Non-destructive in-situ performance monitoring of High-efficiency SPV modules using the infrared thermography in a composite climate of India, Rashmi Singh, Madhu Sharma, Rahul Rawat, O. S.Sastry, Kamlesh Yadav, Chandan Banerjee, MOJ Solar, and Photoenergy Systems, 2018;2(2):54–60.
   DOI: 10.15406/mojsp.2018.02.00024.
5. Performance Monitoring of High-Efficiency Maxeon^{tm} Based SunPower PV Plant in the Composite Climate of India, PDPU Journal of Energy and Management, Vol. 3, No.1, October 2018.
6. Estimation of Dynamic resistance of HIT technology module in dark and illuminated condition, Rashmi Singh, Madhu Sharma, Birinchi Bora, O. S. Sastry, Kamlesh Yadav, Chandan Banerjee, Material Today Proceedings, 2019. https://doi.org/10.1016/j.matpr.2018.11.056.
7. Effect of thermal stress over high-efficiency solar photovoltaic modules

in the composite climate of India, Rashmi Singh, Madhu Sharma, Rajesh Kumar, Rahul Rawat, Chandan Banerjee. (Accepted in Springer Journal-SCI index)

Conference Publications

1. Effect of thermal stress over high-efficiency solar photovoltaic modules in the composite climate of India, Rashmi Singh, Madhu Sharma, Rajesh Kumar, Rahul Rawat, Chandan Banerjee, 6th International Conference on Advances in Energy Research 2017.
2. Performance of High-Efficiency SunPower based MaxeonTM PV plant in outdoor condition, Rashmi Singh, Madhu Sharma, Rahul Rawat, Arun Tripathi, Rajesh Kumar, Chandan Banerjee, World Sustainable Energy Days, Wels, Austria, 2018.
3. Real-time Performance monitoring of high-efficiency Sun Power based MaxeonTM PV plant in a composite climate of India, Rashmi Singh, Madhu Sharma, Rahul Rawat, Chandan Banerjee, Research Enclave, IIT-Guwahati, 2018